On Aspects of Weakly Interacting Physics: Neutrino Oscillation & Dark Sector

Thesis by

Anish Ghoshal

Supervised by:

Dr. Davide Meloni

In Partial Fulfillment of the Requirements

for the Degree of

Doctor of Philosophy

Dipartimento di Matematica e Fisica,

Universita di Roma Tre

Rome, Italy

2020

(Defended October 31, 2019)

This dissertation is the result of my own work. Following the tendency of modern research in theoretical physics, most of the material discussed in this dissertation is the result of collaborative research. I have made major contributions to the publications, both in terms of results and writing. All figures presented in this dissertation were produced or adapted by myself. I hereby declare that my dissertation on *On Aspects of Weakly Interacting Physics: Neutrino Oscillation & Dark Sector* is not substantially the same as any that I have submitted or is being concurrently submitted for a degree, diploma or other qualification at the University Roma Tre, any other University or similar institution. I further state that no substantial part of my dissertation has already been submitted or is being concurrently submitted for any such degree, diploma or other qualification at the University Roma Tre, any other University or similar institution.

Anish Ghoshal

October 2019

I am not crazy, my mother had me tested.

— Dr. Sheldon Lee Cooper, the Big Bang Theory

Acknowledgments

> I have tried to read philosophers of all ages and have found many illuminating ideas but no steady progress toward deeper knowledge and understanding. Science, however, gives me the feeling of steady progress: I am convinced that theoretical physics is actual philosophy. It has revolutionized fundamental concepts, e.g., about space and time (relativity), about causality (quantum theory), and about substance and matter (atomistics), and it has taught us new methods of thinking (complementarity) which are applicable far beyond physics.
>
> — Max Born

> Our imagination is stretched to the utmost, not, as in fiction, to imagine things which are not really there, but just to comprehend those things which 'are' there.
>
> — Richard P. Feynman

I thank my supervisor for providing an opportunity to work on the projects which were close to my heart. I also take the opportunity to express my gratitude for Prof. Enrico Nardi, LNF-INFN for useful discussion related to dark sector physics. I am grateful to all my teachers during my under-graduation and post-graduation days from whom little by little I have developed my current understanding of physics. Finally I thank my parents who have been a continuous support in my life throughout my career so far.

Abstract

The Standard Model (SM) of particle physics describes the electromagentic, weak and strong interactions nicely in terms of particles: bosons, which are mediators of these interactions and fermions, which are the matter content. With no concrete hints for new physics beyond the SM from the experimental side, weakly interacting physics are a subject of focus in the recent times since weakly coupled sector particles may have eluded our detectors hitherto. Among the fermions in the SM, neutrinos are massless and electrically neutral particles which participate only in weak interactions. The experimentally observed phenomenon of neutrino oscillation establishes neutrinos having mass and there is a mixing between the three neutrino flavours. The point to note is the neutrino mass terms in the action introduces off-diagonal elements in the neutrino mass matrix in the flavour basis which depends on neutrino mass and mixing parameters. Measurements of the neutrino oscillation parameters may lead to discovering the underlying symmetries of the neutrino mass matrix thus providing a lead in the ultra-violet (UV) physics beyond the Standard Model. In current and future neutrino oscillation experiments, the oscillation parameters, namely the neutrino mass-squared differences and the mixing angles are being measured with precision. The main three unknowns in the neutrino oscillation in the standard three generation framework are: the neutrino mass hierarchy, octant of θ_{23} and the leptonic phase δ_{CP}. Among several ongoing & future experiments where these unknown oscillation parameters can be probed, Deep Underground Neutrino Experiment (DUNE) is an ambitiously planned experiment and consists of the largest Liquid Argon-TPC neutrino detector. It will have high intensity $\nu_\mu-$beam from Fermilab directed towards Sanford Underground Research Facility (SURF) laboratory. Using ν_μ-disappearance

and ν_e appearance channels, it will be able to measure the three unknowns mentioned earlier with high statistical significance. Beside this, DUNE detector is capable to detecting tau-flavored neutrinos, the species of neutrinos which have been identified very less number of times in any experiment til now. DUNE is going to surpass this with huge tau statistics. In the first half of the thesis we considered the physics potential using this $\nu_\mu \to \nu_\tau$ appearance channel. We studied the physics capabilities in the standard oscillation framework and the sensitivities of the measurement using the ν_τ-appearance channel. Alongside we investigated the impact of systematics, tau detection efficiency and various experimental reaches on the ν_τ-appearance channel. DUNE collaboration also has plans for a tau-optimized flux which will be able to provide almost 4-times larger τ-events. We also performed studies based on this flux. Apart from the standard physics scenarios, new physics especially such coupling to the third generation leptons are weakly constrained and can be concretely probed using the ν_τ-appearance channel. We investigated the measurement sensitivities of new physics in terms the non-standard interaction (NSI) parameters and predicted the bounds DUNE will be able to pose on these.

In the second half of the thesis we focused on the hidden weakly coupled sector physics. Several theoretical models envisage various types of dark matter (DM), among which of particular interest is the possibility that there is a specific type of particle that may serve as a portal between the dark particles of the new type of matter and the ordinary matter of the SM through a new very weak interaction. In a theoretical scenario of DM particles, this new sector can be constituted of possible DM candidates that can be classified based on the masses of the mediators being in the TeV, sub-GeV, eV or lighter. Due to the unsuccessful results from the traditional searches for WIMP particles, there are at least two possible reasons why a DM particle of a new sector has not been discovered yet: first, the mass scale of the new particles, including the mediators of the new forces, is well above the energy scale reached so far in laboratory experiments, mainly investigated in collider experiments. Second, the mass scale is within experimental reaches, but the couplings between the new particles and the SM ones are so feeble that the whole new sector has so far

remained hidden. We reviewed the search for dark photon (mediator between the SM and the hidden sector) in various experiments and observations and studied the current bounds. Dark photon (DP) is particular of interested in terms of anomalies of the discrepancy between the theoretical and experiment value $(g-2)_\mu$ and the electron-positron observed in decays of excited $^{8}8$ Be nuclei In particular, the last anomaly can be resolved by hypothesizing the emission of a 17 MeV dark photon (DP) A' , in the decay ^{8} Be $^{*} \rightarrow ^{8}$ Be + A' followed by $A' \rightarrow e^{+} + e^{-}$. We developed a novel technique to search for this DP in the PADME experiment in the Frascati National laboratory. This method involves the DP being produced by resonance in positron beam-dump experiment. We investigated the sensitivity of PADME using this process and compared it with the bremsstrahlung method of production. Both of them are complementary in the sense that these strategies of DP search will be able to probe different regions of the parameter space.

Keywords: Weakly interacting, Neutrino Physics, Neutrino Oscillation, Long-Baseline Neutrino Experiments (LBL), Deep Underground Neutrino Experiment (DUNE), Leptonic CP Phase, CP Violation, Non-Standard Interaction (NSI), tau, ν_τ appearance, Liquid Argon detector, Fermilab.

BSM U(1), dark sector, dark photon, dark matter, PADME, resonance, bremsstrahlung, ATOMKI, Be-anomaly.

Contents

List of Figures

Chapter 1

Introduction

The Standard Model (SM) of particle physics successfully describes electromagnetism as well as the strong and weak nuclear forces. It classifies all the observed elementary particles and was developed in stages throughout the latter half of the 20th century, by the work of many scientists around the world. Symmetry plays a central role in the SM supplemented with beautiful and well-coordinated unity. What lies at the heart of this theory is the gauge principle: a continuous global symmetry group is made local (gauged) by introducing fields, which serve as mediators for the interactions among particles. The particular symmetry group in the Standard Model is SU (3) $\times$ SU (2) $\times$ U (1). In terms of the particle spectrum, SM has 17 fundamental particles (or quanta of fields) and their corresponding anti-particles. All anti-particles are not entirely new set of particles since some particles are their own anti-particles. Twelve are spin 1/2 fermions. Among them six posses strong interaction due to their colour charges (red, green and blue); these are known as quarks. Quarks also carry electric charges: the up, charm and top quarks have electrical charge + 2/3 while the down, strange and bottom quarks have 1/3 charge. The rest of the fermions do not participate in the strong nuclear interaction and are known as leptons. Three leptons have electric charge 1. They are known as the electron, the muon and the tau-on. While the other leptons are neutral and are known as neutrinos. Neutrinos only feel the weak nuclear force. Apart from the fermions there are the force mediating particles - the gauge bosons with spin-1. The gluon, responsible for the strong nuclear force, is massless and binds quarks together to form bound-state hadrons. Photons are the gauge boson

mediators of electromagnetism and are also massless. However the crucial difference between photons and gluons lies in the fact that gluons themselves carry colour, while photons are electrically neutral. This is so because the symmetry group that describes the strong interaction is SU(3), which is non-abelian, while U(1), the symmetry group of electromagnetism, is abelian. The weak nuclear force is mediated by 3 massive bosons (& therefore short-ranged interaction): $W^{\pm}$ and Z, with electrical charges 1 and 0, respectively. W boson is responsible for the radioactive nuclear processes. The neutral Z boson on the other hand, participates in interactions like that between two neutrinos. The masses of the W and Z bosons come from their interaction with a particle known as the Higgs boson which is a scalar particle. It has no spin and is responsible for the origin of masses of the particles in the Standard Model. The Higgs is important because an explicit mass-term for the gauge bosons breaks the gauge symmetry. Moreover, the SU(2) part of the Standard Model symmetry group is also broken by explicit fermion masses. However, if the symmetry is spontaneously broken by the vacuum expectation value of a scalar field, a mass term is generated without explicitly breaking any symmetries. This is known as the celebrated Brout-Englert-Higgs mechanism [1, 2, 3, 4]. Although SM has been met with enormous theoretical and experimental successes [5, 6, 7, 8, 9, 10], there are several questions unexplained within. These are a few examples [1]:

- Gravity: The Standard Model does not involve gravitational interaction.
- Neutrinos: Neutrinos in the Standard Model are massless. But neutrino oscillations experiments suggest that they have masses.
- Baryon Asymmetry: Matter is much more abundant than antimatter. The Standard Model has no explanation for this.
- CP: The strong CP problem: why does Quantum Chromodynamics (QCD) or the strong interactions not break the CP symmetry ?

[1] We have not included the fine-tuning problems like the Higgs naturalness or the cosmological constant.

- Dark Sector: Cosmological observations require the existence of dark matter but the Standard Model of particle physics provides no candidate to explain these.

This dissertation is concerned with the second, third and the fifth points, as we entertain the notion that BSM physics, in the general form, involving dark photons, SM neutrinos and Non-Standard Interactions (NSI) are useful probes for the weakly coupled sector physics.

1.1 Neutrinos

The origin of neutrinos can be traced back to the late 19th century (1896) when Becquerel discovered radioactivity. It was observed that the nucleus of an unstable atom loses energy by emitting alpha (α), beta (β) and gamma (γ) rays. It was largely believed that the β-decay is governed by the two-body process, similar to the α-particle emission,

$$N_0(A, Z) \to N(A, Z + 1) + e^-,$$

the energy of the electron emitted in the process is equal to the tiny masses differences of the nuclei involved. But the measurements of the electron energy spectra was not conforming to this mechanism as its spectrum is continuous. It was a great puzzle in the 1920s since a two-body in the final state decay means a fixed energy line for the electrons. In this context, Niels Bohr suggested that the energy in the micro-world was conserved only on an average and not on an event-by-event basis. In 1930, Wolgang Pauli postulated the famous "Neutrino Hypothesis" to bring back the principle of energy conservation in β-decay and suggested that the continuum spectra is due to one more invisible light neutral particle involved in the β-decay. Though he himself was not so sure about this postulate. In this hypothesis, one has three particles involved, so the electron would be able to take any momentum from zero to the maximum allowed value, that is, a continuous energy spectra and the rest of the residual energy is carried away by the other light and invisible particle. This

lead Enrico Fermi to formulate his theory of β-decay based on Pauli's hypothesis (1933). Inspite of skepticism, this invisible particle hypothesis was accepted and the name "neutrino" (in Italian, "ino" suffix is used for "small"; neutrino represented a "small neutron" since neutron was the only neutral particle discovered back then) was coined. Thus the process of $\beta-$decay became

$$n \to p + e^- + \bar{\nu}.$$

Furthermore, the conservation of angular momentum dictates that the neutrinos must have spin-1/2 and thus they obey the Fermi-Dirac Statistics. But this theory was only firmly established in 1953 when in 1956, Reines and Cowan detected electron anti-neutrinos from a nuclear reactor at Savannah River via the inverse β decay for the first time [11]. The principle of lepton number conservation lead to postulation of newer kinds of neutrinos after this discovery. Muon decay processes should give rise to muon-flavored neutrino which was subsequently observed at the Brookhaven Laboratories in 1962 [12]. There the first neutrino beam was created from protons coming from an accelerator and projected on a target producing hadrons, mainly pions and kaons and decaying subsequently in the "decay tunnel", generating neutrinos (in particular ν_μ-s with a small contamination of ν_e-s). After the decay tunnel, an absorber was able to stop all the particles except neutrinos. The remaining neutrino beam reached the detector, which was able to identify neutrinos via the charged current neutrino interactions with nuclei ($\nu_\mu N \to \mu X$). Third kind of neutrino, namely the tau-on flavored neutrino was observed in 2000 by the DONUT accelerator experiment [13]. This was particularly difficult since they involve only heavy hadrons, like charmed mesons, which are able to produce ν_τ-s in their decays. Moreover, one needs high energy threshold for producing the τ lepton, 3.4 GeV, and identifying its charge current interactions.

These fundamental particles and their interactions were formulated and embedded in what is now known as the Standard Model (SM) of particle physics [14], an effort to unify the electromagnetic, weak, and strong forces, which was developed throughout

the latter half of the 20th century. This has been described earlier in this chapter.

Although the neutrinos are massless in the SM, the experimentally observed phenomenon of "neutrino oscillation" dictates that neutrinos have non-zero mass. The strangeness oscillations of neutral kaons was observed in 1955 [15]. Bruno Pontecorvo conceived the idea that neutrinos undergo quantum mechanical oscillation among their states and postulated the existence of neutrino-antineutrino oscillations. This is an interference phenomenon in which a neutrino created with a specific lepton flavour (ν_e, ν_μ or ν_τ) can later be measured to have a different flavour [16]. This occurs only if neutrinos are massive and they mix leading to the fact that the flavour eigenstates are not the same as the mass eigenstates. Afterwards its discovery, the second neutrino paved the way for Maki, Nakagawa and Sakata to discuss the possibility of the mixing between two massive neutrinos [17]. Their oscillation theory, for the first time, considered neutrinos as massive particles, even though all the observations were compatible with the massless neutrinos hypothesis. Experiments that looked at neutrinos coming from the Sun observed some anomalies that could be explained considering the oscillations between ν_e and ν_μ since 1968 [18, 19, 20]. The effect of matter in these oscillations was explored by Wolfenstein [21]. He showed that matter effect suppresses oscillations of the solar neutrinos propagating in the Sun and supernova neutrinos inside a star. He considered hypothetical experiments with neutrinos propagating through 1000 km of rock, which back then were thought-experiments only.

However, the first evidence of neutrino oscillation was found by the Super-Kamiokande experiment in 1998 [22] which was concerned about investigating the directional analysis of the fluxes of atmospheric neutrinos which are basically neutrinos that originate from decays or interactions of the cosmic rays inside the atmosphere. This study clearly produced a deficit in the flux of muon-flavored neutrinos traveling a large distance through the Earth. Oscillations between ν_μ-s and ν_τ-s states of the neutrinos explain this anomalous phenomenon. On the back of this evidence, many other neutrino oscillation experiments were constructed and thoroughly studied neutrinos arriving from the Sun (Refs. [23]-[25]), cosmic rays [26], nuclear reactors (Refs.

[27]-[28]) and particle accelerators (Refs. [29]-[34]).

Neutrinos interact in the gauge-basis and therefore detected according to the Lagrangian in their flavour or gauge eigenstates (ν_α). It is related to the mass or energy eigenstates (ν_i) as

$$|\nu_\alpha\rangle = U_{\alpha i}|\nu_i\rangle, \tag{1.1}$$

with $\alpha = e, \mu, \tau$ and $i = 1, 2, 3$. U is the unitary mixing matrix known as the Pontecorvo-Maki-Nakagawa-Sakata (PMNS) matrix.

$$\begin{aligned} U &= \begin{bmatrix} U_{e1} & U_{e2} & U_{e3} \\ U_{\mu 1} & U_{\mu 2} & U_{\mu 3} \\ U_{\tau 1} & U_{\tau 2} & U_{\tau 3} \end{bmatrix} \\ &= \begin{bmatrix} 1 & 0 & 0 \\ 0 & c_{23} & s_{23} \\ 0 & -s_{23} & c_{23} \end{bmatrix} \begin{bmatrix} c_{13} & 0 & s_{13}e^{-i\delta} \\ 0 & 1 & 0 \\ -s_{13}e^{i\delta} & 0 & c_{13} \end{bmatrix} \begin{bmatrix} c_{12} & s_{12} & 0 \\ -s_{12} & c_{12} & 0 \\ 0 & 0 & 1 \end{bmatrix} \\ &= \begin{bmatrix} c_{12}c_{13} & s_{12}c_{13} & s_{13}e^{-i\delta} \\ -s_{12}c_{23} - c_{12}s_{23}s_{13}e^{i\delta} & c_{12}c_{23} - s_{12}s_{23}s_{13}e^{i\delta} & s_{23}c_{13} \\ s_{12}s_{23} - c_{12}c_{23}s_{13}e^{i\delta} & -c_{12}s_{23} - s_{12}c_{23}s_{13}e^{i\delta} & c_{23}c_{13} \end{bmatrix}, \end{aligned}$$

θ_{ij} are the various mixing angles, s & c are respective sine and cosine of the θ_{ij} angles and δ_{CP} is the CP-violating phases in the matrix [2]. The probability that ν_α-flavored neutrino to transform to ν_β-flavored neutrino ($\nu_\alpha \to \nu_\beta$) in a time interval t is given by the amplitude squared $|\langle\nu_\beta(t)|\nu_\alpha\rangle|^2$. Just to sketch an example, oscillation of the three flavours of neutrinos in vacuum, the probability of flavour transition $\nu_\alpha \to \nu_\beta$ can be expressed as [35]

$$\begin{aligned} P_{\alpha\beta} = \delta_{\alpha\beta} \quad &- \quad 4\sum_{i<j} \mathrm{Re}\big(U_{\alpha i}U_{\beta j}U^*_{\alpha j}U^*_{\beta i}\big)\sin^2\{\Delta_{ij}L/4E\} \\ &+ \quad 2\sum_{i>j} \mathrm{Im}\big(U_{\alpha i}U_{\beta j}U^*_{\alpha j}U^*_{\beta i}\big)\sin\{2\Delta_{ij}L/4E\}, \end{aligned} \tag{1.2}$$

where $\Delta_{ij} = m_i^2 - m_j^2$ and i, j runs from 1 to 3. This will be discussed in details

[2]Majorana phases have not been considered as they do not enter in the neutrino oscillation phenomena

in the next chapter. It is evident from this relation the oscillatory terms depend on the mass squared differences of the neutrinos and not the absolute masses of the neutrinos themselves. Moreover, the flavor transition is characterised by the energy of the neutrinos E and the baseline L associated with it. The oscillation probability is maximum when L/E is of the order of $1/\Delta_{ij}$.

Most of the oscillation parameters have been determined with a very small uncertainty till now. But there are still many open questions, for example, the CP violation in the neutrino sector (that is, measurement of the phase δ_{CP}), the mass hierarchy (if the mass of neutrino m_2 is greater than m_3 or not) and the octant of θ_{23} (whether the value of θ_{23} is less than or greater than 45^o). Also now that we are in the era of precision measurements in the neutrino sector, also search for evidences of new physics in the oscillations has gained momentum.

The open questions mentioned above will be explored in future neutrino experiments and one of the most important among them will be the Deep Underground Neutrino Experiment (DUNE), which will have a baseline of 1300 km. We will concentrate the phenomenology related to this experiment in this thesis for the neutrino studies. The standard numerical simulations involving physics potentials and their sensitivity studies in DUNE involve two oscillations channels, namely the ν_e appearance and the ν_μ disappearance channels. However, the ν_τ appearance channel will be directly accessible by DUNE as well. In this thesis we consider a scenario with DUNE where the ν_τ appearance channel has been added to the standard simulations and study its impact on the analysis of sensitivities to neutrino oscillation parameters. The ν_τ appearance channel can be used not only to study standard oscillations, but also to improve the sensitivity limits to new BSM physics parameters like that of Non-Standard Interaction (NSI) and the 3+1 sterile neutrino model.

1.2 Dark Sector

In the second half of the thesis we will be concerned with the problem of dark matter and dark sector physics searches. Dark matter (DM) [36, 37, 38] and neutrino masses

[18, 39] are among the several experimental facts that point towards physics beyond the current fundamental physics framework known as the Standard Model of particle physics or SM. The non-luminous matter component of the universe known as dark matter constitutes about a fifth of the total energy density of our universe a fact now well established courtsey to several evidences in cosmology and astrophysics at different scales [41]. Despite the several experimental searches and the impressive efforts of the community, all the evidence for DM has only been of gravitational nature and the widely considered non-gravitational nature of DM is still unknown [40]. There are many candidates postulated for this [41], and a lot of attention was devoted to the class of beyond Standard Model theories which can provide a weakly interacting massive particle (WIMP) DM candidate, which, as the name suggests, weakly interact with SM particles and contains an appealing connection between the dark sector and the electroweak scale [42].

Several theoretical models envisage various types of DM models, among which of particular interest is the possibility that there is a specific type of particle that may serve as a portal between the dark particles of the new type of matter and the ordinary matter of the SM through a new very weak interaction. In a theoretical scenario of DM particles, this new sector can be constituted of possible DM candidates that can be classified into three broad classes

1. Weakly interacting massive particles (WIMPs). Typically with masses of several GeV.

2. Ultra-light sub-eV particles introduced as a solution to the strong CP problem (axion) and similar pseudo-Goldstone bosons (axion-like particles or ALPs).

3. Sub-GeV hidden sector particles, neutral under SM charges and feebly interacting with the SM through new portal forces.

Due to the unsuccessful results from the traditional searches for WIMP particles, there are at least two possible reasons why a DM particle of a new sector has not been discovered yet: first, the mass scale of the new particles, including the mediators

of the new forces, is well above the energy scale reached so far in laboratory experiments, mainly investigated in collider experiments. Second, the mass scale is within experimental reaches, but the couplings between the new particles and the SM ones are so feeble that the whole new sector has so far remained hidden. This latter case often referred to as the Hidden Sector (HS) or "Dark Sector" (DS) hypothesis, and this motivation has lead to an increasing interest in the high energy physics community. Several novel ideas have been proposed to hunt for new physics at the intensity frontiers for scenarios beyond the SM (BSM) containing new particles with masses in the range between sub-eV and sub-GeV, neutral under the SM forces and interacting feebly with the ordinary matter. HS is motivated from some experimental anomalies like the discrepancy between the measured value of $(g\text{-}2)_\mu$ and the theoretical prediction and the anomaly observed in decays of excited $^{8}8$ Be nuclei. These puzzles can be explained via weakly coupled HS mediators with masses in the MeV range. In particular, the last anomaly can be resolved by hypothesizing the emission of a 17 MeV HS boson, a dark photon (DP) A' , in the decay ^{8} Be $^{*} \rightarrow ^{8}$ Be + A' followed by $A' \rightarrow e^+ + e^-$. This idea is developed where the DP is considered as a natural candidate for super-weakly coupled new state, since its dominant interaction with the SM sector might arise exclusively from a mixed kinetic term coupling the $U(1)'$ and QED field strength tensors. In this work, we studied how DPs can be searched when its production is through the annihilations of e^+ and e^- into an on-shell DP, or non-resonant into photon pairs, one of which ordinary and one dark. The analysis is considered for the PADME experiment at the Frascati National Laboratories, aiming to seek this type of event through the accurate reconstruction of the invariant mass distributions of e^+, e^- pairs produced in a possible decay of A' , or through the reconstruction of the missing mass in the balance between the initial state, constituted by the $e^+ + e^-$ pair (using the positrons of the Frascati Beam Test Facility) and the final state in which only the ordinary photon is detected. If discovered the dark photon explaining the ^{8}Be anomaly, it will be a breakthrough in particle physics as this might open the door to a whole new sector containing hidden particles.

Before concluding this chapter, let me summarize the essential motivation behind

the research concerned with this thesis. We are mainly interested in the weakly coupled sector of the standard particle theory of the Universe in general. One in the neutrino sector which interact through the weak interactions of the Standard Model and the neutrino oscillation experiments are well equipped with measuring the unknown parameters in the neutrino sector as well as looking for beyond Standard Model (BSM) physics linked to it, especially in context to the third generation of the leptons in the SM which have very weak constraints till now. For the planned DUNE experiment we investigated the impact of analysing the ν_τ-appearance channel that is accessible there. The second weakly coupled sector is dark sector or hidden sector and we study the DP phenomenology with respect to this. Particularly we studied the various DP searches and developed a novel method to look for DP in the PADME experiment in a case well-suited to solving the 8-Be nuclear anomaly.

The structure of this thesis is as follows: in the second chapter, we lay out the formalism for neutrino oscillation, in the next we give an overview of the DUNE experiment, in the fourth chapter, we investigate the standard physics scenario in DUNE with ν_τ appearance and in fifth we study the new physics in the form of NSI in our analysis. The sixth and seventh chapters are about the DP models overviews and the search in PADME experiment respectively. Finally we have the ninth chapter to briefly summarize and present conclusions from our study.

I have added material that reviews and clarifies the relevant physics for the reader. Also, as far as possible, I have complemented the previously published research with discussions of recent advances in the literature and in my own understanding.

Chapter 2

The Phenomenon of Neutrino Oscillation

This chapter and the next one are dedicated to reviewing the phenomena of neutrino oscillation; in particular, we will concentrate on the neutrino oscillation in context to Long-Baseline experiment. Likewise we will review the experimental set-up and the main physics opportunities at the DUNE experiment.

2.1 Introduction

Originally proposed by Bruno Pontecorvo [43], neutrinos while propagating undergo oscillation and this phenomenon is described in terms of the transition probability from one flavour to another. The probability depends on the neutrino mass squared differences, mixing angles and the Dirac CP phase. Although experiments detecting neutrinos from many sources were able to constrain with a very good precision the oscillation parameters, there are still some open questions. Moreover, oscillation experiments cannot measure the absolute neutrinos masses; for that purpose, tritium beta decay experiments have been built. The Troitsk [44] and Mainz [45] experiments give an upper bound on electron neutrino $|m_{\nu_e}| < 1.8$ eV. For some weak constraints on muon and tau-flavored neutrino masses, see pion decay experiment bounds: $\mathrm{m}_{\nu_\mu} < 0.17$ MeV [46] and $\mathrm{m}_{\nu_\tau} < 18.2$ MeV [47] respectively. For Majorana neutrino mass bound, see neutrino-less double-beta decay experiment [48, 49] and lastly cosmology gives an upper bound on neutrino mass sum due to neutrino-free streaming constraints

at late universe [50]. For a comprehensive summary, see [51].

We will follow a bottom-up approach and build up the neutrino oscillation probabilities with increasing level of complexities. Let us begin with a simple *2-flavor* neutrino oscillation scenario in vacuum.

2.2 A Look at the Oscillation Probabilities

We will present analytic expressions for the neutrino oscillation probabilities in vacuum, and in presence of matter. Using constant matter density one can derive the exact expressions for a *2-flavor* neutrino oscillation scenario. The same for *3-flavor* needs to be achieved under certain assumptions. One of the popularly used methods to derive the probabilities is the $\alpha - s_{13}$ (double expansion in $\alpha(= \Delta_{21}/\Delta_{31})$ and $\sin\theta_{13}$) approximation where $\Delta_{ij} = m_i^2 - m_j^2$ [52] and θ_{13} is one of the mixing angles of U_{PMNS}. We shall describe the parameters in details later. This approximation is suited to accelerator-based neutrino oscillation studies.

We will concentrate on the latter; other than the planned DUNE experiment [53] which we will describe in details later, some the experimental set-ups which uses accelerator-based neutrinos to study neutrino oscillation are namely the LSND [54], MiniBooNE [55], K2K [56], MINOS [57], T2K [58] and NOνA [59] experiments.

2.2.1 2-Flavors Neutrino in Vacuum

For two generations of neutrinos, say of flavors, ν_e and ν_μ, the flavor and mass eigenstates of the neutrinos are related by:

$$\begin{pmatrix} \nu_e \\ \nu_\mu \end{pmatrix} = \begin{pmatrix} \cos\theta & \sin\theta \\ -\sin\theta & \cos\theta \end{pmatrix} \begin{pmatrix} \nu_1 \\ \nu_2 \end{pmatrix}, \tag{2.1}$$

where θ is the mixing angle between the gauge and mass eigenstates between the neutrinos. Considering the time evolution of the neutrino,

$$i\frac{d}{dt}|\nu(t)>= H|\nu(t)> \tag{2.2}$$

with $H = \frac{1}{2E_\nu}U\text{Diag}[m_1^2, m_2^2]U^\dagger$, then using energy-mass relation, the time evolution the neutrino gives

$$|\nu_e(t)\rangle = e^{-iE_1 t}\cos\theta|\nu_1\rangle + e^{-iE_2 t}\sin\theta|\nu_2\rangle, \tag{2.3}$$

where E_1 and E_2 are the energies of the mass eigenstates ν_1 and ν_2 having mass m_1 and m_2, respectively; the survival probability of the electron neutrino ν_e is given by

$$\begin{aligned} P_{ee} &= |\langle\nu_e|\nu_e(t)\rangle|^2 \\ &= (\cos^2\theta e^{-iE_1 t} + \sin^2\theta e^{-iE_2 t})(\cos^2\theta e^{iE_1 t} + \sin^2\theta e^{iE_2 t}) \\ &= 1 - \sin^2 2\theta \sin^2\{(E_2 - E_1)t/2\}. \end{aligned} \tag{2.4}$$

As neutrinos are relativistic particles, $E \approx p \approx \frac{m^2}{2E}$ and $t \approx L$ (for $c = 1$ and $\hbar = 1$). Therefore, P_{ee} becomes

$$\begin{aligned} P_{ee} &= 1 - \sin^2 2\theta \sin^2\{\Delta_{21}L/4E\} \\ &= 1 - \sin^2 2\theta \sin^2\{1.27\Delta_{21}L/E\}, \end{aligned} \tag{2.5}$$

where in the last line, $\Delta_{21} = m_2^2 - m_1^2$ is in eV^2, L is in km and E is in GeV. Since the total probability should add upto 1, the conversion probability is

$$\begin{aligned} P_{\mu e} &= 1 - P_{ee} \\ &= \sin^2 2\theta \sin^2\{1.27\Delta_{21}L/E\}. \end{aligned} \tag{2.6}$$

Although Eq. 2.6 is a very simplified calculation, some salient features of neutrino oscillation are apparent: the essential oscillatory behaviour is encoded within Δ_{21}-term

which when the neutrinos masses are equal, or becomes vanishing; so, no oscillation. Also, notice that whether $\theta < 45^\circ$ or $> 45^\circ$ does not matter and the probability remains the same for both cases. Similarly, the sign of Δ_{21} does not affect the probability; so there is a degeneracy between $\theta \to \pi/2 - \theta$ and $\Delta_{21} \to -\Delta_{21}$ values.

On the other hand the L and E terms in the probability conspires to decide the sensitivity to the parameters. For example, high L and low E values cause large periodicity leading to averaging out of oscillations, the maximum oscillation being:

$$1.27\Delta_{21}L/E = n\pi/2, \tag{2.7}$$

n being integers ($n = 1$ is known as the first oscillation maximum which is usually what is looked at long-baseline neutrino experiments). For example, the DUNE experiment is designed such that the neutrino flux peaks at the energies where there is maximum of oscillation; for L= 1300 km the neutrino peaks at about 2.5 GeV. This value for $n = 1$ points to a mass squared difference as 2.5×10^{-3} eV^2 which is the best-fit values of the accelerator mass squared difference.

Having understood some preliminary points regarding the oscillatory nature of the probability, let us move on to the *3-flavor* scenario in the next subsection.

2.2.2 3-Flavours Neutrinos in Vacuum

Following Ref. [60], a 3-flavor case, the mixing matrix U_{PMNS} will be a 3×3 unitary matrix and be parameterized by three mixing angles, namely θ_{12}, θ_{23} and θ_{13} and a CP-violating phase δ_{CP}

$$U_{PMNS} = R_{23}\tilde{R}_{13}R_{12}, \tag{2.8}$$

where R_{ij} are the orthogonal rotational matrices:

$$R_{23} = \begin{pmatrix} 1 & 0 & 0 \\ 0 & c_{23} & s_{23} \\ 0 & -s_{23} & c_{23} \end{pmatrix}, \tilde{R}_{13} = \begin{pmatrix} c_{13} & 0 & s_{13}e^{-i\delta_{CP}} \\ 0 & 1 & 0 \\ -s_{13}e^{-i\delta_{CP}} & 0 & c_{13} \end{pmatrix}, R_{12} = \begin{pmatrix} c_{12} & s_{12} & 0 \\ -s_{12} & c_{12} & 0 \\ 0 & 0 & 1 \end{pmatrix} \tag{2.9}$$

leading to

$$U_{PMNS} = \begin{pmatrix} c_{12}c_{13} & s_{12}c_{13} & s_{13}e^{-i\delta_{CP}} \\ -s_{12}c_{23} - c_{12}s_{23}s_{13}e^{i\delta_{CP}} & c_{12}c_{23} - s_{12}s_{23}s_{13}e^{i\delta_{CP}} & s_{23}c_{13} \\ s_{12}s_{23} - c_{12}c_{23}s_{13}e^{i\delta_{CP}} & -c_{12}s_{23} - s_{12}c_{23}s_{13}e^{i\delta_{CP}} & c_{23}c_{13} \end{pmatrix} \tag{2.10}$$

where $c_{ij} = \cos\theta_{ij}$, $s_{ij} = \sin\theta_{ij}$. The gauge eigenstates and mass eigenstates are related to each other by:

$$\begin{pmatrix} \nu_e \\ \nu_\mu \\ \nu_\tau \end{pmatrix} = U_{PMNS} \begin{pmatrix} \nu_1 \\ \nu_2 \\ \nu_3 \end{pmatrix} \tag{2.11}$$

Similar to the 2-flavor case, the neutrino state evolution will be governed by the Hamiltonian [1] $H = \frac{1}{2E_\nu} U_{PNMS}$ Diag $[m_1^2, m_2^2, m_3^2] U_{PNMS}^\dagger$. Writing the relation in terms of $\alpha = e$, μ, τ and i =1, 2, 3, we have

$$|\nu_\alpha(t=0)\rangle = U_{\alpha1}|\nu_1\rangle + U_{\alpha2}|\nu_2\rangle + U_{\alpha3}|\nu_3\rangle \tag{2.12}$$

$$|\nu_\alpha(t)\rangle = U_{\alpha1}e^{-iE_1t}|\nu_1\rangle + U_{\alpha2}e^{-iE_2t}|\nu_2\rangle + U_{\alpha3}e^{-iE_3t}|\nu_3\rangle \tag{2.13}$$

and the survival probability is given by

$$\begin{aligned} P_{\alpha\alpha} &= |\langle\nu_\alpha(t=0)|\nu_\alpha(t)\rangle|^2 \\ &= (|U_{\alpha1}|^2e^{-iE_1t} + |U_{\alpha2}|^2e^{-iE_2t} + |U_{\alpha3}|^2e^{-iE_3t}) \\ &\times (|U_{\alpha1}|^2e^{iE_1t} + |U_{\alpha2}|^2e^{iE_2t} + |U_{\alpha3}|^2e^{iE_3t}) \\ &= |U_{\alpha1}|^4 + |U_{\alpha2}|^4 + |U_{\alpha3}|^4 \\ &+ |U_{\alpha1}|^2|U_{\alpha2}|^2e^{-i(E_1-E_2)} + |U_{\alpha1}|^2|U_{\alpha2}|^2e^{i(E_1-E_2)} \\ &+ |U_{\alpha1}|^2|U_{\alpha3}|^2e^{-i(E_1-E_3)} + |U_{\alpha1}|^2|U_{\alpha3}|^2e^{i(E_1-E_3)} \\ &+ |U_{\alpha2}|^2|U_{\alpha3}|^2e^{-i(E_2-E_3)} + |U_{\alpha2}|^2|U_{\alpha3}|^2e^{i(E_2-E_3)} \end{aligned} \tag{2.14}$$

[1] We have used U and U_{PNMS} interchangeably in the thesis.

Now taking the first three terms of equation 2.15

$$\begin{aligned} |U_{\alpha 1}|^4 + |U_{\alpha 2}|^4 + |U_{\alpha 3}|^4 &= (|U_{\alpha 1}|^2 + |U_{\alpha 2}|^2 + |U_{\alpha 3}|^2)^2 \\ &- 2|U_{\alpha 1}|^2|U_{\alpha 2}|^2 - 2|U_{\alpha 1}|^2|U_{\alpha 3}|^2 - 2|U_{\alpha 2}|^2|U_{\alpha 3}|^2 \\ &= 1 - 2|U_{\alpha 1}|^2|U_{\alpha 2}|^2 - 2|U_{\alpha 1}|^2|U_{\alpha 3}|^2 \\ &- 2|U_{\alpha 2}|^2|U_{\alpha 3}|^2 \end{aligned} \tag{2.15}$$

Note that unitary condition have been used:

$$\sum_{i=1}^{3} U_{\alpha i} U^*_{\beta_i} = \delta_{\alpha\beta} \tag{2.16}$$

Gathering all the terms from equations 2.15 and 2.16

$$-2|U_{\alpha 1}|^2|U_{\alpha 2}|^2 + |U_{\alpha 1}|^2|U_{\alpha 2}|^2(e^{-i(E_1-E_2)} + e^{i(E_1-E_2)}) = -4|U_{\alpha 1}|^2|U_{\alpha 2}|^2 \sin^2 \Delta_{21} L/4E \tag{2.17}$$

which after some algebraic simplification reduces to the expression for $P_{\alpha\alpha}$ as

$$\begin{aligned} P_{\alpha\alpha} &= 1 - 4|U_{\alpha 1}|^2|U_{\alpha 2}|^2 \sin^2 \Delta_{21} L/4E \\ &- 4|U_{\alpha 1}|^2|U_{\alpha 3}|^2 \sin^2 \Delta_{31} L/4E \\ &- 4|U_{\alpha 2}|^2|U_{\alpha 3}|^2 \sin^2 \Delta_{23} L/4E \end{aligned} \tag{2.18}$$

Proceeding in a similar manner, one obtains for the general transition probability, for appearance and disappearance cases,

$$\begin{aligned} P_{\alpha\beta} =& \delta_{\alpha\beta} - 4\Re \left[\sum_{i>j}^{n} U^*_{\alpha i} U_{\beta i} U_{\alpha j} U^*_{\beta j} \sin^2 \left(\Delta m^2_{ij} \frac{L}{4E} \right) \right] + \\ &+ 2\Im \left[\sum_{i>j}^{n} U^*_{\alpha i} U_{\beta i} U_{\alpha j} U^*_{\beta j} \sin \left(\Delta m^2_{ij} \frac{L}{2E} \right) \right] \end{aligned} \tag{2.19}$$

where $\Re$ and $\Im$ represents the real and imaginary parts respectively. Note that the

$\Im$ part comes into play only in disappearance type transitions, so the CP violating parameter δ_{CP} can be probed by this. One can see that the three mass squared differences are a part of equation 2.19 in the three flavour oscillation scenario. We shall derive these probabilities in details considering matter effects in subsequent chapters.

Although we studied the neutrino oscillation in vacuum, in reality the neutrino propagates through some matter, and due to presence of electrons in matter, they suffer coherent forward scattering and their propagation gets modified than that in vacuum. This shall be topic of study of the next subsection: we will understand the features of neutrino oscillations in matter.

2.2.3 2-Flavours Neutrinos in Matter

Whenever neutrinos propagate inside matter neutrino oscillation probabilities are modified from that in vacuum. This is because active neutrino flavors get scattered by the electrons present inside the matter, causing an effective potential (or effective mass) in the path during the travel of the neutrinos. Basically neutrinos interact with the medium and gets scattered coherently: these scattering are elastic in nature and can be of weak charge current (CC) or neutral current (NC) in their electro-weak physics origin. The charge current interactions affect only ν_e since normal matter consists of electron, proton and neutron but the neutral current interactions affect all the three active neutrinos. These interactions are represented by the Feynman diagrams in Fig. 2.1.

NC scattering effective-potential affects all three neutrino flavor propagation equally, so does not show up in the the final expressions of neutrino oscillation probabilities. However, the CC interaction has its effect only on the electron neutrinos and consequently changes the probability expression. We can write the effective interaction Hamiltonian for the CC as, following Ref. [60]:

$$H_{\text{eff}} = \frac{G_F}{\sqrt{2}} \left[\bar{e}\gamma_\mu(1-\gamma_5)\nu_e\right] \left[\bar{\nu}_e\gamma^\mu(1-\gamma_5)e\right], \tag{2.20}$$

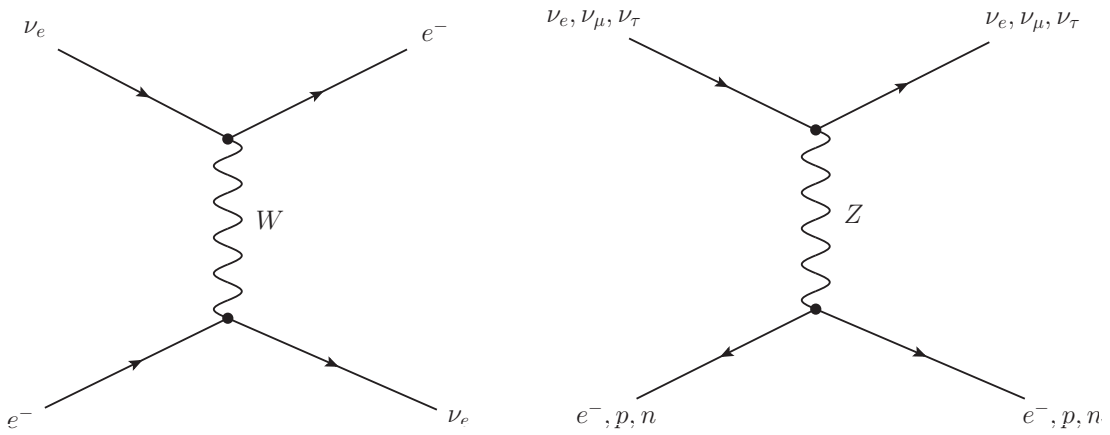

Figure 2.1: CC and NC interactions of neutrinos in matter.

where G_F is the Fermi constant and the symbols have their usual meaning. After some algebraic transformation, one can reduce the expression to

$$H_{\text{eff}} = \frac{G_F}{\sqrt{2}} \left[\bar{e}\gamma_\mu(1-\gamma_5)e\right] \left[\bar{\nu}_e\gamma^\mu(1-\gamma_5)\nu_e\right].$$

Next we take an average of this interaction over the background field, since we are interested in understanding in terms of an interaction potential. Since the electrons are the background we may use the following identities [61]

$$\begin{aligned} \langle\bar{e}\gamma_\mu\gamma_5 e\rangle &\sim \frac{1}{2}, \\ \langle\bar{e}\gamma_i e\rangle &\sim \text{v}, \\ \langle\bar{e}\gamma_0 e\rangle &= N_e, \end{aligned} \tag{2.21}$$

where the first identity is the spin, v is the velocity of electrons and N_e is the number

density of the electrons. In the non-relativistic limit it can be written as

$$\begin{aligned} \bar{H}_{\text{eff}} &= \sqrt{2} G_F N_e \bar{\nu}_{eL} \gamma^0 \nu_{eL} \\ &= v_{CC} \bar{\nu}_{eL} \gamma^0 \nu_{eL} \\ &= v_{CC} j_\nu, \end{aligned} \tag{2.22}$$

where N_e is the electron number density of the medium, $\nu_{eL} = \frac{1-\gamma_5}{2}\nu_e$, $j_\nu = \bar{\nu}_{eL}\gamma^0\nu_{eL}$ and v_{CC} is the interaction effective-potential given by

$$v_{CC} = \sqrt{2} G_F N_e. \tag{2.23}$$

Similarly, for anti-neutrinos, we will have (see Appendix 9.1):

$$\bar{v}_{CC} = -\sqrt{2} G_F N_e. \tag{2.24}$$

Thus the evolution equation becomes

$$i\frac{\partial}{\partial t}\begin{pmatrix} \nu_e \\ \nu_\mu \end{pmatrix} = H_F^{\text{matt}} \begin{pmatrix} \nu_e \\ \nu_\mu \end{pmatrix}, \tag{2.25}$$

with

$$H_F^{\text{matt}} = \begin{pmatrix} -\frac{\Delta_{21}}{4E}\cos 2\theta + v_{CC} & \frac{\Delta_{21}}{4E}\sin 2\theta \\ \frac{\Delta_{21}}{4E}\sin 2\theta & \frac{\Delta_{21}}{4E}\cos 2\theta \end{pmatrix}. \tag{2.26}$$

Let

$$A = 2\sqrt{2} G_F N_e E, \tag{2.27}$$

and substracting $\frac{A}{4E}$ from the diagonal elements, Eq. 2.26 simplifies to

$$H_F^{\text{matt}} = \frac{1}{4E}\begin{pmatrix} A - \Delta_{21}\cos 2\theta & \Delta_{21}\sin 2\theta \\ \Delta_{21}\sin 2\theta & -A + \Delta_{21}\cos 2\theta \end{pmatrix}. \tag{2.28}$$

The energy eigenvalues of $H_F^{\rm matt}$ are obtained by simply diagonalising the above matrix:

$$E_{1,2} = \frac{1}{4E}\left[A \pm \sqrt{(-A + \Delta_{21}\cos 2\theta)^2 + (\Delta_{21}\sin 2\theta)^2}\right]. \tag{2.29}$$

We know, for relativistic species $E_2 - E_1 = (m_2^2 - m_1^2)/2E$. This modifies the neutrino mass squared difference in presence of matter and one may write the effective neutrino mass-squared as:

$$\Delta_{21}^M = \sqrt{(-A + \Delta_{21}\cos 2\theta)^2 + (\Delta_{21}\sin 2\theta)^2} \tag{2.30}$$

Just to point out explicitly, the matter effects are nicely encoded with the A-term and note that this is the term which is causing the modification of the energy eigenstates. In the limit $A \to 0$, one recovers the vacuum oscillation properties. A not only shifts the mass values, but also in a similar manner modifies the mixing between the neutrinos:

$$\tan 2\theta_{eff} = \frac{\Delta_{21}\sin 2\theta}{-A + \Delta_{21}\cos 2\theta}. \tag{2.31}$$

Here θ_{eff} is the mixing angle in matter and U_{eff} the mixing matrix which is required for diagonalizing the matter Hamiltonian matrix $H_F^{\rm matt}$ for converting from flavour basis to mass basis by the transformation $H_M^{\rm matt} = U_{eff}^\dagger H_F^{\rm matt} U_{eff}$. The expressions for the probabilities $P_{e\mu}$ and $P_{\mu\mu}$ become

$$P_{\mu e} = \sin^2 2\theta_M \sin^2(1.27\Delta_{21}^M L/E) \tag{2.32}$$

$$P_{\mu\mu} = 1 - P_{\mu e} \tag{2.33}$$

where we took the matter density to be of constant nature. Some comments are in order: the expression for the vacuum oscillation probability was not sensitive to

the sign of Δ_{21} and octant of θ but due the modification in mass and mixing, the expression now becomes sensitive to both of them. Another interesting phenomenon in this case is the MSW (Mikheyev-Smirnov-Wolfenstein) resonance. This happens when

$$\begin{aligned} \Delta_{21}\cos 2\theta &= A \\ &= 0.76\times 10^{-4}\left[\frac{\rho}{\mathrm{gm/cc}}\right]\left[\frac{E}{\mathrm{GeV}}\right]\mathrm{eV}^2. \end{aligned} \tag{2.34}$$

If this condition is satisfied then we see that the mixing angle becomes maximal i.e., $\pi/4$. This leads to the possibility of total transitions between the two flavours. Since for neutrinos A is positive, resonance can only occur for $\Delta_{21} > 0$ and $\theta < \pi/4$ or $\Delta_{21} < 0$ and $\theta > \pi/4$. For anti-neutrinos the resonance condition is given by $\Delta_{21} > 0$ and $\theta > \pi/4$ or $\Delta_{21} < 0$ and $\theta < \pi/4$. From this it is clear that the enhancement of the neutrino and anti-neutrino probabilities depend on the sign of Δ_{21} and octant of θ. Thus the experimental observation of this resonance effect can lead to the determination of the same.

Next we show the *business* part of our computation where will derive the full *3-flavor* neutrino oscillation probability including all matter effects by diagonalizing the matter Hamiltonian. An approximation regarding that the matter density is constant will also be used for simplification purposes.

2.2.4 3-Flavours Neutrinos in Matter:

In this subsection we will give the derivation of the approximate three flavour probability expressions using the series expansion method [52] in a constant matter density. We will study expansions in terms of the mass hierarchy parameter $\alpha = \Delta_{21}/\Delta_{31}$ and mixing parameter $s_{13} = \sin\theta_{13}$ keeping terms up to second order. The effective Hamiltonian in flavour basis can be written as

$$H_F^{\mathrm{matter}} = \frac{\Delta_{31}}{2E}\left[U\,\mathrm{diag}(0,\alpha,1)U^\dagger + \mathrm{diag}(\hat{A},0,0)\right], \tag{2.35}$$

where $\hat{A} = A/\Delta_{31}$. In order to derive the double expansion, we write the above Hamiltonian as

$$H_F^{\rm matter} = \frac{\Delta_{31}}{2E} R_{23} U_\delta M U_\delta^\dagger R_{23}^T, \tag{2.36}$$

where $U_\delta = {\rm diag}(1, 1, e^{i\delta_{CP}})$. We define,

$$\begin{aligned} H_F'^{\rm matt} &= \frac{\Delta_{31}}{2E} M \qquad (2.37)\\ &= \frac{\Delta_{31}}{2E} \left[R_{13} R_{12} {\rm diag}(0, \alpha, 1) R_{12}^T R_{13}^T + {\rm diag}(\hat{A}, 0, 0) \right] \\ &= \begin{pmatrix} s_{12}^2 c_{13}^2 \alpha + s_{13}^2 + \hat{A} & \alpha c_{12} c_{13} s_{12} & s_{13} c_{13} (1 - \alpha s_{12}^2) \\ s_{12} c_{12} c_{13} \alpha & \alpha c_{12}^2 & -\alpha c_{12} s_{12} s_{13} \\ s_{13} c_{13} (1 - \alpha s_{12}^2) & -s_{12} c_{12} s_{13} \alpha & \alpha s_{12}^2 s_{13}^2 + c_{13}^2 \end{pmatrix}. \end{aligned}$$

Diagonalisation is performed using perturbation theory up to second order in the small parameters α and s_{13} i.e.,

$$M = M^0 + M^1 + M^2, \tag{2.38}$$

where

$$M^0 = {\rm diag}(\hat{A}, 0, 1) = {\rm diag}(\lambda_1^0, \lambda_2^0, \lambda_3^0), \tag{2.39}$$

$$M^1 = \begin{pmatrix} \alpha s_{12}^2 & \alpha s_{12} c_{12} & s_{13} \\ \alpha s_{12} c_{12} & \alpha c_{12}^2 & 0 \\ s_{13} & 0 & 0 \end{pmatrix}, \tag{2.40}$$

$$M^2 = \begin{pmatrix} s_{13}^2 & 0 & -\alpha s_{13} s_{12}^2 \\ 0 & 0 & -\alpha s_{13} s_{12} c_{12} \\ -\alpha s_{13} s_{12}^2 & -\alpha s_{13} s_{12} c_{12} & -s_{13}^2 \end{pmatrix}. \tag{2.41}$$

For eigenvalues we write

$$\lambda_i = \lambda_i^0 + \lambda_i^1 + \lambda_i^2, \tag{2.42}$$

and for the eigenvectors we write

$$v_i = v_i^0 + v_i^1 + v_i^2. \tag{2.43}$$

Since M^0 is already diagonal we have

$$v_i^0 = e_i, \tag{2.44}$$

i.e.,

$$v_1^0 = \begin{pmatrix} 1 \\ 0 \\ 0 \end{pmatrix}, \quad v_2^0 = \begin{pmatrix} 0 \\ 1 \\ 0 \end{pmatrix}, \quad v_3^0 = \begin{pmatrix} 0 \\ 0 \\ 1 \end{pmatrix}. \tag{2.45}$$

Now the first and second order corrections to the eigenvalues are given by

$$\lambda_i^1 = M_{ii}^1 = \langle v_i^0 | M^1 | v_i^0 \rangle, \tag{2.46}$$

$$\lambda_i^2 = M_{ii}^2 + \sum_{j \neq i} \frac{(M_{ii}^1)^2}{\lambda_i^0 - \lambda_j^0}, \tag{2.47}$$

and the corrections to the eigenvectors are given by

$$v_i^1 = \sum_{j \neq i} \frac{M_{ij}^1}{\lambda_i^0 - \lambda_j^0} e_j, \tag{2.48}$$

$$v_i^2 = \sum_{j \neq i} \frac{1}{\lambda_i^0 - \lambda_j^0} \left[M_{ij}^2 + (M^1 v_i^1)_j - \lambda_i^1 (v_i^1)_j \right] e_j. \tag{2.49}$$

Using Eqs. 2.46 and 2.47 and keeping in mind the fact that $E_i = \frac{\Delta_{31}}{2E}\lambda_i$, we obtain the following expressions for the energy eigenvalues

$$E_1 = \frac{\Delta_{31}}{2E}\big(\hat{A} + \alpha s_{12}^2 + s_{13}^2\frac{\hat{A}}{\hat{A}-1} + \alpha^2\frac{\sin^2 2\theta_{12}}{4\hat{A}}\big), \tag{2.50}$$

$$E_2 = \frac{\Delta_{31}}{2E}\big(\alpha c_{12}^2 - \alpha^2\frac{\sin^2 2\theta_{12}}{4\hat{A}}\big), \tag{2.51}$$

$$E_3 = \frac{\Delta_{31}}{2E}\big(1 - s_{13}^2\frac{\hat{A}}{\hat{A}-1}\big), \tag{2.52}$$

and using Eqs. 2.48 and 2.49 we get the three eigenvectors as

$$v_1 = \begin{pmatrix} 1 \\ \frac{\alpha\sin 2\theta_{12}}{2\hat{A}} + \frac{\alpha^2\sin 4\theta_{12}}{4\hat{A}^2} \\ \frac{s_{13}}{\hat{A}-1} - \frac{\hat{A}\alpha s_{13}s_{12}^2}{(\hat{A}-1)^2} \end{pmatrix}, \quad v_2 = \begin{pmatrix} -\frac{\alpha\sin 2\theta_{12}}{2\hat{A}} - \frac{\alpha^2\sin 4\theta_{12}}{4\hat{A}^2} \\ 1 \\ \frac{\alpha s_{13}\sin 2\theta_{12}(\hat{A}+1)}{2\hat{A}} \end{pmatrix}, \tag{2.53}$$

$$\text{and} \quad v_3 = \begin{pmatrix} -\frac{s_{13}}{\hat{A}-1} + \frac{\hat{A}\alpha s_{13}s_{12}^2}{(\hat{A}-1)^2} \\ \frac{\hat{A}\alpha s_{13}\sin 2\theta_{12}}{2(\hat{A}-1)} \\ 1 \end{pmatrix}.$$

such that now the leptonic mixing matrix is:

$$U_\prime = R_{23}U_\delta W, \tag{2.54}$$

with $W = (v_1, v_2, v_3)$. Next, via the $U_\prime$ matrix elements and using Eqs. 2.50, 2.51 and 2.52 we get the analytic expressions for oscillation probabilities. First the $\nu_\mu \to \nu_e$

transition probability and the leading order term for $\nu_\mu \to \nu_\mu$ [2]:

$$\begin{aligned} P_{\mu e} = \; & 4 s_{13}^2 s_{23}^2 \frac{\sin^2(\hat{A}-1)\Delta}{(\hat{A}-1)^2} \\ & + 2\alpha s_{13} \sin 2\theta_{12} \sin 2\theta_{23} \cos(\Delta - \delta_{CP}) \frac{\sin \hat{A}\Delta}{\hat{A}} \frac{\sin(\hat{A}-1)\Delta}{\hat{A}-1} \\ & + \alpha^2 \sin^2 2\theta_{12} c_{23}^2 \frac{\sin^2 \hat{A}\Delta}{\hat{A}^2}, \end{aligned} \tag{2.55}$$

Similarly, the expression for the disappearance probability,

$$\begin{aligned} P_{\mu\mu} = & \, 1 - \sin^2 2\theta_{23} \, \sin^2 \Delta + \alpha \, c_{12}^2 \, \sin^2 2\theta_{23} \, \Delta \, \sin 2\Delta \\ & - \alpha^2 \, \sin^2 2\theta_{12} \, c_{23}^2 \, \frac{\sin^2 \hat{A}\Delta}{\hat{A}^2} - \alpha^2 \, c_{12}^4 \, \sin^2 2\theta_{23} \, \Delta^2 \, \cos 2\Delta \\ & + \frac{1}{2\hat{A}} \, \alpha^2 \, \sin^2 2\theta_{12} \, \sin^2 2\theta_{23} \left(\sin \Delta \, \frac{\sin \hat{A}\Delta}{\hat{A}} \, \cos(\hat{A}-1)\Delta - \frac{\Delta}{2} \, \sin 2\Delta \right) \\ & - 4 \, s_{13}^2 \, s_{23}^2 \frac{\sin^2(\hat{A}-1)\Delta}{(\hat{A}-1)^2} \\ & - \frac{2}{\hat{A}-1} \, s_{13}^2 \, \sin^2 2\theta_{23} \left(\sin \Delta \, \cos \hat{A}\Delta \, \frac{\sin(\hat{A}-1)\Delta}{\hat{A}-1} - \frac{\hat{A}}{2} \Delta \, \sin 2\Delta \right) \\ & - 2 \, \alpha \, s_{13} \, \sin 2\theta_{12} \, \sin 2\theta_{23} \, \cos \delta_{\rm CP} \, \cos \Delta \, \frac{\sin \hat{A}\Delta}{\hat{A}} \, \frac{\sin(\hat{A}-1)\Delta}{\hat{A}-1} \\ & + \frac{2}{\hat{A}-1} \, \alpha \, s_{13} \, \sin 2\theta_{12} \, \sin 2\theta_{23} \, \cos 2\theta_{23} \, \cos \delta_{\rm CP} \, \sin \Delta \left(\hat{A} \sin \Delta - \frac{\sin \hat{A}\Delta}{\hat{A}} \, \cos(\hat{A}-1)\Delta \right) , \end{aligned} \tag{2.56}$$

where $\Delta = \Delta_{31}/4E$. The transformation $\hat{A} \to -\hat{A}$ and $\delta_{CP} \to -\delta_{CP}$ give us the same for the anti-neutrinos. See Appendix for details.

This is the so-called (α, s_{13}) approximation, valid when $\alpha, s_{13} \ll 1$. This series expansion formula cannot be used when $\alpha\Delta = \Delta_{21}L/4E$ is of order 1 since then the oscillatory behaviour is governed by the mass squared difference Δ_{21} as well. Thus we have established that for the Long-baseline experiments for which we are concerned,

[2] We choose these two probability transitions to present as these are two channels to be explored in the DUNE experiment as per planned till now. We will describe the $\nu_\mu \to \nu_\tau$ probability in a subsequent chapter.

in particular for DUNE, these formulae are more than justified to be true and the approximation holds good. For detailed studies on MSW effects see Ref. [62] [3].

Geared up with this, we are in a position to review briefly the current constraints and experimental measurements of the neutrino oscillation parameters. This will be the topic of the next subsection. This shall also enable us to understand how long-baseline experiments and DUNE, in particular, maybe useful to perform future measurements so as to fill-up the gap in our current understanding of the neutrino oscillation phenomena.

2.3 Present Status of Oscillation Measurements

Let us make the following classification of the neutrino oscillation based on the neutrino experiment-type they are inferred from [4]:

- the solar neutrino parameters, namely, θ_{12}, Δ_{21}.
- the atmospheric neutrino parameters namely, θ_{23}, Δ_{31}.
- the reactor neutrino parameter namely, θ_{13}.

We have not included the Leptonic CP phase in this classification for the time being. Solar neutrino experiments and KamLAND reactor data constrains θ_{12} and Δ_{21} [65]. Accelerator long-baseline experiments like MINOS and T2K constrain $|\Delta_{31}|$ and δ_{CP}. The parameters $|\Delta_{31}|$ and θ_{23} are also constrained from Super-Kamiokande. The reactor data (Daya-Bay, RENO and Double-Chooz) constrain θ_{13} and $\Delta_{ee}\big(= s^2_{12}\sin^2(\frac{\Delta_{32}L}{4E}) + c^2_{12}\sin^2(\frac{\Delta_{31}L}{4E})\big)$ [66, 67, 68]. However, the situation is not simple, so to speak: a non-zero value of θ_{13} affects both solar and atmospheric oscillation results, therefore θ_{13} plays a major role in the global fit to neutrino data worldwide.

[3] For the first time, the matter effects were considered in the context of neutrinos coming from the sun where the MSW effect was dominant [63, 64].

[4] This classification is not so rigid as KamLAND is a reactor experiment, it measured θ_{12} and Δ_{21} as well.

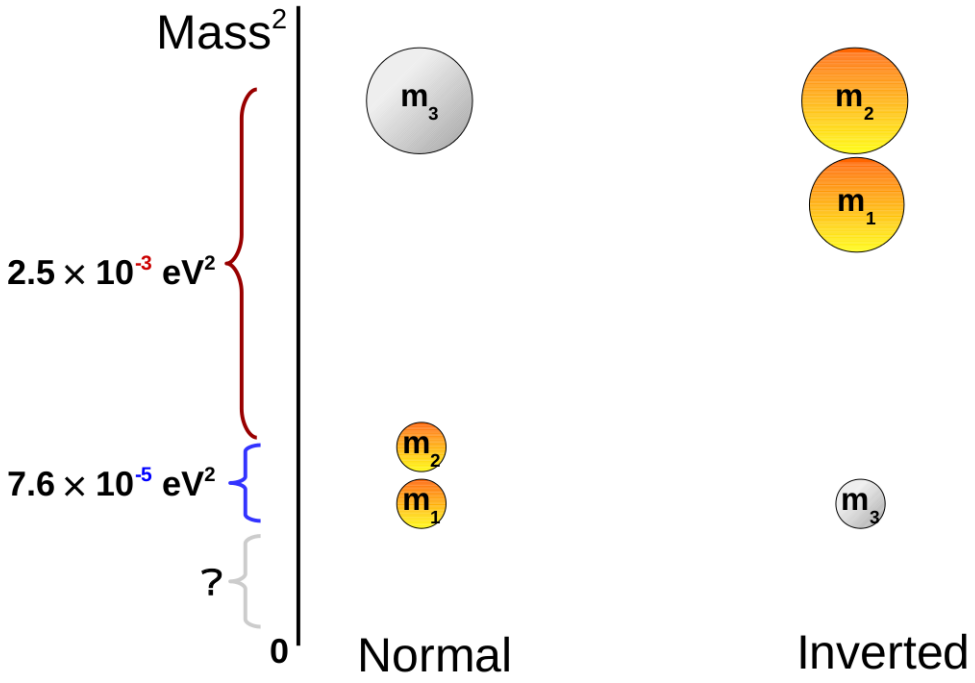

Figure 2.2: Two possible mass orderings of neutrinos. Individual masses m_1, m_2,and m_3 are unknown.

One of the three groups doing the global analysis of the world neutrino data is the Nu-Fit group [69]: we quote their latest values in Table 4.1.

Let us try to put the unknowns discussed above in terms of transition probabilities and measurements context.

Matter effect is crucial when trying to measure neutrino mass hierarchy. For solar neutrinos, the MSW effect in the core of the Sun leads to measurement of θ_{12} be in the first octant which consequently implies $m_2 > m_1$ [70]. However, for the case to understand the Δ_{31} sign, one needs to understand the Earth matter effects [71]. In context to the the long-baseline neutrino experiments the determination of neutrino mass hierarchy is advocated through the electron neutrino appearance channel. More so, in particular, this is the case for DUNE.

The octant of θ_{23} is sensitive mainly to appearance channels (see Eqs. 2.55 and

2.56) in long-baseline neutrino experiments. The reason is as follows: from the probability expressions in matter, we can see that the leading order term of the appearance channel depends on $\sin^2\theta_{23}$; the appearance channel probability increases as the value of θ_{23} increases (for $\theta_{23} < \frac{\pi}{2}$). But in the disappearance channel probability, the leading order term is $\sin^2 2\theta_{23}$ and this gives equal probability for θ_{23} and $\pi/2 - \theta_{23}$.

Even though the sensitivity of disappearance channel to octant sensitivity for the long-baseline experiments is sub-dominant but this channel is useful for the precision measurement of θ_{23} nonetheless. So one can determine the octant of θ_{23} using the combination of appearance and disappearance channels in the long-baseline experiments if θ_{23} is not very close to maximal. Currently the statistics available is insufficient to predict the true octant of θ_{23} to any extent.

It is important to observe that in the appearance channel probability expressions, the octant sensitive term $\sin^2\theta_{23}$ appears with θ_{13}. Thus the precise measurement of θ_{13} also improves the octant sensitivity [72]. Earlier when θ_{13} was not measured very precisely, it was difficult to measure the value of θ_{23} accurately in the long-baseline experiments, that goes without explicitly saying so to speak.

Moreover, the first δ_{CP} measurement came from the appearance channel of a long-baseline experiments (e.g., T2K gives it to about -90^o) but this parameter is difficult to probe as in the $\alpha - s_{13}$ approximation we saw that the dependence in δ_{CP} is sub-leading. On the other hand, in case of the atmospheric neutrino experiments the CP sensitivity suffers a lot due to their dependence on the direction of the incoming neutrinos [73, 74] [5]. For the case of reactor experiments, there is no sensitivity to δ_{CP} as it consists of electron appearance channel which does not depend on δ_{CP}.

The other crucial aspect in unknown measurements is the fact that the measurements are largely affected by the presence of many degeneracies in the neutrino oscillation probabilities. Let us review some of those in the next section.

[5] The disappearance probability of $P_{\mu\mu}$ and appearance $P_{e\mu}$ contain δ_{CP} term always multiplied by $\cos\Delta$ or $\sin\Delta$ factors. Now for a 10% error range in the zenith angle θ_z for the direction of the incoming neutrinos and the energy of the incoming neutrino, the oscillating term value varies over its entire cycle. Thus we get hardly any sensitivity for the δ_{CP} measurement.

2.4 Parameter Degeneracies in the Oscillation Probabilities

Suppose one gets the same neutrino oscillation probabilities for different sets of parameter values, then it is said that there is degeneracy between those oscillation parameters. As a consequence of this, this degeneracy translates into same number of events and it is impossible to distinguish the true parameter value from the fake ones. Thus even if different sets of parameters can give equally good fit to the experimental data it becomes very tough to determine the actual values of the parameters in an unambiguous manner.

During the era of unknown values of θ_{13}, three types of ambiguities in measurements of oscillations were in vogue in the literature:

1. the intrinsic (θ_{13}, δ_{CP}) ambiguity [75]. $P_{\mu e}$ appearance probability takes the same values for different pairs of parameters:

$$P_{\mu e}(\theta_{13}, \delta_{CP}) = P_{\mu e}(\theta'_{13}, \delta'_{CP}). \tag{2.57}$$

2. Δm^2_{31}-δ_{CP} ambiguity [76]. $P_{\mu e}$ channel gives wrong mass hierarchy solutions arising due to a different value of δ_{CP} other than the true value.

$$P_{\mu e}(\Delta m^2_{31}, \delta_{CP}) = P_{\mu e}(-\Delta m^2_{31}, \delta'_{CP}). \tag{2.58}$$

3. the ambiguity of octant of θ_{23} [77]. The intrinsic octant degeneracy of the $P_{\mu\mu}$ channel is due the existence of identical solutions for θ_{23} and $90^0 - \theta_{23}$ values:

$$P_{\mu\mu}(\theta_{23}) = P_{\mu\mu}(90^o - \theta_{23}). \tag{2.59}$$

These ambiguities collectively is known as eight-fold degeneracy [78]. For the $P_{\mu e}$ appearance channel, the octant degeneracy shows up because the leading order dependency on θ_{23} is on $\sin^2\theta_{13}\sin^2\theta_{23}$. For a given value of δ_{CP}, many sets of

$(\theta_{13}, \theta_{23})$ values are allowed if θ_{13} in unknown. There exists a plethora of proposals to break the degeneracies and perform better sensitivity measurements, see Refs. [79, 80, 81, 82, 83, 84, 85, 86, 87, 88, 89, 90] for a list. In particular Ref. [84] proposed to utilize the spectral information to resolve the (θ_{13}, δ_{CP}) degeneracy. However, the reactor angle θ_{13} has been measured to good precision, therefore the intrinsic degeneracy is largely said to be resolved, also improving upon the octant sensitivity. In today's context since the value of δ_{CP} is known only with a relatively high uncertainty, therefore the ambiguities in determining the oscillation parameters that continue to exist are the hierarchy-δ_{CP} degeneracy and the octant-δ_{CP} degeneracy [91].

In the next chapter we will focus particularly at the DUNE experiment and describe in details the experimental set-up and numerical simulations we considered sketching a preliminary idea upon the motivation as well how the current study in thesis may help in understanding physics opportunities related to ν_τ appearance analysis in DUNE.

Chapter 3

Overview of the DUNE experiment

3.1 Introduction

The Deep Underground Neutrino Experiment (DUNE) [53] is considered as one of the most important of the future neutrino experiments with collaboration of about 1000 scientists from 175 institutions in 32 countries people (2nd highest in any experimental collaboration till date) with an average rate of increase of 100 persons per year. The construction work started in 2017, with expected whole experimental set-up to be complete within 2017 and data taking scheduled from the mid 2020-s.

3.2 Experimental Set-up

DUNE will have two neutrino detectors alongside the most intense neutrino beam from the Long Baseline Neutrino Facility (LBNF) located at Fermilab, in Batavia, IL, USA. Like all the accelerator beams, it will be mainly composed of ν_μ (or $\bar{\nu}_\mu$); the beam has tiny ν_e (or $\bar{\nu}_e$) contamination of about 0.9% [53, 92]. The far detector is planned at 1300 km far from the beam source, at Sanford Underground Research Laboratory (SURF), in South Dakota. It will consist of four 10-kt Liquid Argon Time Projection Chambers (LAr-TPCs). Recently this kind of detector has been found to be most useful in the studies of neutrino interaction processes since its spatial resolution and its time resolution is very good; moreover, it can detect neutrinos very precisely leading to unprecedented energy-reconstruction of complex neutrino

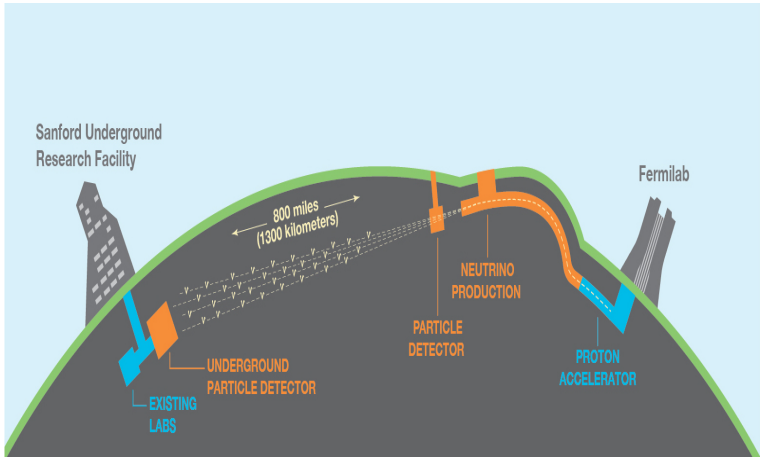

Figure 3.1: *Schematic description of the DUNE experiment.*

interactions with high efficiency over a broad energy range [93, 94]. A schematic description of the DUNE experimental-setup is given in Fig. 3.1.

3.2.1 The Near Detector

Fermilab is the host for the beam facility and the near detector which is currently under consideration as a part of the main experiment [95]. Extracting the proton beam from the Fermilab Main Injector (MI) and colliding in the target area, the pions and kaons are generated and focused by the so called "neutrino horns". They decay producing neutrinos in the final state, which are mostly ν_μ, and the neutrino beam is thus achieved. The beam is designed in order to provide a proton beam power of 1.2 MW, (upgrade-able to 2.4 MW).

The near detector system studies the energy spectrum characterization source beam compositions, and neutrino interaction cross-sections thereby reducing the flux uncertainties and systematics related to it [1]. It is noteworthy to mention that the construction details of the near detector for DUNE is yet to be finalized. The reference design being considered is similar to NOMAD tracker [53]; however there have been considerations for calorimeters [97] or gaseous argon TPC-type [98, 99] detectors as well.

[1]Recently BSM physics search capabilities including heavier neutrinos was done in Ref. [96].

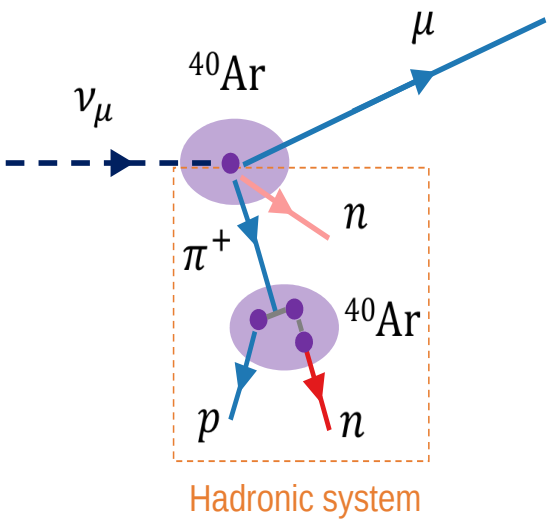

Figure 3.2: *An illustration of neutrino detection in Liquid-Argon detector.*

3.2.2 The Far Detector

SURF (Soudan Underground Research Facility) is the host for the far site and detector modules, utilities and cryogenic systems.

The detector is located deep underground and having four similar 10-kt fiducial mass modules [2] of Liquid-Argon Time Projection Chambers (LAr-TPC). This is basically a large tank filled with Liquid Argon so that the neutrinos as they pass through interact with Argon nuclei and show their typical signatures (see Ref. [94] for details and a recent study). Liquid Argon has the following advantages:

- It produces ionization charge than can be used to track particles and measure their energy,

- It gives off scintillation light, that brings to a good timing resolution.

ICARUS used in CNGS long baseline experiment [3] was the first to use this kind of detector. In case of the DUNE far detector module they are far bigger than the ICARUS one and studies related to different compositions of Argon inside the detector

[2] A total of 40-kt mass means a huge ν statistics, beating that of all experiments before.
[3] It will be used in the future for the SBN program at Fermilab [100, 101].

have been performed [53]. A schematic description of ν-interaction and consequent detection in Liquid Argon is given in Fig. 3.2.

Just to conclude this subsection with a comment on the LAr-TPC type detector, it usually has a long read-out time ($\sim$O(2 ms)) between two consecutive detected interactions. However, neutrino interactions are too infrequent (due to their weakly interacting nature) to be affected significantly by this lag in the detector. Ref. [94] studied the neutrino energy reconstruction in DUNE detector recently in details and found improved migration matrices that may be used for future estimations which may lead to possible increase in detection efficiencies by 25% or so, compared to what we have presently.

3.2.3 Physics opportunities with DUNE

Having a muon neutrino beam, $\nu_\mu \to \nu_e$ and $\nu_\mu \to \nu_\mu$ neutrino oscillation will be precisely measured in a three-neutrino paradigm or beyond. The DUNE experiment provides a "compact, scale-able" approach to achieve sensitivity to the oscillation physics goals of neutrinos and astro-particles physics. Some of the main goals are [92, 102, 103, 104]:

- Determining the CP violating phase δ_{CP} in the PMNS matrix leads to matter-antimatter asymmetry if the value of δ_{CP} different from 0 or π. As an evidence of the CP violation in the leptonic sector, this measurement is of extreme importance.

- Determining the sign of the parameter Δm^2_{31}. This will tell us whether the neutrino mass hierarchy is normal or inverted.

- Determining the octant sensitivity θ_{23} is a very important measurement due to what discussed in Sec. 2.4.

- Search for the proton decay in various modes.

- Detection and measurement of a ν_e flux coming from a supernova within our galaxy.

Beside these, study of BSM scenarios in DUNE include NSI and sterile neutrino models. DUNE will be able to measure atmospheric neutrinos, and to some extent those coming from the sun and other astrophysical objects as well. Apart from these, there are physics cases in DUNE for precision tests about interactions physics. In particular measurements of neutrino cross sections, nuclear effects, nucleons structure and Weinberg angle and signatures of dark matter are agenda of the DUNE collaboration [92].

There is however one Standard physics scenario that maybe done in DUNE: a measurement of τ-flavored neutrino with a higher statistics than any other experiments till date. This is facilitated by the $\nu_\mu \to \nu_\tau$ transitions. This is one of main topics of this thesis both in the standard and NSI scenarios but before delving into such a study, let us briefly review the DUNE far detector performances.

3.2.4 Study of the Detector

As DUNE's main plan is to measure the PMNS matrix CP-violating phase and the atmospheric mass splitting (Δm^2_{31}) sign, they designed a beam optimized for the study of this particular CP-vialation (CPV) and mass hierarchy starting from a NuMi (Neutrino Main Injector) reference beam. The NuMi beam [105] now operating for MINERvA and NOνA experiments, has been used in the past for the former MINOS experiment [32]. LBNF facility at Fermilab will provide the neutrino beam and that will be focused to Soudan Laboratories in South Dakota which is about 1300km away.

Standard Flux

In our simulation, we have considered two neutrino fluxes, the standard and the optimized, as described in Sec. 3.3.3. The values from Table 3.2 have been used, in the case of the standard flux, as post smearing matrices and detection efficiencies (see Fig. 3.3) for the ν_e appearance and ν_μ disappearance channels [53, 92]. We have implemented our simulation following these and the systematic uncertainties assumptions [106]. In Fig. 3.3, one may note that the with electron channel it possible

Particle type	Detection Threshold	Energy resolution	Angular resolution
μ	30 MeV	Contained tracks: track length Exiting tracks: 30%	1°
π	100 MeV	μ-like contained tracks: track lenght π-like contained tracks: 5% Showering or exiting tracks: 30%	1°
e/γ	30 MeV	$2\% \oplus 15\%/\sqrt{E}[GeV]$	1°
p	50 MeV	p<400 MeV/c: 10% p>400 MeV/c: $5\% \oplus 30\%/\sqrt{E}\,[GeV]$	5°
n	50 MeV	$40\%/\sqrt{E}\,[GeV]$	5°
other	50 MeV	$5\% \oplus 30\%/\sqrt{E}\,[GeV]$	5°

Table 3.1: *Energy and spatial resolution for particles in the DUNE detector. Table taken from Ref. [92].*

to reach 90% max. efficiency at low energies. Similarly for the muons, one may be able to reach even 100% efficiency but less dependent on neutrino energies involved. However, while for the muon channel there is no significant efficiency for the background processes, but for the electron channel there is high efficiency involved coming from the processes corresponding to the electron contamination of beam background. Since the LAr-TPC kind of detector is unable to distinguish the charge of the particles generated by the neutrino interactions, the sum of neutrino and anti-neutrino events is considered as our total number of events.

ν_e appearance channel		
Signal	ν_e and $\bar{\nu}_e$ CC events from ν_μ oscillations	2% sys
Backgrounds	Beam ν_e and $\bar{\nu}_e$ CC events	5% sys
	Misidentified ν_μ and $\bar{\nu}_\mu$ CC events	5% sys
	Misidentified ν_τ and $\bar{\nu}_\tau$ CC events	20% sys
	Misidentified NC events	10% sys
ν_μ disappearance channel		
Signal	ν_μ and $\bar{\nu}_\mu$ CC events	5% sys
Backgrounds	Misidentified ν_τ and $\bar{\nu}_\tau$ CC events	20% sys
	Misidentified NC events	10% sys

Table 3.2: *Backgrounds and signal systematic uncertainties proposed by the collaboration for the standard flux simulations. Table taken from Ref. [106].*

This beam will be generated using collisions of 80 GeV protons on a 1.5 metres

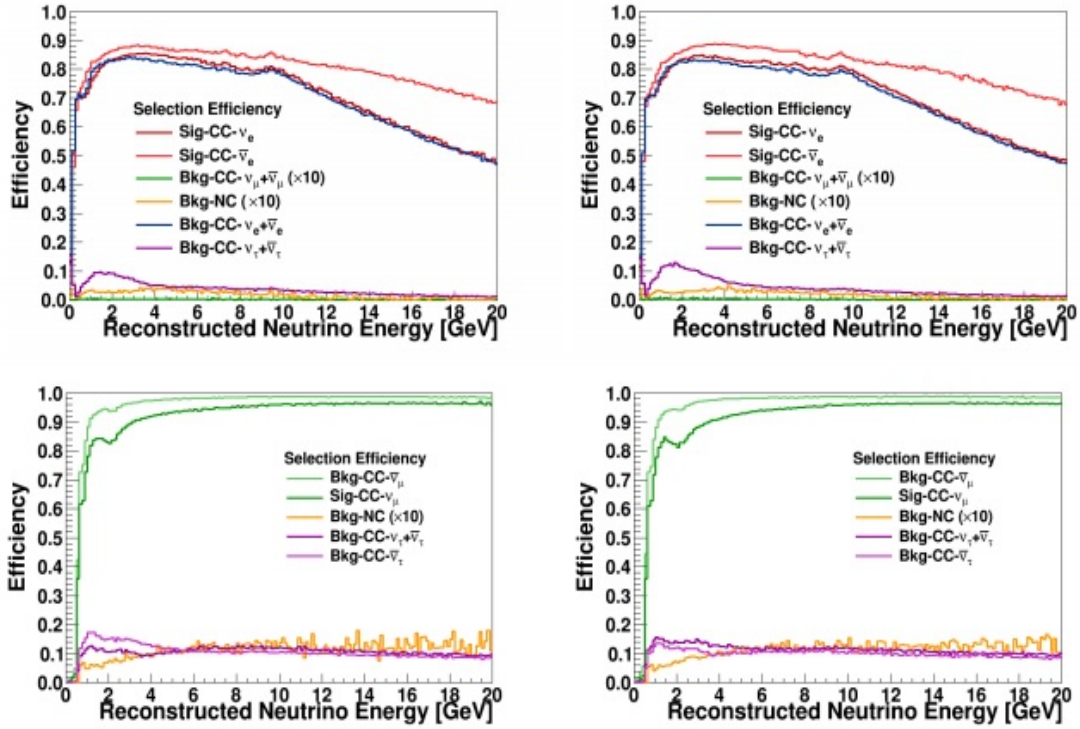

Figure 3.3: *Selection efficiencies (left neutrino and right antineutrino mode) for ν_μ and $\bar{\nu}_\mu$ (bottom), ν_e and $\bar{\nu}_e$ (top) as a function of the reconstructed neutrino energy. [92].*

long target. The beam power will be 1.07 MW, that corresponds to 1.47×10^{21} protons on target (POT).

This flux is optimized for studying CP-violating sensitivity and is commonly studied in the literature for simulations regarding DUNE analyses. This flux actually provides a relatively large sample of ν_e coming from $\nu_\mu \to \nu_e$ oscillations. Henceforth, in this thesis, we will refer to this as *the standard flux* [106]. Using this flux in the experiment we will also be able to collect a huge ν_τ sample, even if most of the neutrinos will not reach the threshold energy of 3.4 GeV for the τ production. Since we intend to study the ν_τ appearance channel in DUNE, there is also a possibility to optimize the neutrino flux so as to produce neutrinos with energies higher than the τ-threshold. This possibility is being actively studied by the DUNE collaboration in many different forms [107, 108]. We have studied the physics sensitivities using such a particular flux; we call it "tau-optimized" or simply "optimized" flux. However, we defer a detailed description of the flux to a later section.

3.3 DUNE with ν_τ Appearance

As this is a preliminary study of the ν_τ appearance and detection, we considered the DUNE detector to be similar to the ICARUS one, which has been the only LAr-TPC detector built to look at ν_τ-s. The detector being too small it itself did not find any events; moreover, the CNGS baseline was not suitable to reach the atmospheric oscillation peak, namely the maximum of the term in $\sin^2\left(\frac{\Delta m^2_{31} L}{4E}\right)$. Thus studies about detection efficiencies and backgrounds for this detector have only been done using simulations [92].

3.3.1 A Typical ν_τ Sample

ν_e and ν_μ samples in DUNE have been studied in details and can be found in Ref. [92]. In this section, we discuss in details the same about the ν_τ-sample. The ν_τ appearance sample is composed of ν_τ and $\bar{\nu}_\tau$ CC interactions resulting from $\nu_\mu \to \nu_\tau$ and $\bar{\nu}_\mu \to \bar{\nu}_\tau$

oscillations. Backgrounds to this channel can be ν_e CC, ν_μ CC and NC interactions. Focusing on the leptonic decay of the tau generated by ν_τ CC interactions, it is possible to look only at the electron channel (18% branching fraction). From the ICARUS proposal [109], it is clear that, in a LAr-TPC, choosing the right kinematic cuts, the electron channel backgrounds can be reduced to only ν_e CC events coming from two main components which are the intrinsic ν_e beam and $\nu_\mu \rightarrow \nu_e$ oscillations. Regardless of the kinematical cuts, some of the backgrounds expected for ICARUS should be negligible for DUNE. For example, events that lead to a mis-identification of a charm meson with a τ lepton are going to be only a few at LBNF beam energy.

3.3.2 Different set-ups of our study

For the ν_τ, the signal efficiency has been studied with two possible values:

- For the electronic decay of τ, the branching fraction is about 18% [51]. This is the maximum reachable efficiency for this particular detection channel. However this also comes along with the assumption that DUNE is able to re-construct 100% of the final electrons coming from the τ. This we consider as an optimistic case.

- A value of 6% has been used for the ν_τ and $\bar{\nu}_\tau$ appearance channels. This value is motivated from that considered by Ref. [110]. This we consider as a pessimistic value.

For ν_τ signal systematics uncertainties, we consider two possible cases in our simulation throughout the thesis:

- A value of 20%, same as what the DUNE collaboration used for ν_τ CC background to ν_e appearance and ν_μ disappearance channels in their study of the detector.

- A value of 10%, which is an optimistic value. But it will help us to understand to what extent improving the systematics in this channel may help the physics sensitivities.

Lastly, we remark the number of ν_e CC background events has been set to a constant value so as to reproduce, at the best fit parameters values, the Signal-to-Background (S/B) values [4]:

- of 2.45 as discussed achievable in Ref. [110].
- of 18.6, as discussed in Ref. [109]. As we mentioned, it is clear that choosing the right kinematical cuts, the electron channel background can be reduced to only ν_e CC events coming from two main components, which are the intrinsic ν_e beam and $\nu_\mu \to \nu_e$ oscillation [5].

This phenomenological parameter, S/B, we call it as the "experimental reach" and the study the effect of increasing or decreasing the "experimental reach"-s on our physics sensitivities and leave the final value to the experimental collaboration to decide what can be possible to achieve.

We emphasize the fact that not only the impact of individual above-mentioned factors is important but also an understanding of how these factors compete with each other in terms of the final resultant sensitivity is worthwhile to investigate since DUNE collaboration is still on the verge of finalizing the actual experimental set-up.

3.3.3 Comparison between the Standard and Optimized Flux

DUNE will be the experiment with the biggest ν_τ sample so far. Indeed, the only accelerator experiment which was able to see $\nu_\mu \to \nu_\tau$ transitions was OPERA, and collected 10 ν_τ events (8 signal events and 2 background events) with a 6.1 σ significance [114, 115, 116].

However, the neutrino flux suited for studying CP violation and mass hierarchy searches, known as the standard flux, has a mean neutrino energy that is below the threshold for the $\nu_\tau N \to \tau X$ interaction, which is 3.4 GeV. Moreover, neutrinos

[4] We noticed a small number of ν_τ events is being overshadowed by the background in our correlation and sensitivity studies; the number of background events change considerably due to different true values of the oscillation parameters leading to the sensitivity in which it is more difficult to disentangle the contribution of the $\nu_\mu \to \nu_\tau$ transition.

[5] There is negligible intrinsic ν_τ component in the beam.

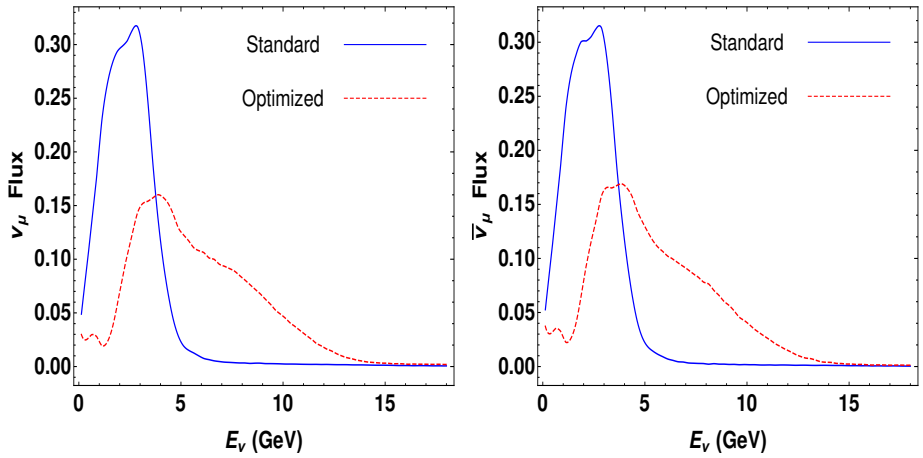

Figure 3.4: *Fluxes comparison in Arbitrary Units. Standard (blue, solid) and optimized (red, dashed) cases. The two figures show the fluxes in neutrino (left panel) and anti-neutrino modes (right panel).*

with an energy bigger than the threshold are far from the peak of the $\nu_\mu \to \nu_\tau$ oscillation probability at DUNE baseline. For these reasons the number of ν_τ-s that can be detected by DUNE using the standard flux (roughly 75 per year) is very small compared to the number of ν_e-s and ν_μ-s.

Moving the position of the horns and the focus of the proton beam, and increasing the proton energy up to 120 GeV (1.2 MW, 1.1×10^{21} POT) it is possible to obtain a flux optimized for the ν_τ appearance. This flux can increase the number of ν_τ CC events by a factor of 10. In Ref. [108] different optimized fluxes are described. In this thesis, the flux obtained with a 1.0 m long target (NuMi style) has been considered, using flux files from [107]. The ν_τ CC events with this flux are expected to be 809 per year. This reference value from [108] has been used to find the normalization for the optimized flux.

Fig. 3.4 shows a comparison between the standard (CP violation optimized) and the ν_τ optimized fluxes for neutrino and anti-neutrino modes. It is clear that the number of neutrinos with an energy bigger than the τ production threshold is increased in the optimized case. Furthermore, also the total number of unoscillated ν_μ and ν_e CC events, that are summarized in Tab. 3.3, is bigger in the case of the ν_τ optimized flux than in the case of the standard flux. This is mainly due to the more

	Standard Flux		**Optimized Flux**	
	ν mode	$\bar{\nu}$ mode	ν mode	$\bar{\nu}$ mode
ν_μ CC	30175	3225	85523	4933
$\bar{\nu}_\mu$ CC	1025	9879	1256	26221
ν_e CC	371	136	856	258
$\bar{\nu}_e$ CC	44	109	84	215

Table 3.3: *Estimate of non-oscillated events for the two considered fluxes.*

energetic protons involved than in the standard flux and results in producing higher energy neutrinos and thus involve larger neutrino-nucleus interactions cross sections.

Having set up some basic preliminaries regarding the DUNE experiment and computation of non-oscillated events (parameter independent) for normalization purposes, we next go to standard physics sensitivity studies in the next chapter.

Chapter 4

ν_τ appearance in DUNE: Standard Physics

In this chapter we discuss the inclusion of the $\nu_\mu \rightarrow \nu_\tau$ oscillation channel sticking to standard physics scenarios. DUNE collaboration never studied this channel in their analysis [92]. During the preparation of this doctoral thesis, a similar study involving τ-detection in the hadronic channel was published [111] [1]. However we consider the τ detection in the electronic decay mode following the ICARUS collaboration. This chapter and the next chapter are based on our work in Ref. [113].

4.1 Introduction

The OPERA experiment [114, 115, 116] recently observed 10 ν_τ interactions [2]. Ref. [117] studied the impact of such measurements in standard and non-standard scenarios.

DUNE will be the first experiment to look at ν_τ detection in LAr-TPC-s; Monte Carlo simulation regarding the ν_τ appearance is available in DUNE but only as a background process. The process for ν_τ detection always involves an associated secondary particle (a muon, an electron or hadron), consequently it is difficult to study. We will need to use some assumptions regarding the electronic decay channel, following the method as proposed in ICARUS.

[1] An introductory study about the ν_τ appearance in DUNE can be found in [112].
[2] 8 signal events & 2 background events.

Extensively discussed channels in DUNE are the ν_e appearance and ν_μ disappearance channels which are used to estimate the sensitivity reach of the experiment for the oscillation parameters of the standard 3-ν framework as well as in the investigation of the parameter space of the NSI and of the sterile $3+1$ neutrino models. As already mentioned, we consider the $\tau \to e$ leptonic decay as our ν_τ detection channel, unlike [111], which focused on the τ hadronic decays. Our numerical simulations have been performed utilizing the GLoBES software [118, 119]. We performed full numerical computation and took into account various detection efficiencies, signal to background ratios (S/B) and systematic uncertainties as quoted in Section 3.3.2. We explored the performances of the DUNE far detector considering standard flux and also the ν_τ-*optimized flux*. In both cases we have considered 3.5 years of data taking in the neutrino mode and 3.5 years in the anti-neutrino modes for a total of 7 years.

In order to configure for the tau neutrino appearance signal, the DUNE GLoBES file from [106] was edited to include the $\nu_\mu \to \nu_\tau$ and $\bar{\nu}_\mu \to \bar{\nu}_\tau$ appearance channels and the relevant efficiencies, systematics and backgrounds of the transition channels included in our numerical simulations as described in details in Sec. 3.3.2.

Let us next quickly recap some of oscillation probability features, with respect to the phenomenology and configurations involved in the DUNE experiment, in particular.

4.2 Relevant recap of Oscillation Probability

Just to re-consider some useful points we are carrying forward from our discussion on the oscillation probabilities, and the matter effect in oscillation, the biggest impact in the probabilities can be found (see Sect. 2.2.3), when the so called atmospheric MSW resonance condition is satisfied:

$$\frac{2Ev_{cc}}{\Delta m^2_{31}} = \cos 2\theta_{13}, \tag{4.1}$$

where

$$v_{cc} \sim 7.56 \times 10^{-14} \left(\frac{\rho}{g/cm^3} \right) Y_e \ \ eV. \tag{4.2}$$

Taking some typical values of the matter density ρ (3 g/cc), the number of electron per nucleus Y_e (0.5) and the best fit values for the oscillation parameters (shown in Table 4.1) the resonance condition will be satisfied for neutrino energies >> 9 GeV. This energy is far from the peak of the neutrino fluxes in DUNE; so matter effects do not play much of a role here. It goes without saying that while performing the simulation, full matter effects and 3-flavor neutrinos have been taken into account numerically. So, let us quickly see some of the *3-flavor* vacuum oscillation probabilities that were computed in Sect. 2.2.2 pertaining to the DUNE experimental scenario.

Neglecting terms containing the solar mass difference $\Delta m^2_{21} = m^2_2 - m^2_1$ and the small $\sin\theta_{13}$, in vacuum $\nu_\mu \to \nu_\tau$ oscillation probability reads (from Sec. 2.2.2):

$$P_{\mu\tau} \approx \cos^4\theta_{13} \sin^2 2\theta_{23} \sin^2\left(\frac{\Delta m^2_{31} L}{4E} \right) . \tag{4.3}$$

Eqn.4.3 shows that the ν_τ appearance channel is particularly sensitive to θ_{23} and to the atmospheric mass-squared splitting $\Delta m^2_{31} = m^2_3 - m^2_1$. However, also the other two channels are expected to be sensitive to the same two parameters since, neglecting solar terms, we have:

$$P_{\mu e} \approx 4 \sin^2\theta_{13} \cos^2\theta_{13} \sin^2\theta_{23} \sin^2\left(\frac{\Delta m^2_{31} L}{4E} \right) , \tag{4.4}$$

and, from unitarity condition,

$$P_{\mu\mu} \approx 1 - (\sin^2 2\theta_{23} \cos^4\theta_{13} + \sin^2 2\theta_{13} \sin^2 2\theta_{23}) \sin^2\left(\frac{\Delta m^2_{31} L}{4E} \right) . \tag{4.5}$$

In DUNE the mean neutrino energy in the standard flux has been chosen (about 2.5 GeV) in order to maximize the atmospheric term; since the minimum ν_τ energy needed to be converted in a τ lepton is around 3.4 GeV, the number of ν_e and ν_μ events will be much bigger than the number of ν_τ CC. For this reason, we expect that

constraints on θ_{23} and Δm^2_{31} will be mainly set by $\nu_\mu \to \nu_e$ and $\nu_\mu \to \nu_\mu$ channels. Notice also that next terms in the Δm^2_{21} and θ_{13} of Eqn.4.3 would exhibit a $\sin \delta_{CP}$ dependence, so we expect this channel to be also partially sensitive to CP violation searches. However, due to the very large leading term, the changes in probability $\mathrm{P}_{\mu\tau}$ due to the CP violation phase will be comparatively very small and definitely less important than the corresponding CP violating terms in $P_{\mu e}$.

In summary, considering the $\nu_\mu \to \nu_\tau$ oscillation probability and the lack of statistics, the ν_τ appearance channel is expected to have a negligible impact on standard physics studies. It will be evident from our numerical results. However even before commencing to compute and understand physics parameter sensitivities we will try to garner an understanding of the ν_τ statistics and relevant background statistics in all of the DUNE appearance and disappearance channels.

In the next section we will take a look at the computational tool we used and the relevant neutrino detection event-rate calculation performed. Besides, we will define some statistical analysis procedures used to analyse the DUNE experimental simulation study according to our computation.

4.3 GLoBES Software

GLoBES is a sophisticated software package for the simulation of long baseline neutrino oscillation experiments. It helps to incorporate correlations and degeneracy studies in the oscillation parameter space and often includes advanced routines for specific treatment of arbitrary systematical errors. The user interface for simulating a long-baseline experiment is called AEDL, the Abstract Experiment Definition Language which provides an easy way to define experimental setups. The user may define priors that allow the inclusion of arbitrary external physical information. Lastly, there are lot of documentation and experimental set-ups available so that we have an active community and a discussion between phenomenology and experiments [118, 119].

4.3.1 Events rates

In this chapter we discuss the χ^2 analysis method. In a typical neutrino detector for DUNE (say) one gets electron and muon events governed by the neutrino oscillation probability $P_{\mu e}$ and survival probability $P_{\mu\mu}$. The number of oscillated electron events at the detector contains the contribution of the appearance channel $P_{\mu e}(\vec{x})$, $\vec{x}$ being a vector of oscillation parameters. Let the ν_μ flux at the detector be Φ_μ; then the number of electron neutrinos at the detector can be written as

$$N_e = \Phi_\mu P_{\mu e}(\vec{x}) \sigma_e \epsilon, \tag{4.6}$$

where σ_e is the cross section of the electron neutrinos and ϵ is known as the detector efficiency. In the detector, neutrinos undergo charge current interactions to produce electrons.

$$\nu_e + n \rightarrow p + e^-.$$

The signal produced by that electron is considered as the signature of the detected neutrino and this is called an 'event'. Now the energy of this electron needs to be reconstructed: the true energy of the neutrinos E_t is reconstructed from the measured energy E_m. The expression for total number of events can be obtained by

$$N_e(E_m) = \int_{E-\Delta E/2}^{E+\Delta E/2} \Phi_\mu(E_t)\ P_{\mu e}(\vec{x}, E_t)\ R(E_t, E_m)\ \sigma_e(E_t)\ \epsilon\ dE_t, \tag{4.7}$$

N_e is the number of detected neutrinos with energy between the energy range $E - \Delta E/2$ and $E + \Delta E/2$, $R(E_t, E_m)$ is the Gaussian resolution (smearing) function, which gives the spread of E_m for a given E_t and can be written as

$$R(E_t, E_m) = C_1 \exp\left[- \frac{(E_t - E_m)^2}{2\sigma_E^2} \right], \tag{4.8}$$

with normalisation coefficient C_1 and

$$\sigma_E = \alpha E + \beta\sqrt{E} + \gamma. \tag{4.9}$$

The values of α, β and γ are different for different detectors depending upon its properties.

Using the events rates generated by these, one needs to understand the sensitivity of oscillation parameters. For performing statistical analysis, typically χ^2 analysis is used, for which each energy bin can be obtained by either the Gaussian or Poisson formula (usually if the number of events is less than 5, then the latter is used). Gaussian formula is given by

$$\chi^2_{\rm stat} = \sum_i \frac{((N_e)_i^{\rm th} - (N_e)_i^{\rm exp})^2}{(N_e)_i^{\rm exp}}. \tag{4.10}$$

Similarly, Poission formula is given by:

$$\chi^2_{\rm stat} = \sum_i 2\left[(N_e)_i^{\rm th} - (N_e)_i^{\rm exp} - (N_e)_i^{\rm exp}\log\left(\frac{(N_e)_i^{\rm th}}{(N_e)_i^{\rm exp}}\right)\right]. \tag{4.11}$$

Next one needs to incorporate the systematic errors for realistic simulation of experiments. These systematics are basically the uncertainties related to the measurement of the actual neutrino flux and neutrino interaction cross-sections [3]. In our study we used the widely accepted pull method [120, 121, 122]. To give an example, in order to include a 5% overall normalization error in our analysis, the modification we need is in terms of events in the i-th bin $N_i^{\rm th}$. This can be written as:

$$N_i^{\rm th} \to N_i^{\rm th}(1 + 0.05\xi), \tag{4.12}$$

where ξ is known as the pull variable. Total χ^2 is then given by:

$$\chi^2 = \chi^2_{\rm stat} + \chi^2_{\rm sys} \tag{4.13}$$

[3] In case of atmospheric neutrinos, direction of the neutrino too.

where the $\chi^2_{\rm sys}$ term is arising due to deviating $N_i^{\rm th}$ from its mean value. Similarly it can be extended for more than one sources of systemtics which then will be summed over. Therefore, the χ^2 is given by in total by:

$$\chi^2 = \min_{\xi} \left\{ \sum_c \chi^2_c + \left(\frac{\xi_N}{\sigma_N} \right)^2 \right\},$$

where the subscript c depicts χ^2 for each neutrino oscillation channel separately and the overall signal normalization is represented respectively by the last term known as the pull term. The different values used for σ_N have been quoted in Section 3.3.2. If one wishes to determine the combined sensitivity of various experiments, χ^2 for each experiment is calculated corresponding to a given test parameter value. Then the resultant χ^2's are simply added and minimised over the test parameter set after adding the priors.

After having setup the necessary computational definitions and strategies we move on to the computation regarding estimating the rate of neutrinos to be observed in DUNE.

4.4 Standard DUNE Scenario

The usual analysis of DUNE considers neutrino oscillation in the $\nu_\mu \to \nu_e$ appearance and $\nu_\mu \to \nu_\mu$ disappearance channels. On top of this we investigated the $\nu_\mu \to \nu_\tau$ appearance channel in our study. The experiment running time considered in our work is 3.5 years in the neutrino mode + 3.5 years in the anti-neutrino mode for both fluxes, which correspond to the standard exposition time proposed by the collaboration. Throughout the analysis done in this thesis, unless otherwise explicitly stated, we have used mixing parameters with their error bars from Ref. [69]; for the convenience of the reader we also summarize them in Table 4.1.

Parameter	Central Value	Relative Uncertainty
θ_{12}	33.82°	2.3%
θ_{23} (NH)	49.6°	2.0%
θ_{23} (IH)	49.8°	2.0%
θ_{13} (NH)	8.61°	1.4%
θ_{13} (IH)	8.65°	1.5%
δ_{CP} (NH)	215°	13%
δ_{CP} (IH)	284°	10%
Δm^2_{21}	7.39×10^{-5} eV^2	2.8%
Δm^2_{31} (NH)	2.525×10^{-3} eV^2	1.3%
Δm^2_{32} (IH)	-2.512×10^{-3} eV^2	1.3%

Table 4.1: *Central value and relative uncertainty of neutrino oscillation parameters from a global fit to neutrino oscillation data [69]. As in [53], for non-Gaussian parameters the relative uncertainty is computed using 1/6 of the 3σ allowed range. We have used these values as central values for our simulation unless otherwise stated explicitly in the text.*

4.4.1 Rates

The event rates for signal and background in both neutrino and antineutrino modes in the standard 3-neutrino paradigm for DUNE in the ν_μ appearance channel and ν_e disappearance channel are reported in Table 4.2, where efficiencies have been taken into account based on the post-smearing matrices provided in the DUNE simulation [106]. It is evident the ν_μ disappearance channel dominates over the ν_e appearance channel events.

Our next objective is to estimate the 3 main goals for the DUNE experiment we talked about. They are namely, the mass hierarchy sensitivity, CP Violation sensitivity and the measurement and sensitivity of the θ_{23} octant.

4.5 Discovery Potentials

During the estimation of discovery potentials, the topic of this section, the neutrino oscillation parameters are all allowed to vary, constrained by a Gaussian prior with 1σ width as given by the relative uncertainties shown in Table 4.1. We have used the standard flux for our numerical computation in this purpose.

	signal	**backgrounds**			
		intrinsic ν_e	mis ν_μ	mis ν_τ	NC
neutrino mode	$\nu_\mu \rightarrow \nu_e \oplus \bar{\nu}_\mu \rightarrow \bar{\nu}_e$	288.2	3.1	19.9	26
	1188 $\oplus$ 11.5				
	$\nu_\mu \rightarrow \nu_\mu \oplus \bar{\nu}_\mu \rightarrow \bar{\nu}_\mu$			28.2	75.3
	7601 $\oplus$ 519.2				
antineutrino mode	$\bar{\nu}_\mu \rightarrow \bar{\nu}_e \oplus \nu_\mu \rightarrow \nu_e$	171.8	2.9	13.4	15.2
	209 $\oplus$ 64				
	$\bar{\nu}_\mu \rightarrow \bar{\nu}_\mu \oplus \nu_\mu \rightarrow \nu_\mu$			16.5	44.1
	2591 $\oplus$ 1489				

Table 4.2: *Total number of signal and background events for neutrino and anti-neutrino modes, computed for ν_μ disappearance and ν_e appearance channels, using the oscillation parameters as in Table 4.1.*

4.5.1 Mass Hierarchy Sensitivity

The experimental sensitivity for the mass hierarchy of neutrinos is quantified using a test statistic, $\Delta\chi^2 = \chi^2 - \chi^2_{\text{min}}$, which is defined as [92]:

$$\Delta\chi^2_{MH} = \Delta\chi^2_{IH} - \Delta\chi^2_{NH}$$

for true Normal Hierarchy. And

$$\Delta\chi^2_{MH} = \Delta\chi^2_{NH} - \Delta\chi^2_{IH}$$

for true Inverted Hierarchy.

In the simulations, the χ^2 function has been marginalized over all the oscillation parameters; all possible true values of the δ_{CP} phase have been scanned upon while the δ_{CP} fit values have been kept free.

Fig. 4.1 shows mass hierarchy sensitivity for various true values of the phase δ_{CP} in the standard DUNE scenario. 5 σ sensitivity is achieved for all values of δ_{CP} which means the resolution of the MH degeneracy will be possible.

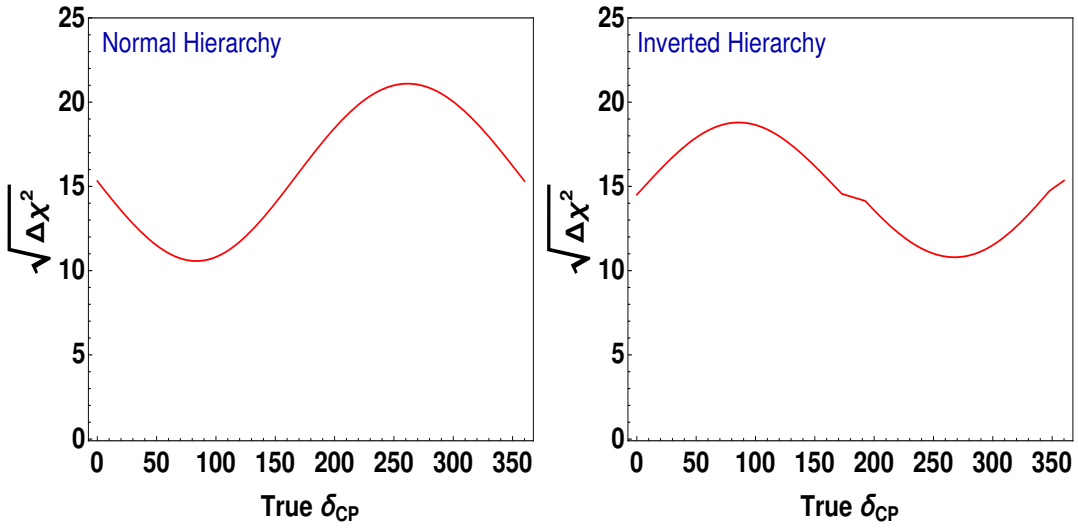

Figure 4.1: *Mass hierarchy sensitivity in DUNE considering the ν_μ disappearance and ν_e appearance channels with standard flux for Normal ordering (left) and Inverted ordering (right) of neutrino masses.*

4.5.2 CP violation sensitivity

The CP violation (CPV) sensitivity means whether a δ_{CP} value may be distinguished from 0° (or 180°) since these values represent no CPV as the PMNS matrix becomes real. Typically, the sensitivity with which CP violation can be discovered is defined as:

$$\Delta\chi^2_{CPV} = Min[\Delta\chi^2_{CP}(\delta^{test} = \frac{\pi}{2}), \Delta\chi^2_{CP}(\delta^{test} = 0)],$$

where

$$\Delta\chi^2_{CP} = \Delta\chi^2_{\delta^{test}_{CP}} - \Delta\chi^2_{\delta^{true}_{CP}}.$$

In order to find out the most probable data for given a set of input parameters, i.e., in which no statistical fluctuations have been applied, true and test values of the parameters are considered. In Eqn. 4.10, true values are the ones used to obtain N_{th} and test values are the ones to scan over to find the expected no. of events to minimize the χ^2 function. E.g., the predicted spectra and the true spectra becomes identical for the most probable data set; in CP violation, $\chi^2_{\delta^{\rm true}_{CP}}$ is identically zero and the χ^2_{CP} value for a typical experiment is given by $\chi^2_{\delta^{\rm test}_{CP}}$.

Since the true value of δ_{CP} is unknown, a scan is performed over all possible values

of δ_{CP}. Both the neutrino mass hierarchy and the θ_{23} values are also assumed to be unknown and are varied in the fits, with the lowest value of $\Delta\chi^2$ thus obtained is used to estimate the sensitivities. The χ^2 has been marginalized over all the other oscillation parameters considering their central values and their uncertainties from Table 4.1 (NH has been assumed).

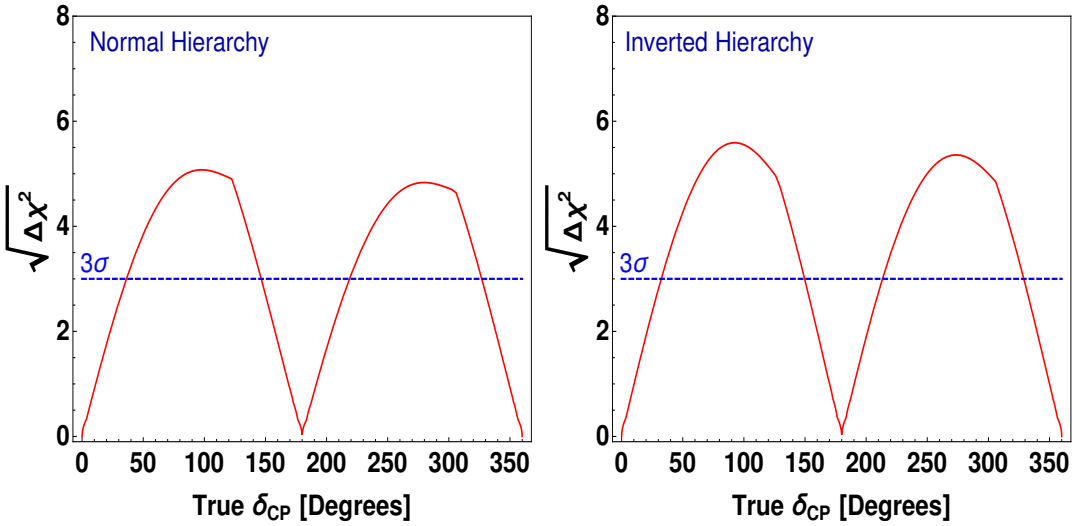

Figure 4.2: *CP violation sensitivity in DUNE with ν_μ disappearance and ν_e appearance channels using the standard flux. Normal Hierarchy (NH) is assumed in the left panel, and Inverted Hierarchy (IH) is assumed in the right panel.*

Figs. 4.2 depicts the δ_{CP} sensitivity obtained in the standard DUNE scenario. We observe that it is possible to reach a 3 σ sensitivity for most of the δ_{CP} parameter values. In particular for the Normal Hierarchy case the range δ_{CP} is between [35° to 155°] and [215°, 330°] where this occurs. For maximal CP violation value, that is, for $\delta_{CP} = 90°$, the sensitivity reaches 5 σ leading to the much awaited discovery of CP-violation in the leptonic sector. For $\delta_{CP} = 270°$ which also represents maximal CP violation, 5 σ is not achieved but is very close ($\sim 4.85\ \sigma$). In the case of Inverted Hierarchy (IH) both maximal CP violation values will correspond more than 5 σ discovery limits.

Also we remind the reader that the standard flux is optimized for CP violation searches, as discussed in Sectn. 3.2.4, so DUNE performs very well in this regard as expected.

4.5.3 Sensitivity Study of the θ_{23} Octant

The uncertainty in the determination of whether the octant of θ_{23} is in the higher or in the lower octant ($> 45^o$ or $< 45^o$) comes from the fact that its measurements till date are mainly due to the ν_μ disappearance channel which depends on $\sin^2 2\theta_{23}$. DUNE having simultaneous access to both ν_μ disappearance and ν_e appearance channels is useful to probe the octant hypothesis. Sensitivity is estimated following [93, 123]:

$$\Delta\chi^2 = \chi^2(\pi/2 - \theta_{23}^{true}) - \chi^2(\theta_{23}^{true})\,, \tag{4.14}$$

without imposing any priors on the atmospheric angle. So, the θ_{23} octant sensitivity plot can be obtained fixing the true value of this mixing angle in one octant and using as a fit value one in the other octant.

In our simulation, the χ^2 function has been marginalized over all parameters. The χ^2 minimum has been computed for different δ_{CP} true values, in order to obtain a band of possible values of χ^2 without considering any external priors on δ_{CP}. The fit value of the CP violating phase has been kept free.

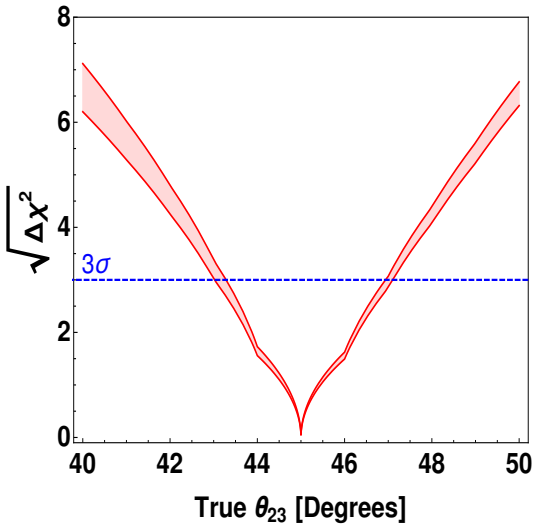

Figure 4.3: *Octant sensitivity using ν_μ disappearance and ν_e appearance channels with the standard flux. The band shows all possible $\sqrt{\Delta\chi^2}$ values obtained changing the δ_{CP} true value.*

Figs. 4.3 show that with the standard flux it is possible to recognize at 3 σ the

octant of θ_{23} if $\theta_{23} < 43^\circ$ or $\theta_{23} > 47^\circ$. This however also means that if the actual value of θ_{23} is close to the best fit of (49.6°) as in Table 4.1, DUNE physics sensitivity is such that this degeneracy will be resolved. This itself is a very important result in the neutrino physics sector.

Now some important comments are called for. Firstly, though we presented our results for all the three discovery potentials for the standard DUNE scenarios using the ν_e appearance and ν_μ disappearance channels in DUNE, we computed the same using the addition of ν_τ appearance in DUNE and found the ν_τ appearance cannot improve the sensitivities to any major extent. Secondly, it is worthwhile to point out the results in this section have been achieved using the latest Nu-fit oscillation parameter values, so our results can be treated as being done for the first time in the literature using these values. The existing work which studied DUNE considered the best-fit neutrino oscillation values which were available back then. Thirdly, we also computed the discovery potential results using the tau-optimized flux as well. However they lead to worsening of the sensitivities due to the increase of the number of events leading to bigger backgrounds for all the channels. For example, the increased ν_τ CC background in the ν_μ disappearance channel leads to big loss in sensitivity in DUNE as this is the dominant channel in DUNE. It can also be seen from Fig. 3.3 where using the standard flux, this background is almost negligible as the efficiency is very small. However, while using the optimized flux, the number of ν_τ CC events is roughly 10 times bigger, so this background becomes relevant. Motivated by the possibility of having increased statistics in the DUNE detector and the increased probability of the ν_τ-appearance channel compared to that of the ν_e-appearance channel we study the physics potential of sensitivity studies using the ν_τ-appearance channel.

Next let us estimate the event rates for ν_τ-appearance channel only along with its corresponding background and efficiencies.

4.6 Dune with ν_τ Appearance

In this section we estimate the event rates for the ν_τ appearance in DUNE.

The expected rates of the ν_τ signal and background (Bkg) from the two fluxes considered here are reported in Table 4.3 for the standard flux and in Table 4.4 for the optimized flux. In both tables we specify the two sources of electron backgrounds coming from the intrinsic ν_e component of the beam, [$\nu_e \oplus \bar{\nu}_e$ CC Background (beam)], and from $\nu_\mu \to \nu_e$ oscillations, [CC Background (oscillation)].

ν **mode**	
ν_τ Signal	277
$\bar{\nu}_\tau$ Signal	26
Total Signal	303
$\nu_e + \bar{\nu}_e$ CC Bkg (beam)	333 + 38
$\nu_e + \bar{\nu}_e$ CC Bkg (oscillation)	1753 + 12
$\bar{\nu}$ **mode**	
ν_τ Signal	68
$\bar{\nu}_\tau$ Signal	85
Total Signal	153
$\nu_e + \bar{\nu}_e$ CC Bkg (beam)	117 + 104
$\nu_e + \bar{\nu}_e$ CC Bkg (oscillation)	90 + 188

Table 4.3: *Rates after oscillation for Signals and Backgrounds (Bkg) in the case of the standard flux and for Normal Hierarchy (NH). $\delta_{CP} = 215°$ is considered [69]. No selection efficiency is considered.*

ν **mode**		$\bar{\nu}$ **mode**	
ν_τ Signal	2673	ν_τ Signal	98
$\bar{\nu}_\tau$ Signal	34	$\bar{\nu}_\tau$ Signal	983
Total Signal	2707	Total Signal	1081
$\nu_e + \bar{\nu}_e$ CC Bkg (beam)	688 + 63	$\nu_e + \bar{\nu}_e$ CC Bkg (beam)	176 + 177
$\nu_e + \bar{\nu}_e$ CC Bkg (oscillation)	1958 + 11	ν_e CC Bkg (oscillation)	76 + 324

Table 4.4: *Same as table 4.4 but for the optimized flux.*

These numbers are small when compared with a total of 2043 (2369) $\nu_\mu \to \nu_e \oplus \bar{\nu}_\mu \to \bar{\nu}_e$ CC signal events for the standard (optimized) flux and with a total of 14206 (67143) $\nu_\mu \to \nu_\mu \oplus \bar{\nu}_\mu \to \bar{\nu}_\mu$ CC signal events.

We clearly observe that the DUNE experiment is able by itself to provide a τ sample around 300 events in FHC mode and 150 in RHC mode because of the generous ν_μ flux components above the tau production threshold. On top of that, as per the

plan for the optimized flux, there is a huge gain in statistics by roughly a factor of 10 with respect to standard taus, thereby justifying the possibility to explore scenarios of new physics with taus.

4.7 Correlation Studies

In this section we study the correlation among the oscillation parameter measurements in DUNE with ν_τ using the various set-ups and fluxes as discussed in Sec. 3.3.2. This will lead to a complete understanding of how systematics may affect the final sensitivity reaches, how performing experimental cuts may lead to better sensitivities (encoded by the experimental reach S/B values), the impact of τ detection efficiency and finally the performances of DUNE in terms of the two neutrino fluxes considered, namely, the standard flux and the tau-optimized flux.

We expect the uncertainties related to ν_τ measurements to play a very significant role. Our choices of systematics are 10% and 20%. The former is very optimistic value. The DONUT collaboration which observed the first ν_τ [124, 125] could bring down to about 40% systematics measuring the tau cross-section. However that value is quite old and the DUNE collaboration itself uses 20% systematics for ν_τ channel but when as a background channel. The detection of a ν_τ interactions is very tricky due to τ lepton which is generated in the ν_τ CC interaction has tiny lifetime ($\sim 10^{-12}$ s). For the neutrino energies in DUNE, almost none of the τ's tracks can be identified. Therefore, just like ICARUS, DUNE's LAr-TPC can recognize the τ from its the decay products. But the neutrinos after the decay is invisible to the detector thereby piling up the uncertainty on the reconstructed energy of the lepton. The flux-related uncertainties can be reduced by measuring the fluxes at the near detector site.

Standard Flux

In this section we exclusively use the standard flux configurations with an exposure of $3.5 + 3.5$ years in the neutrino and anti-neutrino modes respectively, for investigating the sensitivity and correlation among the standard physics parameters obtained from

the ν_τ appearance channel. We cannot observe any improvement in the three sensitivities discussed in the previous section (CP violation, Mass Hierarchy and θ_{23} octant) by the addition of ν_τ appearance channel. The main reasons are the features of the ν_τ-appearance oscillation probabilities which do not vary much with parameter values, and add to that the small number of events in the ν_τ channel compared to the ν_μ disappearance. Thus ν_τ-s cannot compete with respect to the capability of the other channels in the standard physics scenario to improve the sensitivity. Therefore, the features of ν_τ-appearance is not evident at all from such plots; so we do not present the plots obtained using the other two channels (the standard ones in DUNE) and instead show the results obtained using the ν_τ-appearance channel only. As already stated above, we outline that this help us understand the behaviour of this channel in terms of variation of the oscillation parameters, moreover it will also enable us to study the impact of systematics and other factors related to this channel as well.

We present the results when we marginalized over all other oscillation parameters other than those displayed in the axes of the plots in the figures. We kept the true values of standard oscillation parameter according to the best-fit values and varied over their given uncertainty range, as in Table 4.1 unless otherwise mentioned explicitly. In Fig.4.4 we report correlation plots in the planes $(\theta_{13}, \Delta m^2_{31})$ (top left), $(\theta_{23}, \Delta m^2_{31})$ (top right) and $(\theta_{13}, \theta_{23})$ (bottom left). In each panel we show four different cases: (Red, DotDashed) refers to ν_τ detection efficiency of 6% and $S/B = 2.45$, (Brown, Dashed) to the same S/B but 18% of detection efficiencies while the (Blue, Dotted) and the (Black, Solid) lines refer to 6% and 18%, respectively, and the same $S/B = 18.6$. Contours are at 68% confidence level (CL) and are obtained assuming a 10% systematic error on the signal.

It is clear that when the ν_τ detection efficiency is increased from 6% to 18%, the number of signal events is increased and this results in smaller allowed regions in the correlation plots. The allowed range for θ_{13} can be reduced by up to 18%, as we can see in the correlation plot in the $(\theta_{13}, \Delta m^2_{31})$ plane. On the other hand, the θ_{23} range can be reduced approximately by 15%, as shown in the $(\theta_{23}, \Delta m^2_{31})$ plane. For Δm^2_{31}, instead, an improvement of approximately 30% can be reached passing from the worst

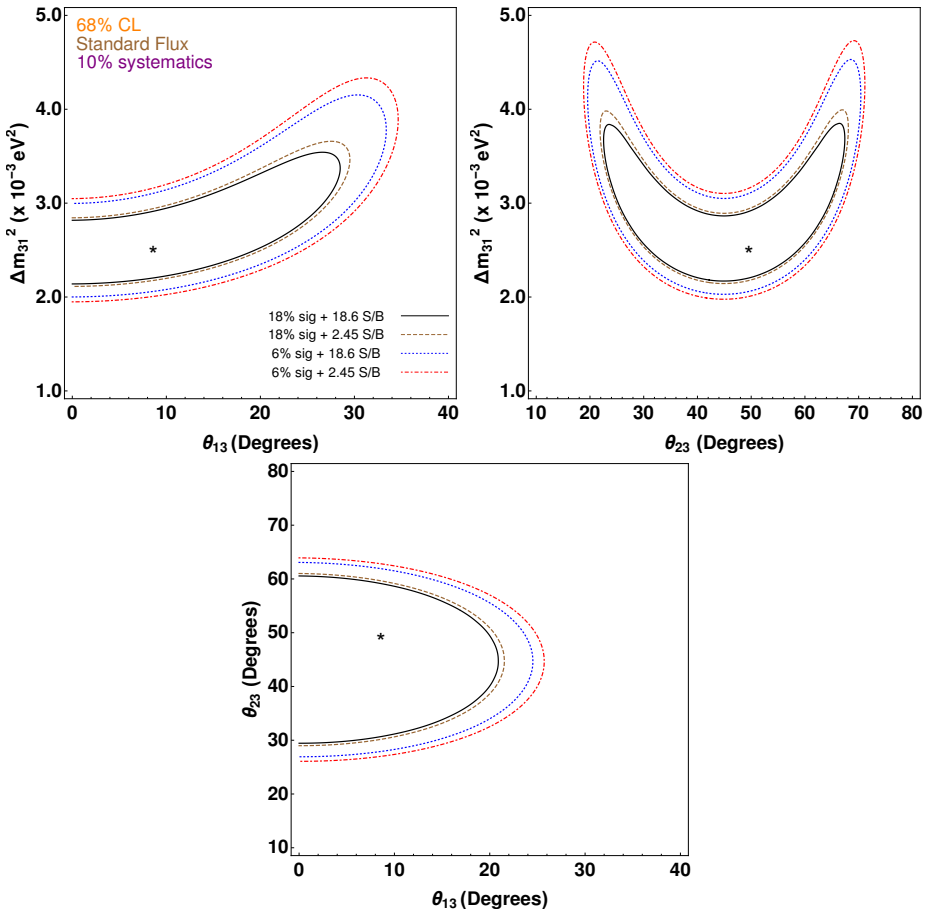

Figure 4.4: *Expected contours at 68% CL in the oscillation parameter planes (as mentioned in each graph axis) for* $S/B = 2.45$*, with* ν_τ *detection efficiency of 6% (Red, DotDashed) and 18% (Brown, Dashed) and for* $S/B = 18.6$ *with* ν_τ *detection efficiency of 6% (Blue, Dotted) and 18% (Black, Solid). Standard flux has been assumed in the simulation, using only the* ν_τ *appearance channel in the Normal Hierarchy case with a 10% signal uncertainty. Marginalization over all undisplayed parameters has been performed. Stars represent the simulated true values.*

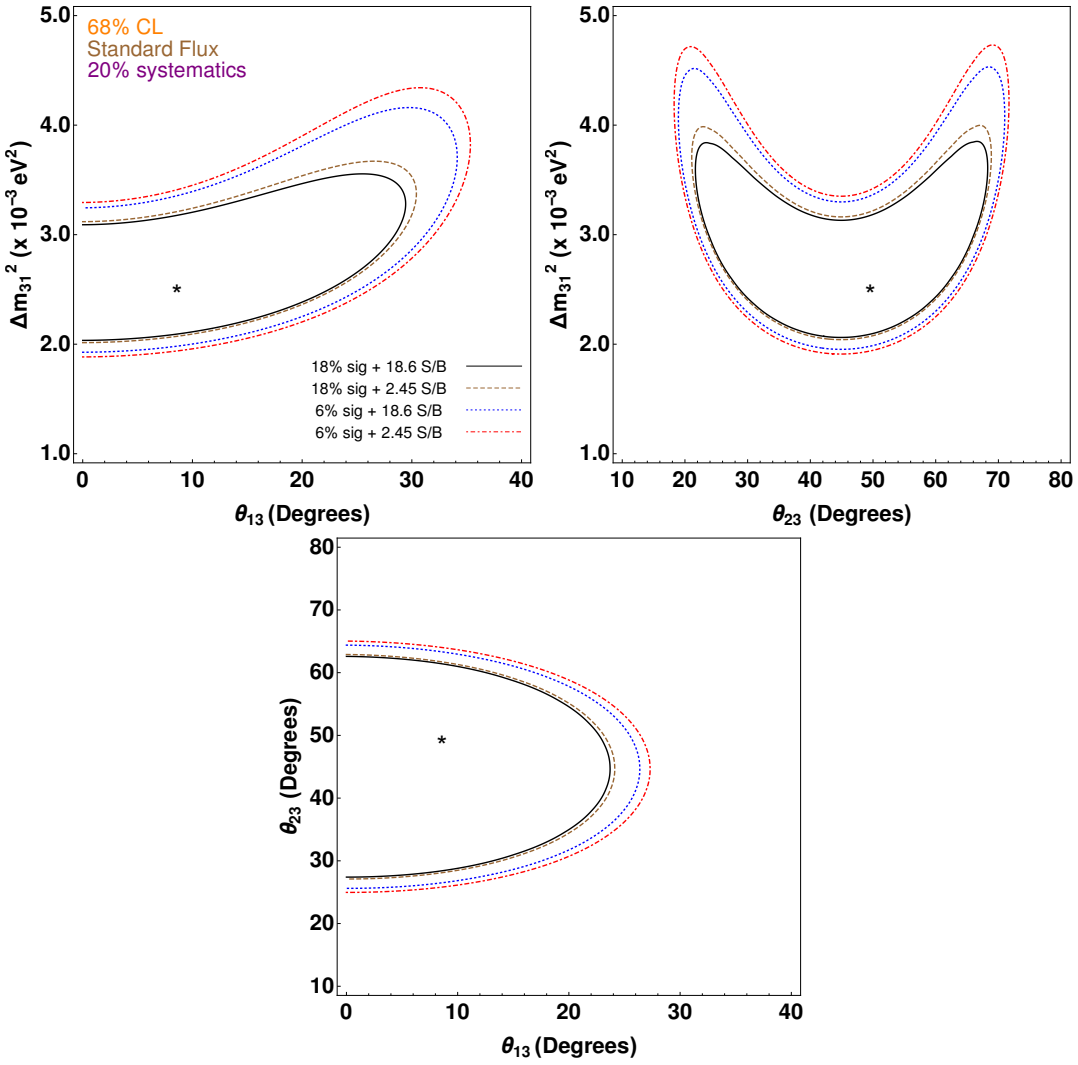

Figure 4.5: *Same as figure 4.4 but with 20% signal uncertainty.*

case ($S/B = 2.45$, with ν_τ detection efficiency at 6%) to the best one ($S/B = 18.6$, with ν_τ detection efficiency at 18%).

In figure 4.5 we depict the same plots as in figure 4.4 but with 20% systematic uncertainty on the signal. We see that doubling the systematic uncertainty from 10% to 20% results in a decrease in sensitivity of approximately 8% for all mixing parameters.

For a given systematics value, the reduction of the regions at 68% confidence level is bigger if we increase the detection efficiency than if we increase the S/B ratio value. In particular, there can be a reduction of the allowed range up to 18% for θ_{13} (in the

θ_{13} vs Δm^2_{31} correlation plot) and up to 15% for θ_{23} (in the θ_{23} vs Δm^2_{31} correlation plot) for increasing the detection efficiency with a fixed S/B. On the other hand, fixing the efficiency and increasing the S/B, the decrease of the allowed ranges can reach only approximately upto 5%. We may say that parameter which is less affected by efficiencies and S/B ratios, is θ_{23}, while the one which is affected the most is the atmospheric mass splitting.

Optimized Flux

In this section, we exclusively use the tau optimized flux configurations with an exposure of 3.5 + 3.5 years for investigating the sensitivity and correlation among the standard physics parameters as obtained from the ν_τ appearance channel only.

Since the flux is optimized for tau as to produce a larger statistics in all cases, the impact of tau detection efficiency increment or S/B ratio increment on the sensitivities is not so much as was in the case of the standard flux (see Fig. 4.6). Similar to the standard flux results, here too, the interplay among the detection efficiency, S/B and systematics uncertainty leads to similar sensitivities (χ^2 values) for various combinations. For example, higher S/B values and smaller detection efficiencies may keep us in the same place in the parameter place with respect to the case where lower systematics and higher detection efficiencies. Analyzing the correlation plots, we observe that the smallest allowed ranges found in the case of the standard flux can be further reduced up to 10% for θ_{23} and 15% for θ_{13} if the optimized flux is considered.

Finally, in figure 4.7 we present the results obtained for a 20% signal uncertainty. As before, the improvement in the sensitivity is smaller than in the case of the standard flux. The parameter which is affected the most by the systematics is the atmospheric mass splitting. As expected, when the efficiency and the S/B ratio are bigger and the systematics are lower, the allowed parameters spaces are smaller. Furthermore, due to the increased statistics, results with optimized flux are always better than the ones obtained using the standard flux. The reduction of the allowed ranges in the case of the optimized flux, fixing the other channel simulation details

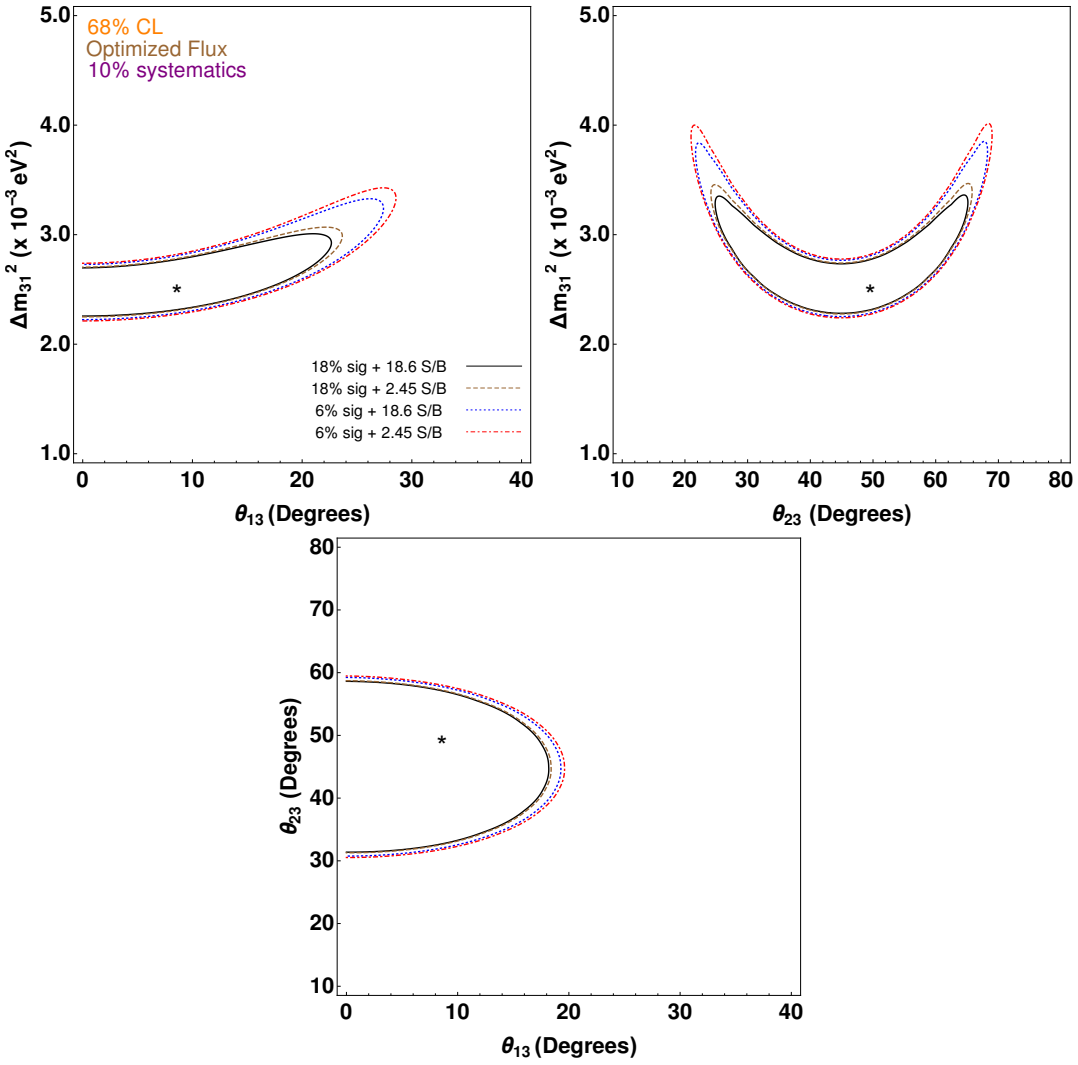

Figure 4.6: *Expected contours at 68% CL in the oscillation parameter planes (as mentioned in each graph axis) for $S/B = 2.45$, with ν_τ detection efficiency of 6% (Red, DotDashed) and 18% (Brown, Dashed) and for $S/B = 18.6$ with ν_τ detection efficiency of 6% (Blue, Dotted) and 18% (Black, Solid). The tau optimized flux has been assumed in the simulation, using only the ν_τ appearance channel in the Normal Hierarchy case with a 10% signal uncertainty. Marginalization over all undisplayed parameters has been performed. Stars represent the simulated true values.*

can reach, for example, 10% for θ_{23} and 15% for θ_{13}.

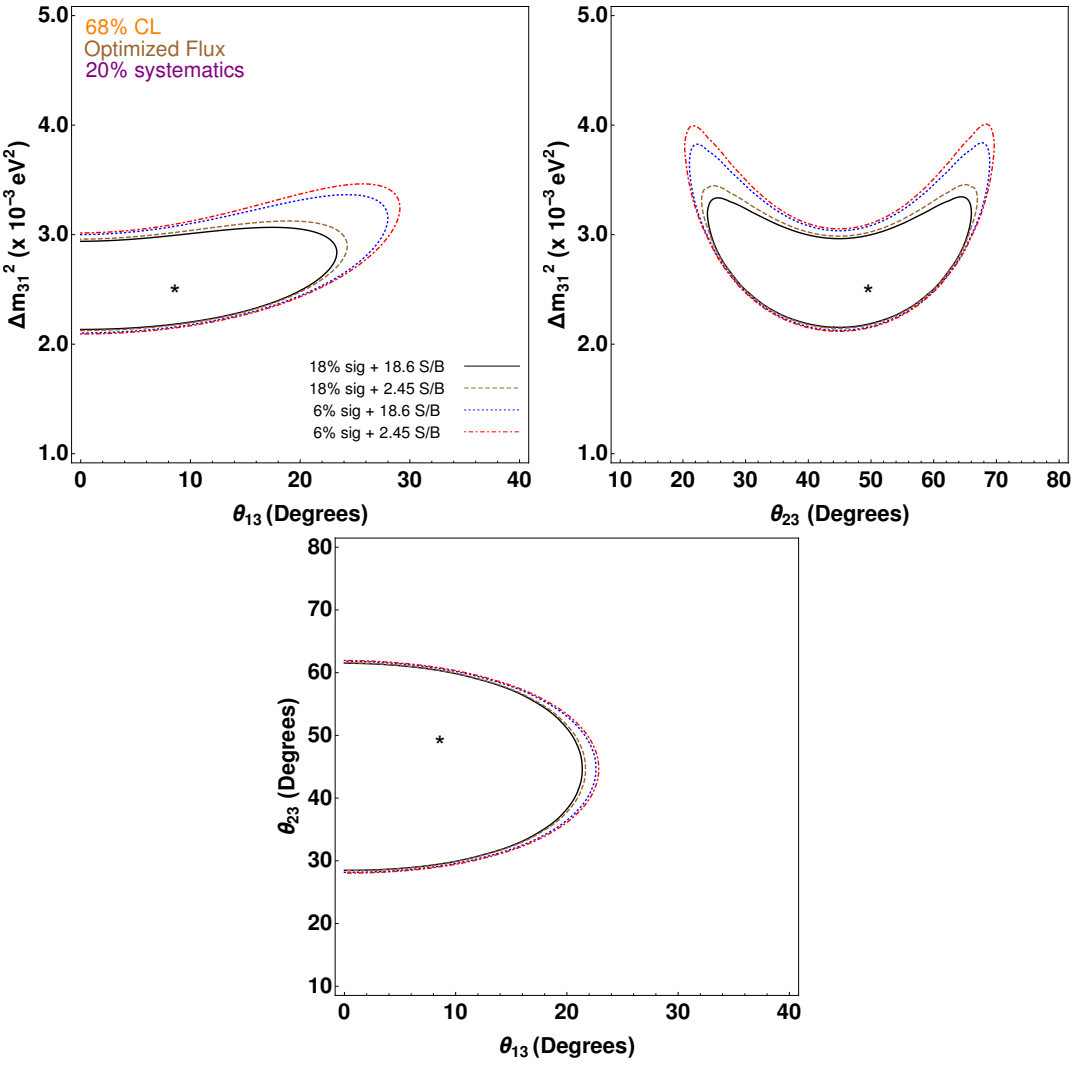

Figure 4.7: *Same as figure 4.6 but with 20% signal uncertainty.*

4.8 A Comparison with OPERA Results

OPERA recently released the observation of 10 ν_τ events [116]. The background for $\nu_\mu \to \nu_\tau$ consists of charm decays to τ leptons and neutral current events. Ref. [117] studied the physics sensitivities employing the OPERA events and obtained a bound on the Δm^2_{31} sensitivity. Using OPERA events one gets: $\Delta m^2_{31} = (2.7 \pm 0.7) \times 10^{-3}$ eV^2.

From Figs. 4.8 and 4.9, one sees DUNE performs much better in context to the Δm^2_{31} sensitivity. A larger S/B gave a better sensitivity to the mixing parameters: in

particular, for $S/B = 18.6$ the correlation plots (Figs. 4.4, 4.6, 4.5 and 4.7) showed a reduction of the mixing angles allowed ranges of approximately 5% if compared to the case $S/B = 2.45$. In a similar manner, Figs. 4.8 and 4.9 depict roughly the same reduction but here in context to the relative uncertainty of Δm^2_{31}.

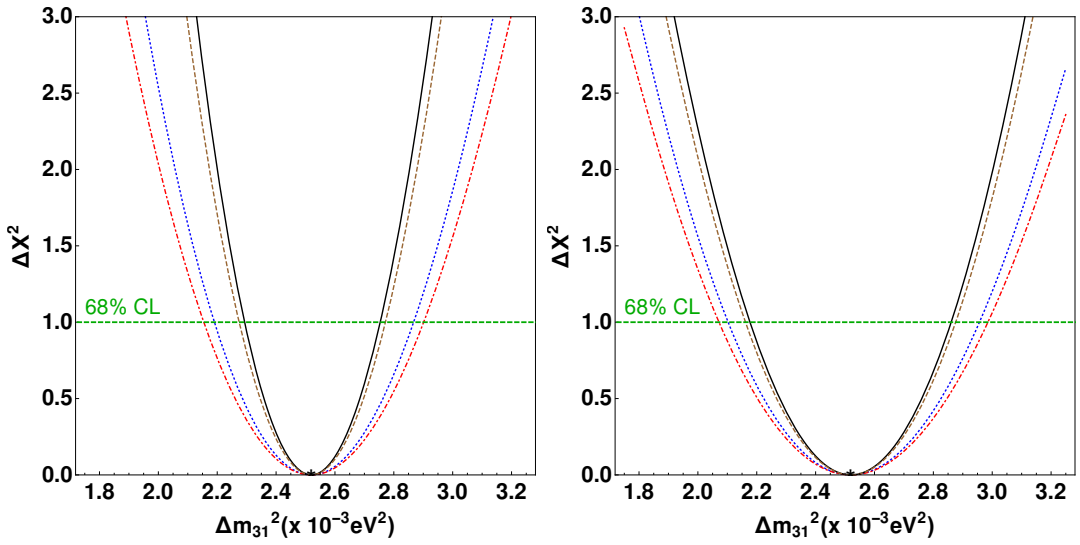

Figure 4.8: *Expected* $\Delta\chi^2 = \chi^2 - \chi^2_{min}$ *as a function of the true* Δm^2_{31} *is plotted. For* $S/B = 2.45$*, with* ν_τ *detection efficiency of 6% (Red, DotDashed) and 18% (Brown, Dashed) and for* $S/B = 18.6$ *with* ν_τ *detection efficiency of 6% (Blue, Dotted) and 18% (Black, Solid). The standard flux has been assumed in the simulation, using only the* ν_τ *appearance channel in the Normal Hierarchy case with a 10% signal uncertainty (left) and 20% signal uncertainty (right). Marginalization over all undisplayed parameters has been performed. Stars represent the simulated true values.*

Thus we conclude that an increase in efficiency allows a better performance of the DUNE detector than a larger S/B. The DUNE setup discussed here with an 18% τ detection efficiency reaches a much better sensitivity (smaller relative uncertainty value of about 8%).

Notice also that with such optimized flux, DUNE can reach a relative uncertainty of 4.5% in the measurement of the atmospheric mass difference if 10% systematics on the signal is assumed.

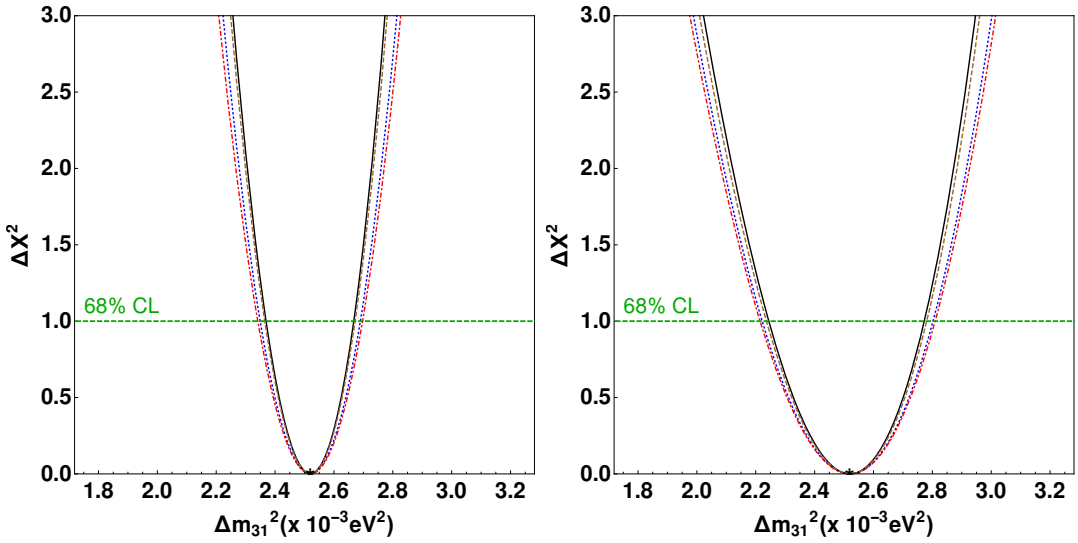

Figure 4.9: *Expected* $\Delta\chi^2 = \chi^2 - \chi^2_{min}$ *as a function of the true* Δm^2_{31} *is plotted. For* $S/B = 2.45$*, with* ν_τ *detection efficiency of 6% (Red, DotDashed) and 18% (Brown, Dashed) and for* $S/B = 18.6$ *with* ν_τ *detection efficiency of 6% (Blue, Dotted) and 18% (Black, Solid). The tau optimized flux has been assumed in the simulation, using only the* ν_τ *appearance channel in the Normal Hierarchy case with a 10% signal uncertainty (left) and 20% signal uncertainty (right). Marginalization over all undisplayed parameters has been performed. Stars represent the simulated true values.*

4.9 Inference

We infer from the results of this chapter that in the context of the three-massive-neutrinos paradigm ν_τ-appearance can also be used to constrain some of the other oscillation parameters in principle but the bounds are not competitive with what DUNE without ν_τ-appearance channel may put (see Appendix). Figs. 4.4, 4.6, 4.5 and 4.7 depict the allowed regions of parameters space obtained after 3.5 + 3.5 years of DUNE data taking, considering the inclusion of ν_τ-appearance. We studied correlation at 68% CL in the $\theta_{23} - \theta_{13}$, $\theta_{23} - \Delta m^2_{31}$ and $\theta_{13} - \Delta m^2_{31}$ planes. We do not present any parameter space that includes the δ_{CP} since we found ν_τ-appearance channel has almost no sensitivity to δ_{CP}. We presented the results when we marginalized over all other oscillation parameters. However, we also checked even if the solar parameters and the mass ordering are held fixed at their current best-fit values, the results stay the same. In comparing the results with that of the OPERA capability, we found the

Δm^2_{31} bounds are significantly improved both in cases for the standard (by 18 %) and optimized (by 21.5 %) fluxes.

To summarize, the impact of the ν_τ-appearance channel is marginal or even negligible when it comes to measuring the standard oscillation parameters within the three-massive-neutrinos paradigm. However we must keep in mind that we have studied only the ν_τ detection via the electronic channel which has a branching fraction pretty small (about 18%). Therefore, if ultimately one is able to combine this sensitivity capability with that in the hadronic decay channel of τ, the channel which was studied in Ref. [111] the resultant sensitivity may have interesting possibilities for standard physics scenario due to increased statistics.

After analysing the standard physics scenario we move on to the Non-Standard Interaction hypothesis in the neutrino sector. Having $\nu_\mu \to \nu_\tau$ appearance channel available we expect to get stringent bounds on the NSI parameters that get associated with the ν_τ-appearance probability. This is the topic of the next chapter.

Chapter 5

ν_τ appearance in DUNE: Non Standard Interaction

Several neutrino experiments have paved the way to search for various new physics scenarios; one model-independent way to study new physics (NP) is done in the framework of what is known as the non-standard interaction [52, 126, 127]. Now that we introduced the ν_τ appearance channel in DUNE, we expect to derive sensitivity bounds better than those existing in some of the NSI parameters.

5.1 Introduction

We begin by reminding the reader that the NSI sector involving (ν_τ, τ), there are physics motivations of great importance since the third generation may be more sensitive to NP effects because of their heavier masses [1]. Therefore, here it presents an unprecedented opportunity to constrain new physics (NP) effects on third generation leptons in neutrino experiments. Thirdly , if a symmetry like $L_\mu - L_\tau$ symmetry as motivated by many physics motivations is present in the leptonic sector, $\chi_{\mu\tau}$ mediator is of specific interest and may also be sensitive to dark matter searches in DUNE [128]. Lastly, there are some hints of lepton flavor universality violations from B-physics anomalies which may point towards lepton non-universal new physics with the largest effects involving the third generation leptons [129]. Through mixing with

[1] In some 2HDM models generating neutrino masses, the masses are proportional to Higgs boson couplings, so neutrino mass generation involving new physics is likely attached to the third generation.

other generation the new physics effect may affect other generations as well, but suppressed through their mixing.

5.2 NSI considerations

Originally Wolfestein proposed NSI as an alternative to explain neutrino flavor oscillation phenomena [130]. Since the effect is sub-dominant it is now regarded as the model for phenomenological NP signature: typically, if the SM is regarded as a low-energy effective theory of some higher theory in the UV, then BSM would enter as higher-dimensional operators, suppressed by the energy scale at which new physics comes into play. One of the diligent ways to capture the effects is to write these interaction Lagrangians in terms of four-fermion interactions, [131]:

$$-\mathcal{L}^{eff}_{\rm NSI} = \varepsilon^{fP}_{\alpha\beta} 2\sqrt{2} G_F (\bar{\nu}_\alpha \gamma_\rho L \nu_\beta)(\bar{f}\gamma^\rho P f)\,, \tag{5.1}$$

where G_F is the Fermi constant, $\varepsilon^{fP}_{\alpha\beta}$ is the parameter which describes the strength of the NSI, f is a first generation SM fermion (e, u or d), P denotes the chiral projector $\{L, R = (1 \pm \gamma^5)/2\}$, and α and β denote the neutrino flavors e, μ or τ. This Lagrangian describes neutral current (NC) interactions and will be our focus here; it basically modifies the matter Hamiltonian and consequently the transition probability of the neutrinos in matter. Long-baseline neutrino experiments with a beam of neutrinos which are well-understood are suited to probe matter NSI because they are more sensitive towards neutral current interactions which affect the neutrino propagation coherently. See Refs. [132] for NSI studies in long-baseline experiments.

The strength of the new interaction is parameterized in terms of the complex $\varepsilon_{\alpha\beta} = |\epsilon_{\alpha\beta}| e^{i\phi_{\alpha\beta}}$ couplings. Thus the state evolution equations are given by:

$$i\frac{d}{dt}\begin{pmatrix}\nu_e\\ \nu_\mu\\ \nu_\tau\end{pmatrix} = \left[U_{PMNS}\begin{pmatrix}0 & 0 & 0\\ 0 & \Delta_{21} & 0\\ 0 & 0 & \Delta_{31}\end{pmatrix}U^\dagger_{PMNS} + A\begin{pmatrix}1+\epsilon_{ee} & \epsilon_{e\mu} & \epsilon_{e\tau}\\ \epsilon^*_{e\mu} & \epsilon_{\mu\mu} & \epsilon_{\mu\tau}\\ \epsilon^*_{e\tau} & \epsilon^*_{\mu\tau} & \epsilon_{\tau\tau}\end{pmatrix}\right]\begin{pmatrix}\nu_e\\ \nu_\mu\\ \nu_\tau\end{pmatrix} \tag{5.2}$$

where $\Delta_{ij} = \Delta m^2_{ij}/2E$, U_{PMNS} is the neutrino mixing matrix, $A \equiv 2\sqrt{2}G_F n_e$ with n_e being the electron density in the Earth crust. What is relevant for neutrino propagation in matter is the vector part V of interaction $\varepsilon^{fV}_{\alpha\beta} = \varepsilon^{fL}_{\alpha\beta} + \varepsilon^{fR}_{\alpha\beta}$ since the neutrino propagation in a medium is sensitive to the combination $\varepsilon_{\alpha\beta} = \varepsilon^{eV}_{\alpha\beta} + N_u/N_e\,\varepsilon^{uV}_{\alpha\beta} + N_d/N_e\,\varepsilon^{dV}_{\alpha\beta}$. Following what is usually done in the literature, we will discuss the bounds from DUNE in terms of $\varepsilon_{\alpha\beta}$.

All in all, beside the standard oscillation parameters, the parameter space is enriched by six more moduli $|\epsilon_{\alpha\beta}|$ and three more phases $\phi_{\alpha\beta}$. Thus we see the main effects of NSI are nicely parameterized in terms of certain coefficients that makes the oscillation dependent on them and are therefore constrain-able by experiments. The values of these coefficients give us the idea of new physics in the neutrino sector. Along propagation we will consider that the effects of the NSI parameters on the transition probability is dependent on the NSI parameters $(\varepsilon_{\mu\tau}, \varepsilon_{\tau\tau})$. Myriad of studies in the context to NSI have been done in the literature; see Refs. [126, 133, 134, 135, 136, 137, 138, 139] for some of the important implications in phenomenology, and in particular for the same in the DUNE experiment context, see Refs. [140, 141, 142].

5.2.1 Concerned Probabilities

In the context of our study, oscillation in the $\nu_\mu - \nu_\tau$ sector is studied using perturbation theory and is given by [126, 136, 137]:

$$\begin{aligned} P(\nu_\alpha \to \nu_\beta; \varepsilon_{e\mu}, \varepsilon_{e\tau}, \varepsilon_{\mu\mu}, \varepsilon_{\mu\tau}, \varepsilon_{\tau\tau}) &= P(\nu_\alpha \to \nu_\beta; 2 \text{ flavor in vacuum}) \\ &+ P(\nu_\alpha \to \nu_\beta; \varepsilon_{e\mu}, \varepsilon_{e\tau}) \\ &+ P(\nu_\alpha \to \nu_\beta; \varepsilon_{\mu\mu}, \varepsilon_{\mu\tau}, \varepsilon_{\tau\tau}), \end{aligned} \tag{5.3}$$

where α and β denote one of μ and τ, and ε's are the NSI parameters. The first term in Eq. 5.3 is just the probability of two flavor oscillation in vacuum:

$$P(\nu_\mu \to \nu_\tau; 2 \text{ flavor in vacuum}) = 4\cos^2\theta_{23}\sin^2\theta_{23}\sin^2\frac{\Delta m^2_{31}L}{4E}, \tag{5.4}$$

The second and third terms are:

$$
\begin{aligned}
& P(\nu_\mu \to \nu_\tau; \varepsilon_{e\mu}, \varepsilon_{e\tau}) \\
= \;& 4\cos^2\theta_{23}\sin^2\theta_{23}|\Xi|^2\left(\frac{aL}{4E}\right)\sin\frac{\Delta m^2_{31}L}{2E} \\
- \;& 8\cos^2\theta_{23}\sin^2\theta_{23}|\Xi|^2\sin\frac{AL}{4E}\sin\frac{\Delta m^2_{31}L}{4E}\cos\frac{\Delta m^2_{31}-a}{4E}L \\
+ \;& 4\cos^2\theta_{23}\sin^2\theta_{23}|\Theta_\pm|^2\left(\frac{A}{\Delta m^2_{31}-a}\right)\left(\frac{AL}{4E}\right)\sin\frac{\Delta m^2_{31}L}{2E} \\
- \;& 8\cos^2\theta_{23}\sin^2\theta_{23}|\Theta_\pm|^2\left(\frac{A}{\Delta m^2_{31}-a}\right)^2\cos\frac{AL}{4E}\sin\frac{\Delta m^2_{31}L}{4E}\sin\frac{\Delta m^2_{31}-a}{4E}L \\
+ \;& 8\cos^2\theta_{23}\sin^2\theta_{23}(\cos^2\theta_{23}-\sin^2\theta_{23})|\Xi||\Theta_\pm|\cos(\xi-\theta_\pm)\left(\frac{A}{\Delta m^2_{31}-A}\right)\left(\frac{A}{\Delta m^2_{31}}\right)\sin^2\frac{\Delta m^2_{31}L}{4E} \\
+ \;& 8\cos\theta_{23}\sin\theta_{23}|\Xi||\Theta_\pm|\left(\frac{A}{\Delta m^2_{31}-A}\right)\sin\frac{AL}{4E}\sin\frac{\Delta m^2_{31}L}{4E} \\
& \times\left[\sin^2\theta_{23}\cos\left(\xi-\theta_\pm-\frac{\Delta m^2_{31}-A}{4E}L\right)-\cos^2\theta_{23}\cos\left(\xi-\theta_\pm+\frac{\Delta m^2_{31}-A}{4E}L\right)\right], \qquad (5.5)
\end{aligned}
$$

and

$$
\begin{aligned}
& P(\nu_\mu \to \nu_\tau; \varepsilon_{\mu\mu}, \varepsilon_{\mu\tau}, \varepsilon_{\tau\tau}) \\
= \;& -2\cos^2\theta_{23}\sin^2\theta_{23}\left(\sin^2\theta_{13}\frac{\Delta m^2_{31}}{a}-\mathcal{S}_1\right)\left(\frac{AL}{2E}\right)\sin\frac{\Delta m^2_{31}L}{2E} \\
& +\cos^2\theta_{23}\sin^2\theta_{23}\mathcal{S}_1^2\left(\frac{AL}{2E}\right)^2\cos\frac{\Delta m^2_{31}L}{2E} \\
- \;& 8\cos\theta_{23}\sin\theta_{23}(\cos^2\theta_{23}-\sin^2\theta_{23}) \\
& \left[\cos\theta_{12}\sin\theta_{12}\sin\theta_{13}\cos\delta\left(\frac{\Delta m^2_{21}}{a}\right)-|\mathcal{E}|\cos\phi\right]\left(\frac{A}{\Delta m^2_{31}}\right)\sin^2\frac{\Delta m^2_{31}L}{4E} \\
+ \;& 4\cos\theta_{23}\sin\theta_{23}(\cos^2\theta_{23}-\sin^2\theta_{23})\mathcal{S}_1|\mathcal{E}|\cos\phi\left(\frac{a}{\Delta m^2_{31}}\right) \\
& \left[\left(\frac{aL}{2E}\right)\sin\frac{\Delta m^2_{31}L}{2E}-2\left(\frac{a}{\Delta m^2_{31}}\right)\sin^2\frac{\Delta m^2_{31}L}{4E}\right] \\
+ \;& 4\cos^2\theta_{23}\sin^2\theta_{23}|\mathcal{E}|^2\left(\frac{A}{\Delta m^2_{31}}\frac{AL}{2E}\right)\sin\frac{\Delta m^2_{31}L}{2E} \\
+ \;& 4|\mathcal{E}|^2\left[(\cos^2\theta_{23}-\sin^2\theta_{23})^2-4\cos^2\theta_{23}\sin^2\theta_{23}\cos^2\phi\right]\left(\frac{A}{\Delta m^2_{31}}\right)^2 \\
\times \;& \sin^2\frac{\Delta m^2_{31}L}{4E}, \qquad (5.6)
\end{aligned}
$$

respectively, where $a = \frac{\Delta m^2_{21}}{\Delta m^2_{31}}$. Some simplified notations involving the NSI ε's have been used: are as follows:

$$\begin{aligned}
\Theta_{\pm} &\equiv \sin\theta_{13}\frac{\Delta m^2_{31}}{a} + (\sin\theta_{23}\varepsilon_{e\mu} + \cos\theta_{23}\varepsilon_{e\tau})e^{i\delta} \equiv |\Theta_{\pm}|e^{i\theta_{\pm}}, \\
\Xi &\equiv \left(\cos\theta_{12}\sin\theta_{12}\frac{\Delta m^2_{21}}{a} + \cos\theta_{23}\varepsilon_{e\mu} - \sin\theta_{23}\varepsilon_{e\tau}\right)e^{i\delta} \equiv |\Xi|e^{i\xi}, \\
\mathcal{E} &\equiv \cos\theta_{23}\sin\theta_{23}(\varepsilon_{\mu\mu} - \varepsilon_{\tau\tau}) + \cos^2\theta_{23}\varepsilon_{\mu\tau} - \sin^2\theta_{23}\varepsilon^*_{\mu\tau} \equiv |\mathcal{E}|e^{i\phi}, \\
\mathcal{S}_1 &\equiv (\cos^2\theta_{23} - \sin^2\theta_{23})(\varepsilon_{\tau\tau} - \varepsilon_{\mu\mu}) + 2\cos\theta_{23}\sin\theta_{23}(\varepsilon_{\mu\tau} + \varepsilon^*_{\mu\tau}) \\
&- \cos^2\theta_{12}\frac{\Delta m^2_{21}}{a}.
\end{aligned} \tag{5.7}$$

$\Theta_{\pm}$, Ξ, and $\mathcal{E}$ are complex and $\mathcal{S}_1$ is real. The matter potential is given by

$$\begin{aligned}
A &= 2\sqrt{2}G_F N_e E \\
&= 7.6324 \times 10^{-5}\text{eV}^2\frac{\rho}{\text{gcm}^{-3}}\frac{E}{\text{GeV}}.
\end{aligned} \tag{5.8}$$

For the DUNE experiment, value of the matter density is given by $\rho = 2.8\,\text{g/cm}^3$. The other conjugate oscillation probability can be obtained easily; T conjugate channels is obtained by the replacement $\delta \to -\delta$ and for CP conjugate channels one needs to replace $\delta \to -\delta$ and $A \to -A$.

The transition probability is sensitive to changes in the absolute values of $\epsilon_{\mu\tau}$ much more than to changes to its imaginary part, $\phi_{\mu\tau}$, the phase. In particular, when $\phi_{\mu\tau}$ takes values $\frac{\pi}{2}$ or $\frac{3\pi}{2}$, the sensitivity is the weakest. Moreover, in the ν_τ appearance channel, we expect sensitivity to $\epsilon_{e\mu}$ and $\epsilon_{e\tau}$ only when they take large values. NSIs could also fake expected event spectra due to standard neutrino oscillations, but with a different set of parameter values. This could therefore lead to new degeneracies in the oscillation parameter space. An important challenge for future experiments is thus to find ways to break these degeneracies to obtain maximum sensitivity to oscillation parameters. Degeneracies between NSI parameters and the three-massive-neutrinos-paradigm parameters have been extensively studied in the literature [141, 142, 143, 144, 145, 146, 147, 148, 149, 150, 151, 152, 153, 154, 155, 156, 157]. These

also include the ones done in particular to the studies of NSI effects in the MINOS, T2HK and NOνA experiments. However, due to large systematic uncertainties and limited statistics, these experiments cannot make a definitive measurement of the matter NSI.

In Fig. 5.1, $P(\nu_\mu \to \nu_\tau)$ and its CP conjugate channel is plotted as expected in the DUNE experimental scenario energies. Both cases, one considering NSI and one without NSI along propagation have been shown. Analyses have been done with $(\varepsilon_{\mu\tau}, \varepsilon_{\tau\tau}) = (0, 0)$ (top panel) and with experimental upper bound of $(\varepsilon_{\mu\tau}, \varepsilon_{\tau\tau}) = (0.07, 0.147)$ (bottom panel) ([133, 134, 135]). Other NSI parameters are always taken to be zero.

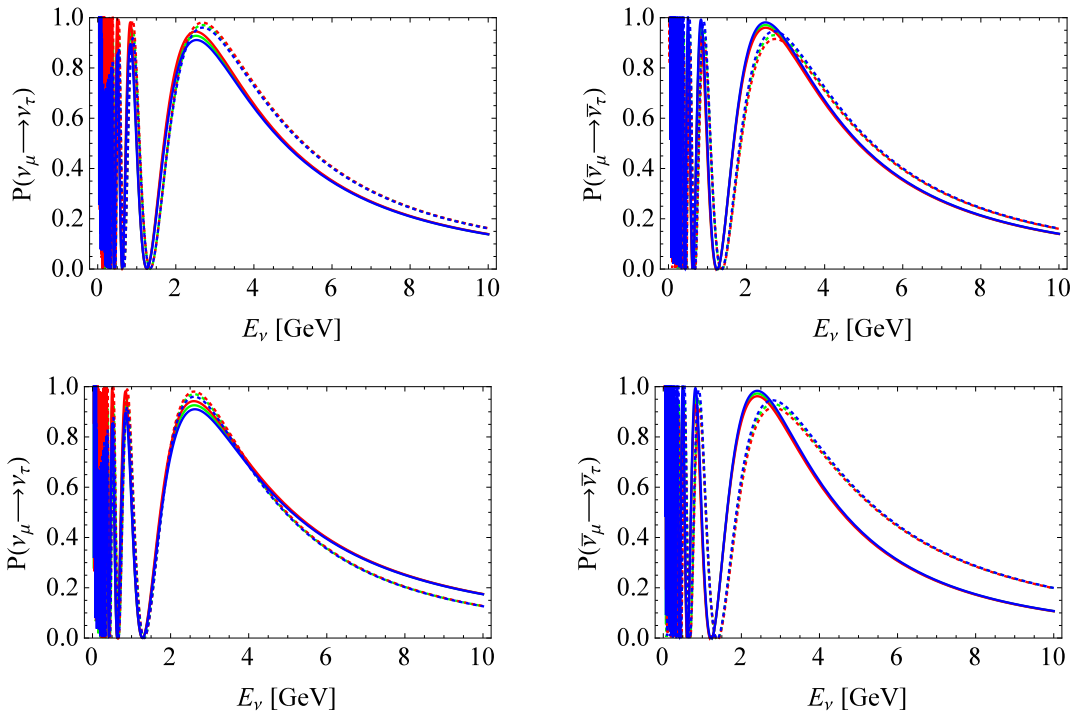

Figure 5.1: *The transition probability of the $\nu_\mu \to \nu_\tau$ (left) channel and its CP conjugate channel $\bar{\nu}_\mu \to \bar{\nu}_\tau$ (right) in the presence of matter effect for the DUNE energy range and baseline. The solid/dotted lines correspond to NH/IH. The green, red, and blue lines correspond to $\delta = (0, \pi/2, -\pi/2)$, respectively. NSI parameters are taken to be $(\varepsilon_{\mu\tau}, \varepsilon_{\tau\tau}) = (0, 0)$ (top) and $(\varepsilon_{\mu\tau}, \varepsilon_{\tau\tau}) = (0.07, 0.147)$ (bottom). Plot taken from Ref. [112].*

In conclusion to this subsection it is therefore straight-forward to surmise that

some of the NSI parameter measurements, will be easily accessible from the ν_τ channel. Therefore we pursue to simulate the experiment including the presence of NSI, and obtain results on the sensitivity to these parameters, which is the topic for the next section.

5.3 Constraining the NSI parameters

First we will state the current constraints on the measurements (global fits to neutrino data) of NSI parameters, then we will describe the limits obtained on these parameters in the standard DUNE scenario. Lastly we will present the results containing the analysis in DUNE with ν_τ appearance channel.

5.3.1 Existing Bounds on the NSI parameters

Direct constraints on NSI can be derived from scattering processes [158] and from neutrino oscillation data [159]. Latest constrains on NSI parameters from global fits were quoted in [160], from which we extracted the limits reported in table 5.1, and used in our numerical analysis. We want to outline that, in order to compute the

NSI parameters	Limits
$\epsilon_{ee} - \epsilon_{\mu\mu}$	(-0.2, 0.45)
$\lvert\epsilon_{e\mu}\rvert$	< 0.1
$\lvert\epsilon_{e\tau}\rvert$	< 0.3
$\epsilon_{\tau\tau} - \epsilon_{\mu\mu}$	(-0.02, 0.175)
$\lvert\epsilon_{\mu\tau}\rvert$	< 0.03

Table 5.1: *Current constraints on the NSI parameters at 90% CL obtained from a global fit to neutrino oscillation data [160]. No bounds on the phases $\phi_{\alpha\beta}$ are available so far.*

oscillation probabilities in presence of NSI, we may subtract from the diagonal entries any one of the diagonal elements $\epsilon_{\alpha\alpha}$ as the oscillation phenomenon is insensitive to overall factors. Therefore one may consider, as done in table 5.1, the *shifted* parameters $\epsilon_{ee} - \epsilon_{\mu\mu}$ and $\epsilon_{\tau\tau} - \epsilon_{\mu\mu}$ instead of ϵ_{ee} and $\epsilon_{\tau\tau}$ respectively and set $\epsilon_{\mu\mu}$ to 0,

which is also motivated by the strong external bounds [126]. Throughout the thesis we refer to the parameters $\epsilon_{ee} - \epsilon_{\mu\mu}$ & $\epsilon_{\tau\tau} - \epsilon_{\mu\mu}$ as ϵ_{ee} & $\epsilon_{\tau\tau}$ respectively.

5.3.2 Analysis in the Standard DUNE scenario

Matter NSIs hypothesis have been investigated for the DUNE neutrino oscillation phenomena in Refs. [140, 141, 142, 148, 147, 149, 150]. Let us briefly chalk out some of the effects: the presence of matter NSIs in general reduces the sensitivity of DUNE to the standard oscillation parameters due to conspiracies occurring among the standard and non-standard oscillation parameters. Essentially they give rise to new kinds of degeneracies for long baseline experiments [141, 142]. In particular, it has been shown in Refs. [142, 144] that for quite bigger values of the NSI parameters a degeneracy between the sign of Δm^2_{31} and δ_{CP} is obtained. This naturally translates into worsening the DUNE sensitivity of the neutrino mass ordering measurements [142, 147]. On the other hand, for θ_{23} and δ_{CP} measurements, there exists two other degeneracies. The first is due to an interplay between the oscillation parameter $|\theta_{23} - \frac{\pi}{4}|$ and the NSI parameter $\epsilon_{\tau\tau}$ thereby reducing the θ_{23} octant distinguishing capability of DUNE and creating fake solutions [141, 142]. Another degeneracy is present due to δ_{CP} and the NSI parameters ϵ_{ee} and $\epsilon_{e\tau}$ including the phase. Naturally this means δ_{CP} measurements (and CP Violation sensitivity) is compromised at DUNE. We will discuss more on the degeneracies in subsequent subsections. The impact of source and detector NSIs at DUNE was studied in Ref. [155] and the effect of systematics was estimated in [161]. DUNE can improve on measuring the $|\epsilon_{e\mu}|$ 3 times than its current limit and the uncertainty of $|\epsilon_{e\mu}|$ can be reduced by 30-40%. These studies were based on considering the standard DUNE ν_e appearance and ν_μ disappearance channels only and did not include the ν_τ appearance channel.

After this quick review let us delve into understanding the $\nu_\mu \to \nu_\tau$ transition in DUNE.

5.3.3 The importance of $\nu_\mu \to \nu_\tau$ channel

After the full treatment of probability in the presence of NSI in Sec. 5.2.1, it will be good to just ascertain some quick points on the $\nu_\mu \to \nu_\tau$ transition probability. The $\nu_\mu \to \nu_e$ oscillation probability is affected by the $\epsilon_{e\mu}$ and $\epsilon_{e\tau}$ parameters, as well as by ϵ_{ee}. However, statistics in DUNE is dominated by the disappearance channel $\nu_\mu \to \nu_\mu$ which is mainly affected by the presence of $\epsilon_{\tau\tau}$ and $\epsilon_{\mu\tau}$. The dependence of probabilities on these parameters have been studied, among others, in [136, 162, 163].

For the appearance probability $\nu_\mu \to \nu_\tau$, the leading analytic behavior in terms of the small ϵ parameters was described in Sec. 5.2.1. From Eqn. 5.4, we estimate:

$$P_{\mu\tau} = P^{SM}_{\mu\tau} + \left(\frac{1}{2}\epsilon_{\tau\tau}\cos^2(2\theta_{23}) + 2\cos(2\theta_{23})\mathrm{Re}\{\epsilon_{\mu\tau}\}\right)(AL)\sin\left(\frac{\Delta m^2_{31}L}{2E}\right) + \mathcal{O}(\epsilon^2), \tag{5.9}$$

where we neglected the small solar mass squared difference Δm^2_{21}; $P^{SM}_{\mu\tau}$ is the oscillation probability in absence of NSI already discussed in section 4.2. Additional terms, which depend on both the real and imaginary parts of $\epsilon_{\mu\tau}$, are at second order in the perturbative expansion, and are expected to provide only small sensitivity in the regions with $\phi_{\mu\tau} \sim \pm\pi/2$. Since the term containing $\epsilon_{\tau\tau}$ is very small for an almost maximal atmospheric angle, the probability $P_{\mu\tau}$ is sensitive to large values of $\epsilon_{\tau\tau}$ only, unlike for $\epsilon_{\mu\tau}$ to which we expect a maximal sensitivity.

In the next subsection we will present correlation studies among the NSI parameters themselves, among NSI and standard oscillation parameters, and sensitivity studies regarding the measurement of NSI parameters.

5.4 Numerical Results

We present a comprehensive set of results obtained from our study of the NSI hypothesis in DUNE neutrino porpagation in this section.

5.4.1 Correlation among NSI parameters

In this section we study the impact of the additional channel on standard oscillation parameters.

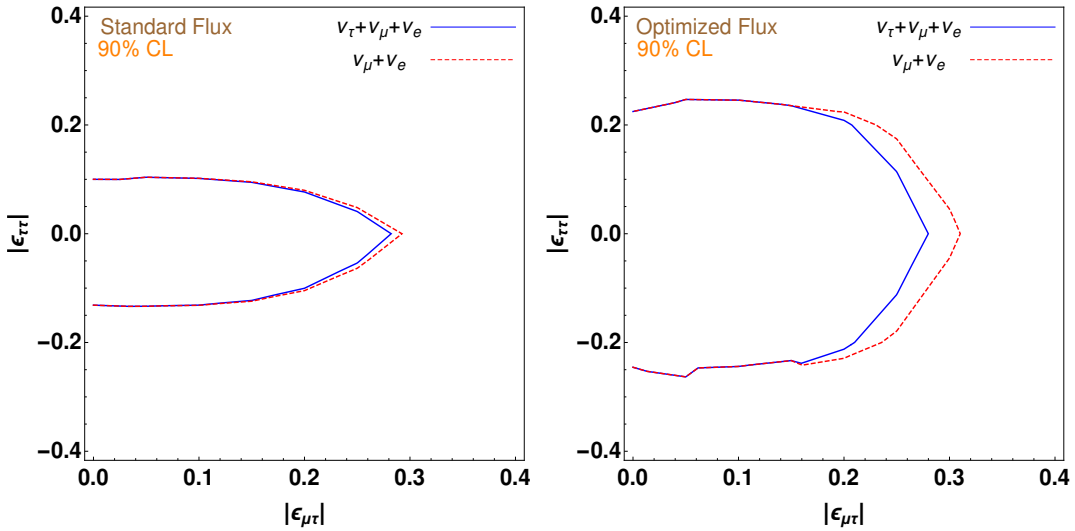

Figure 5.2: *Correlation plots among NSI parameters $|\epsilon_{\tau\tau}|$ versus $|\epsilon_{\mu\tau}|$ at 90% CL using the standard flux (left) and the optimized flux (right). All other standard and NSI parameters have been marginalised over. The solid, blue line show the effect of the ν_τ appearance channel addition. 20% ν_τ signal uncertainty, 6% tau detection efficiency and 2.45 S/B values detection efficiency has been assumed so as to depict the "worst-case" scenario among all sets considered. Normal hierarchy is assumed.*

We present correlation plots which represent the ability of the experiment to distinguish measurement sensitivity of oscillation parameters from one another. We observe from our results that only the $\epsilon_{\mu\tau}$ sensitivity is increased with minor or no affect of the other NSI parameter sensitivity. In the figure 5.2, we have plotted $|\epsilon_{\tau\tau}|$ versus $|\epsilon_{\mu\tau}|$. True values of the NSI parameters have been set to zero. All the standard oscillation parameters and the NSI parameters except those presented in the axes of the plot have been marginalized over. The study using the standard flux is on the left and the same using optimized flux is on the right; ν_τ statistics is significantly more in case of the optimized flux, as expected, due to the increase in ν_τ events but however, the other two channels in DUNE, namely the ν_μ disappearance and the ν_e appearance suffer due to increase in their background consequently rendering the total effect to

be such that the resultant sensitivity in the standard flux case is better than in the optimized flux case.

5.4.2 Correlation among NSI and Standard Oscillation Parameters

Let us study the bounds on $|\epsilon_{\mu\tau}|$ from our analysis in DUNE, with and without considering the ν_τ appearance channel. True values of the NSI parameters have been set to zero. All the standard oscillation parameters and the NSI parameters except those presented in the axes of the plot have been marginalized over.

In Figs. 5.3 we report the behavior of the θ_{23} as a function of $|\epsilon_{\mu\tau}|$ values; the dotted line represents the results obtained considering ν_μ disappearance and ν_e appearance only whilst the solid black line depicts when ν_τ appearance is also added to the analysis. Marginalization has been performed over all the rest oscillation parameters not shown the axes of the plots, including standard parameters and the NSI ones. θ_{23}-octant degeneracy is clearly visible. Our result is only shown for the "worst-case". We also performed the same for the "best case" and found the same behaviour only improving the $|\epsilon_{\mu\tau}|$ part of the correlation. The figure basically tells us that the only parameter that improves is the $|\epsilon_{\mu\tau}|$. We do not estimate the improvement on $|\epsilon_{\mu\tau}|$ from this figure as we will do it in details in a later section considering all possible cases of the experimental configurations.

In Fig.5.4, we have studied the correlations between $|\epsilon_{\mu\tau}|$ and its CP phase $\phi_{\mu\tau}$. Figure on the left is using the standard flux and that on the right is using the optimized flux. The lines show 90% CL contour curves in the $|\epsilon_{\mu\tau}| - \phi_{\mu\tau}$ parameter space. It can be inferred from this result that when we try to determine of $|\epsilon_{\mu\tau}|$, it is strongly correlated and depends on the CP phase value we have assumed. In particular, at $\phi_{\mu\tau} = \pm\pi$, the most stringent of these bounds are being reached. In order to remain at the same $P_{\mu\tau}$ values, one should be near to the CP conserving values of the phase, i.e, $\phi_{\mu\tau} = \frac{\pi}{2}$ or $\phi_{\mu\tau} = \frac{3\pi}{2}$ for lesser values of $|\epsilon_{\mu\tau}|$. Nothing much can be said about the sensitivities from the figures. This means DUNE shall not be able to put strong

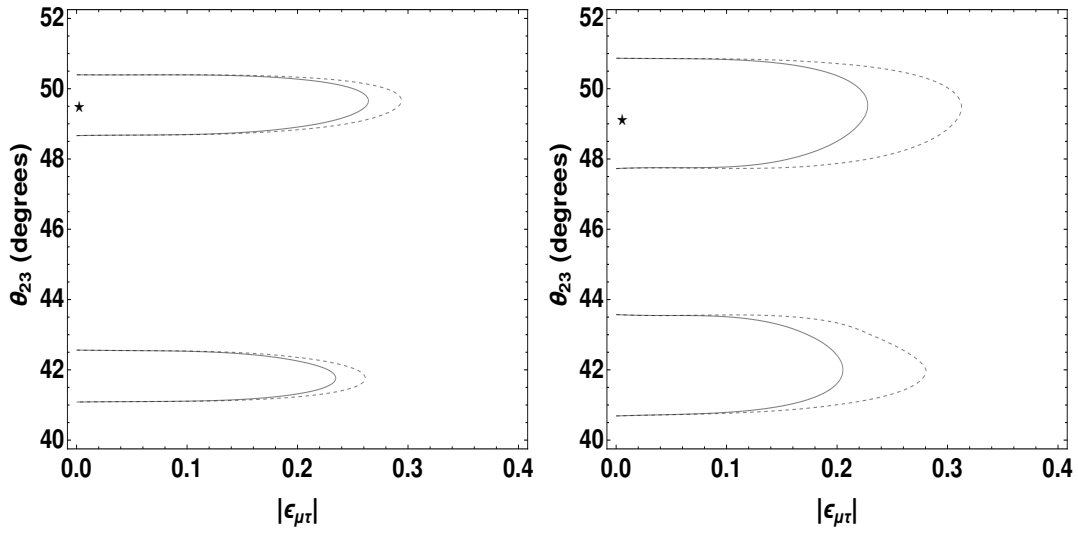

Figure 5.3: *Correlation plots among θ_{23} vs $|\epsilon_{\mu\tau}|$ for the standard neutrino flux (left) and optimized neutrino flux (right) at 90% CL. The solid and dashed lines are for the cases when ν_τ appearance channel are present and absent respectively. All other standard and NSI parameters have been marginalised over. 20% ν_τ signal uncertainty, 6% tau detection efficiency and 2.45 S/B values detection efficiency has been assumed so as to depict the "worst-case" scenario among all sets considered. Normal hierarchy is assumed. Star represents the simulated true values.*

bounds on this parameter.

In Fig. 5.5, the correlation between $|\epsilon_{\mu\tau}|$ and Δm^2_{31} is reported. The plots show there is no strong correlation among these two parameters, but however, the inclusion of the ν_τ appearance channel helps in increasing the sensitivity of $\epsilon_{\mu\tau}$ thereby also affecting this correlation in a straight-forward way to and we obtain the best-fit values to be.

We studied this using both the standard flux and the optimized flux and we notice that, the impact of ν_τ is significantly more in case of the optimized flux, as expected, due to the increase in ν_τ but however, the other two channels in DUNE, namely the ν_μ disappearance and the ν_e appearance suffer due to increase in their background consequently rendering the total effect to be such that the resultant sensitivity in the standard flux case is better than in the optimized flux case.

Lastly before ending this sub-section, we would like to state that the two degeneracies we mentioned in the earlier section. The re-appearance of $\epsilon_{\tau\tau}$ and $|\theta_{23} - \frac{\pi}{4}|$

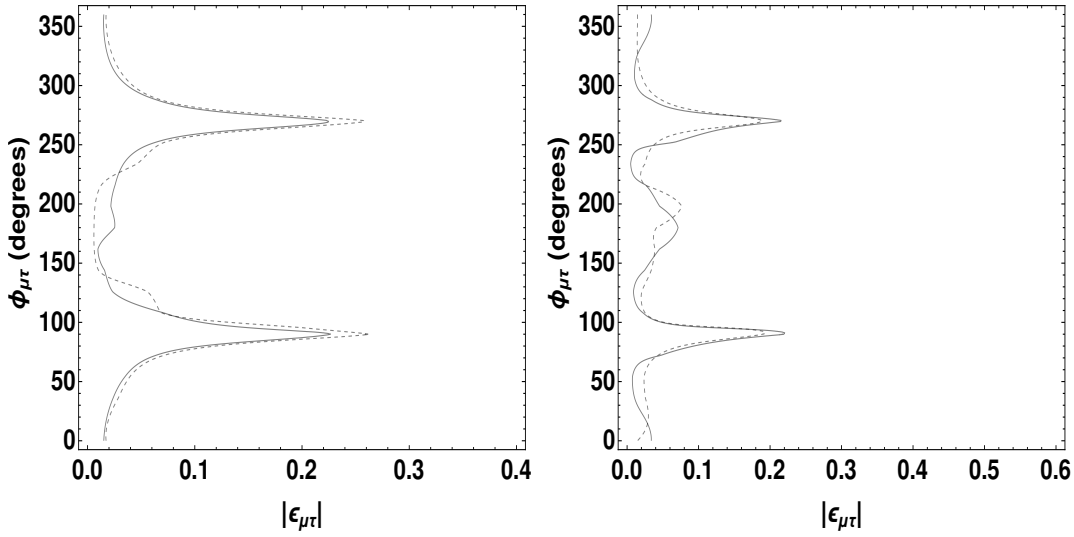

Figure 5.4: *Correlation plots among $\phi_{\mu\tau}$ vs $|\epsilon_{\mu\tau}|$ for the standard neutrino flux (left) and optimized neutrino flux (right) at 90% CL. The solid and dashed lines are for the cases when ν_τ appearance channel are present and absent respectively. All other standard and NSI parameters have been marginalised over. 20% ν_τ signal uncertainty, 6% tau detection efficiency and 2.45 S/B values detection efficiency has been assumed so as to depict the "worst-case" scenario among all sets considered. Normal hierarchy is assumed.*

degeneracy and the CP violating δ_{CP} and NSI parameter ϵ_{ee} and $\epsilon_{e\tau}$ degeneracy (including its phase) (see Figs. 3 and 4 in Ref. [142]), we studied using the ν_τ-appearance channel. Neither there was resolution on the two degeneracy cases, nor there was any significant sensitivity improvement. This is expected since the only parameter which improves to some extent is $\epsilon_{\mu\tau}$. So we have not presented those results here.

Thus we move on to the next section where we will study the $|\epsilon_{\mu\tau}|$ parameter sensitivity, and study it in details considering all possible configurations and understand the effect of systematics on its measurement. We will also compare our bounds with those derived from other existing studies.

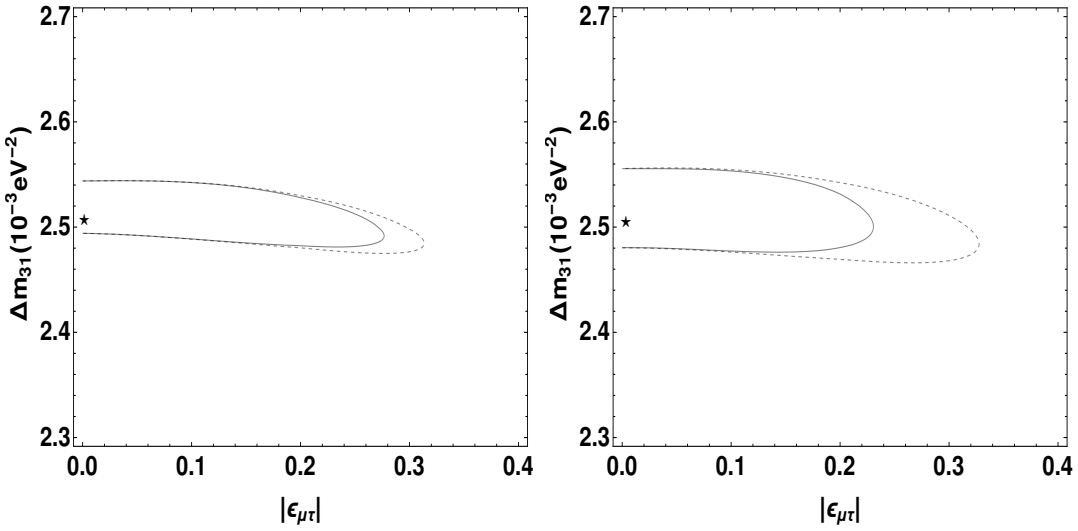

Figure 5.5: *Correlation plots among Δm^2_{31} vs $|\epsilon_{\mu\tau}|$ for 10% (left panel) and 20% (right panel) ν_τ signal systematic uncertainty. The standard neutrino flux has been assumed in the simulations. Horizontal dashed line indicates the 90 % CL limit (1 degree of freedom). The meaning of the curves is the same as the previous plots. Star represents the simulated true values.*

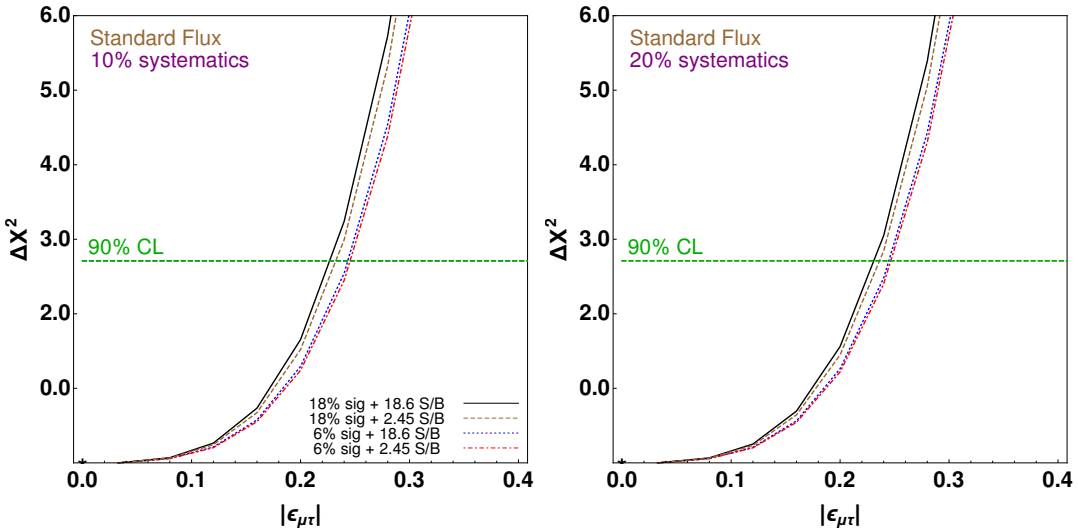

Figure 5.6: *$\Delta\chi^2$ vs $|\epsilon_{\mu\tau}|$ for 10% (left panel) and 20% (right panel) ν_τ signal systematic uncertainty. The standard neutrino flux has been assumed in the simulations. Horizontal dashed line indicates the 90 % CL limit (1 degree of freedom). The meaning of the curves is the same as the previous plots.*

5.4.3 Effect of Systematics, Experimental Reach and ν_τ Detection Efficiency

In figures 5.6 and 5.7 we report the $\Delta\chi^2$ as a function of $|\epsilon_{\mu\tau}|$ for 10% (left panel) and 20% (right panel) systematic uncertainties for the ν_τ signal, for the standard

and optimized fluxes, respectively. Plots have been obtained marginalizing over all standard and non standard parameters according to the constraints reported in tables 4.1 and 5.1, except for the solar parameters θ_{12} and Δm^2_{21} and the NSI parameter $|\epsilon_{\mu\tau}|$, which have been fixed to their best fit values. All the NSI phases have been left free with no bounds.

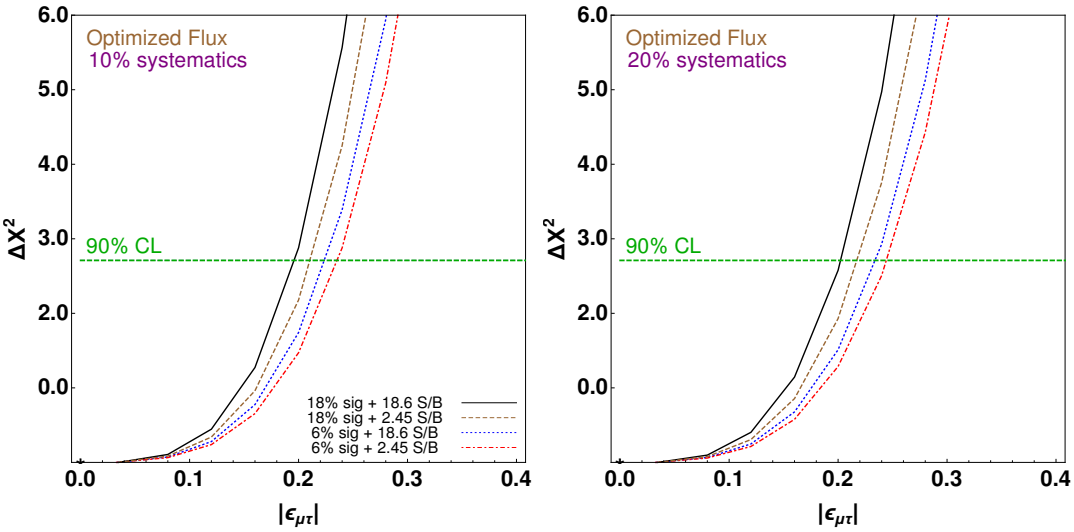

Figure 5.7: *Same as figure 5.6 but for the optimized flux.*

The common feature of the above figures is that there is a significant improvement in the bound for $|\epsilon_{\mu\tau}|$ by increasing the efficiency from 6% upto 18%, and the S/B from 2.45 upto 18.6; one can envisage an overall improvement at 90% CL of approximately 10% in the parameter relative uncertainty in the case of the standard flux and 18% using the optimized flux.

Sensitivity limits at 90% CL reached with all the three appearance and disappearance channels in DUNE using the two fluxes are presented in the Tables 5.2 and 5.3. The worst case scenario using the standard flux gives us a limit on the $|\epsilon_{\mu\tau}| \lesssim 0.25$ while the most stringent limit can be set using the optimized flux with the best efficiency (18%), the best S/B (18.6) and 10% systematic uncertainty, $|\epsilon_{\mu\tau}| \lesssim 0.20$. This limit is approximately 35% smaller than the one that can be set by DUNE using only ν_e appearance and ν_μ disappearance channels with standard flux, $|\epsilon_{\mu\tau}| < 0.32$, as estimated in Ref. [161]. We observe that a fit to the OPERA ν_τ events [116] did

in Ref. [117] predicted the bound $|\epsilon_{\mu\tau}| \lesssim 0.41$ (marginalising over all parameters including NSI parameters) which is almost a factor of two larger than the worst limit DUNE can set.

	Standard Flux (10% **sys**)			
	S/B = 2.45		S/B = 18.6	
Efficiency of ν_τ detection	6%	18%	6%	18%
$\lvert\epsilon_{\mu\tau}\rvert$	[0,0.2452]	[0,0.2320]	[0,0.2431]	[0,0.2264]
	Optimized Flux (10% **sys**)			
	S/B = 2.45		S/B = 18.6	
Efficiency of ν_τ detection	6%	18%	6%	18%
$\lvert\epsilon_{\mu\tau}\rvert$	[0,0.2349]	[0,0.2101]	[0,0.2232]	[0,0.1955]

Table 5.2: *Summary of 90% CL bounds on NSI parameter $|\epsilon_{\mu\tau}|$ that DUNE may set for 10% systematic uncertainty for the ν_τ appearance channel.*

	Standard Flux (20% **sys**)			
	S/B = 2.45		S/B = 18.6	
Efficiency of ν_τ detection	6%	18%	6%	18%
$\lvert\epsilon_{\mu\tau}\rvert$	[0,0.2463]	[0,0.2359]	[0,0.2445]	[0,0.2306]
	Optimized Flux (20% **sys**)			
	S/B = 2.45		S/B = 18.6	
Efficiency of ν_τ detection	6%	18%	6%	18%
$\lvert\epsilon_{\mu\tau}\rvert$	[0,0.2440]	[0,0.2169]	[0,0.2335]	[0,0.2021]

Table 5.3: *Same as table 5.2 but for a 20% systematic uncertainty for the ν_τ appearance channel.*

We checked that the other NSI parameters do not benefit so much from the ν_τ appearance channel and the sensitivity reach remains roughly the same as in the standard DUNE scenario with ν_e appearance and ν_μ disappearance only.

5.5 Discussion

The DUNE experiment is being proposed as a high precision next-generation neutrino experiment to be built in the USA. The baseline of DUNE is suitable for observing the neutrino mass hierarchy and measuring the CP phase δ_{CP} but only ν_e appearance

and ν_μ disappearance have been considered in most of the analysis. We studied the impact of the inclusion of $\nu_\mu \to \nu_\tau$ and $\bar{\nu}_\mu \to \bar{\nu}_\tau$ channels in the DUNE experiment, considering the electronic decay of τ.

Very few ν_τ events have been identified in experiments till now. The DUNE experimental setup is expected to collect and isolate sample high in ν_τ-statistics in the Far Detector and this will dwarf all existing data samples in terms of size and purity. Under this circumstance, we explored some of the important physics opportunities with 7 years running of DUNE with the ν_τ-appearance channel. The essential challenges of ν_τ-related searches is that τ-production threshold is high (due to large τ-lepton mass) results in low statistics compared to other channels; moreover, τ-lepton decays very fast, which in most of the cases too fast to be detected, producing either a lepton or hadrons with missing energy carried by neutrinos. For these reasons it is also very difficult to reconstruct the topology and the total energy of a ν_τ interaction. These are manifested in our choices of efficiencies and systematics and consequently reflected in our poor sensitivity results. Similar analysis was considered in [111] but for the hadronic decay of the τ. Usually, the muonic tau decay is not an option for detection as distinguishing a muon coming from the tau decay from a muon coming from a ν_μ CC interaction is very difficult. We considered the electronic decay mode of the tau, as considered in ICARUS [109] and nonetheless, we adopted an "effective description" approach in the sense that we studied to what extent each factors of detection efficiency, systematics, and experimental reaches (S/B) affect the results. We considered τ detection in the electronic channel, as proposed by the ICARUS collaboration and studied the sensitivity of standard and non-standard physics and the effects of 10% and 20% systematics cases, 2.45 and 18.6 S/B values (experimental reach) and τ detection efficiencies of 6% and 18% on the measurement of the parameters. We used two distinct neutrino fluxes dubbed as 'standard' and 'optimized' fluxes. It goes without saying that the complementarity of the various oscillation channels and new physics hypotheses on the neutrino oscillation phenomena, including the very successful three-massive-neutrinos paradigm, and NSI imply unique correlations among oscillation channels which in several scenarios offer information that cannot

be accessed in ways other than the ν_τ appearance channel.

At the background level, small statistics and weak sensitivity of the ν_τ appearance probability to the standard oscillations parameters, is a result of ν_e CC background events which are large and depends on the oscillation parameters. We found that the performances of the ν_τ appearance channel can be improved using a larger background. This counter-intuitive result is an artifact of few signal events being masked by background events and χ^2 being controlled by the background. We chose to fix the number of background events in our simulation so that on one hand these are parameter independent and on the other we can achieve the S/B ratios predicted for ICARUS. We further comment that this treatment is just for phenomenological way of understanding the impact of the ν_τ appearance channel; for experimental possibilities of achieving the same S/B, see Ref. [110].

There's an interesting possibility to search for ν_τ appearance in the near detector in DUNE; this strategy is sort of "background-free" since there should be no ν_τ-s from the beam, and has been adopted in a study in NOνA [164]. The sensitivity to some of the physics scenarios we described in this thesis will possibly be increased.

Based on the simulations we performed and presented in the chapters 4 and 5, we make some conclusions:

- For the standard physics, the addition of ν_τ appearance channel does not improve the sensitivities of any of the standard neutrino oscillation parameter set by the other two channels already being considered in DUNE, even with the optimized flux set-up. This can be traced to (a) limitation in statistics and (b) leading order dependency of probability on Δm^2_{31} and θ_{23}.

- The performances of the tau optimized flux in the ν_e appearance and ν_μ disappearance channels result generally in worsening of the sensitivities, thus overshadowing the advantage one may get from the increase in the ν_τ statistics. This is mainly due to the increased background events in both the ν_e and ν_μ channels.

- In the new physics cases, the NSI parameter sensitivities are hardly affected by

the addition of the new channel, except for the coupling $|\epsilon_{\mu\tau}|$ for which improved limits (about 15% better than the no-τ case) was found.

Finally, we remark that it may be possible to improve the above-mentioned sensitivities if we add to this analysis the tau hadronic decay channel as well [111], which has a better ν_τ detection efficiency and consequently a bigger statistics. Not only this, other means of achieving greater statistics like increasing the experiment running time from 7 to 10 years or including ν_τ statistics from other experiments like OPERA may be a direction to consider in the future. Also, understanding the physics sensitivities from the DUNE near detector which we have not considered here maybe useful.

Chapter 6

Dark Sector Physics: Phenomenology of Dark Photon

This chapter and the next one is dedicated to the physics of dark sector, particularly the dark photon (DP). Here we will discuss the theoretical and observational physics motivations and subsequently some models for the study of dark photon. Along with that we will also present a brief overview of the experimental searches for DP till date. In the next chapter, we will develop an indigenous method to search for DP in the PADME experiment in the National Laboratory at Frascati (LNF-INFN).

6.1 Introduction

As discussed in the thesis introduction, the SM provides a consistent description of our universe except for some cases where BSM physics is required. One of the most diligent and phenomenological considerations to capture the impact of new physics is through what is known as the dark sectors (or hidden sectors). The "darkness" of this sector is usually attributed to a a new spectrum of particles without having the strong, weak, or electromagnetic charges of the SM. Of course, they interact gravitationally (if massive). However, they may "talk" to or interact with the SM particles through some mediators, a scenario commonly known in the literature as "portal" formulation of the dark sector [165, 166, 167]. There are a plethora of models having these hidden sector formulation and their comprehensive description is extremely broad; however there is a standard way of classifying these models which

helps to explore the related phenomenology effectively yet systematically. This is done via considering the mediator spin and parity [1]. The most familiar ones are [168]:

- "Scalar" Portal [2]: A scalar ϕ(x), leading to the Higgs portal through the operator $(\mu\phi + \lambda\phi^2)$ ($H^\dagger$ H), H is the SM Higgs doublet.
- "Vector" Portal: A vector field A$'$ (x), through the operator $\frac{\epsilon}{2}F_{\mu\nu}F'^{\mu\nu}$, where $F'_{\mu\nu} = \partial_\mu A'_\nu - \partial_\nu A'_\mu$.
- "Fermion" Portal, also commonly considered as the "neutrino portal": A fermion N(x), having the interaction $\sim$ y_N L^c H N, where N plays the role of a right-handed neutrino.

We will concentrate on the "Vector"-portal in this thesis.

6.2 Dark Photon Model

Dark photon also known as hidden photon or A$'$ boson, is a massive vector boson arising due to a new $U(1)'$ gauge symmetry on top of the Standard Model symmetries. This particle mixes with the ordinary photon (γ) via kinetic-mixing term [169, 170]. This mixing allows γ-A' oscillations and produces a small coupling between A$'$ and the electrically charged matter like the electron. Although this new mediator means there exists a new kind of force in nature, there are reasons why it has not been observed yet:

- This new particle is very heavy (around TeV), therefore outside the reach of the current energy scale being achieved in the high energy laboratory experiments. In this case, the forces mediated by them is extremely short ranged.

[1] Note that these are essentially constrained by the Gauge and Lorentz symmetries of the action.

[2] In a similar manner, one may build a pseudo-scalar portal where the mediator is a pseudo-scalar boson (see Ref. [168])

- The new particle interacts very feebly with SM sectors; consequently too weak to be observed.

The first possibility keeps being actively investigated mainly in collider experiments, with the current high energy frontier set by the LHC experiments. However, the so far unsuccessful search for new heavy states has triggered in recent years an increasing interest in the second possibility, with many proposals and many new ideas to hunt for new physics at the intensity frontier (see Refs. [165, 166] for a review).

We shall consider the second possibility in this thesis. DPs are characterized by their coupling to the electromagnetic current J_{μ}^{EM},

$$\mathcal{L} \sim \epsilon e A'_{\mu} J_{\mu}^{EM} \tag{6.1}$$

Note that this interaction is suppressed relative to the electron charge e by the parameter ϵ, which can be small. This parameter can take values in the range $10^{-4} - 10^{-2}$ if generated at one-loop or $10^{-6} - 10^{-3}$ if the mixing is generated at two-loop order of interaction [171, 172, 173] [3]. Having an extra $U(1)'$ gauge symmetry on top of the SM symmetries means that at low energy (EW scale) after symmetry breaking the DP mixes directly with the SM photon (See Appendix 10.1 for details). The effective Lagrangian goes as:

$$\mathcal{L}_{eff} = \mathcal{L}_{SM} - \frac{1}{4} F'_{\mu\nu} F'^{\mu\nu} + \frac{1}{2} m^2_{A'} A'_{\mu} A'^{\mu} - \frac{1}{4} \epsilon F'_{\mu\nu} F^{\mu\nu} \tag{6.2}$$

where F′ is the field strength of the hidden gauge field A′, $F_{\mu\nu}$ the SM EM field strength and $\mathrm{m}_{A'}$ the mass of the DP [169]. Notice that in this model the only new independent parameters are the coupling or the kinetic mixing (ϵ) and the mass of the DP ($\mathrm{m}_{A'}$). The mass generation mechanism of DP can be achieved via the Higgs-like mechanism due to spontaneous symmetry breaking by a dark scalar and can take a large range of values (from sub-eV until GeV) [169, 175]. Since the DP couples to the electron which has mass (m_e) of about 0.5 MeV, one may divide the DP models

[3] DP mass can also be generated via Stuckelberg mechanism which is relevant in string theories [174].

according to their decay[165, 171, 176, 170]:

- For $m_{A'} > 1$ MeV, a DP decays dominantly into charged particles e^+e^-, $\mu^+\mu^-$, or $\pi^+\pi^-$, or to light hidden-sector particles (if present in the dark sector), which again decays to SM particles. See Fig. 6.1 for the predicted branching ratios of A$'$ decaying into SM particles. The scenario is often dubbed as the visible DP model if the end products are visible particles. If the DP decays into hidden sector states, the model is referred to as the invisible decay model. The DP may couple also to other non-SM particles in the hidden sector. For example, there maybe new matter (fermionic) states charged under the new U(1)$'$ which may include particles that constitute the DM. If decays of the DP to the hidden sector states are kinematically forbidden such couplings are irrelevant to the phenomenology and the standard branching ratios hold true as shown in the figure. A DP with mass $m_{A'} \sim MeV - GeV$ is compatible with explaining experimental anomalies like the anomaly observed in decays of excited 8-Be nuclei to electron-positron pairs [177, 178, 179, 180] and the long-standing discrepancy between the measured value of $(g - 2)_\mu$ and the theoretical prediction [167]. Usually electron (positron) or proton fixed-target experiments and hadron colliders offer stringent limits on such particles [165, 166].

- For $m_{A'} < 1$ MeV, the DP cannot decay to e^+e pairs as this is kinematically forbidden [4]. The kinetic mixing implies that the propagation eigenstates of the photons and the interaction eigenstates of the photons are different, leading to $\gamma \rightarrow A'$ oscillation phenomena which are proposed to be searched for in typical light-shining-through-the-wall experiments [181] and Helioscopes observations [182]. The oscillation mechanism may also be responsible for A' as the observed DM relic density in the universe. Direct DM detection experiments may test this scenario; moreoever, indirect observations through the A$'$ decaying into three photons can also be observed above the astrophysical diffuse X-ray backgrounds [183, 184]. CMB bounds on such oscillation are also essential probes of this

[4] only a much slower decay to three photons maybe allowed

sector [185].

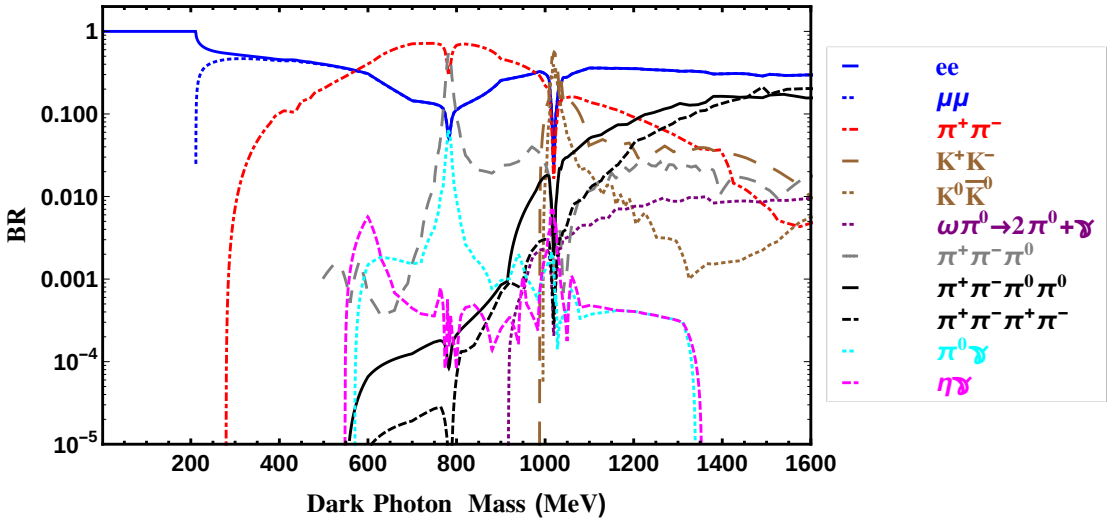

Figure 6.1: Dark photon decay branching ratios into SM particles (figure taken from Ref. [205]).

There are several theoretical studies on this kind of $U(1)'$ extended models (see Refs. [172, 173, 174] for some of the main ideas and related phenomenology). In the next section, we shall briefly describe the quest to understand the DM characteristic through this vector portal.

6.3 DP as a mediator of Light DM

If there is BSM physics not at particularly high energies, then the dark sector particles and their interactions with the SM could well be within experimental reach. However these particles must couple very feebly to the SM particles or else we already would have seen them. Just to give an example, if the hidden sector contains particles with mass below 1 GeV they would have easily escaped detection by underground experiments seeking for halo DM. This motivates complementary searches and search strategies in order to probe this mass region. Many interesting and testable scenarios consider light DM with mass in the $\sim$ (1 MeV - 1 GeV) range, charged under a new

$U(1)'$ symmetry and that interacts with the SM particles via the exchange of a vector boson A$'$. Since decay process is determined by the ratio of the DM and the mediator A$'$ masses, the DP can decay only into SM particles (visible decay) or dominantly to light DM states (invisible decay) depending upon their relative masses. Several DM models attribute the stability of the DM via some discrete symmetry under which SM fields and dark sector fields are oppositely charged, consequently the DM particles do not have direct couplings to the SM and cannot decay. However, the DM may interact with the SM through some mediators coupling to both the SM and the DM. The gauge and Lorentz symmetries of the SM lagrangian restrict the ways in which the mediator can couple to the SM. If the mediator is a vector force carrier from an additional U(1)$'$ gauge group under which DM is charged, a kinetic mixing interaction is gauge invariant under both $U(1)'$ and $\mathrm{U}(1)_Y$. Consequently, a mixing $\frac{\epsilon}{2}F'_{\mu\nu}F^{\mu\nu}$ is induced and is responsible for the phenomenology considered in a light DM model. In this case, the particle spectrum in the dark sector is important in establishing constraints on the model, as well as the parts of parameter space favored by cosmological and astrophysical observations of DM. Simply based on the nature of its spin, DM can be a fermion, χ, or a scalar boson, ϕ, that couples to the DP through the hidden sector gauge interactions.

$$\mathcal{L} = \chi^c(i\not{D} - m_\chi)\chi, \tag{6.3}$$

for a fermion DM and

$$\mathcal{L} = (D^\mu\Phi^\dagger)D_\mu\Phi - m^2|\Phi|^2, \tag{6.4}$$

for a scalar DM with $D_\mu = \partial_\mu - ig'A'_\mu$; we use the symbols g$'$ as the dark sector coupling between the mediator and the light DM [165]. Although the parameter space of the model looks broad, different regions are compatible for different reasons. In fact, several specific regions are particularly important targets, from theoretical point-of-view or because exploring these regions decisively tests some of the experimental anomalies observed [165, 166, 171, 170].

If a thermal process is responsible for production of DM, freeze-out of DM χ

consists of DM annihilations into SM particles. First scenario is where the secluded annihilation of DM to pairs of mediators via $\chi\chi \to A'A'$ (for $m_{A'} < m_e$). Then this is followed by mediator decaying into SM particles and direct annihilation to SM final states via virtual mediator exchange in the s-channel without an intermediate step, $\chi\chi \to A' \to SM\ SM$. [186]. This sets up a minimum value for the SM-mediator coupling ϵe which is compatible with a thermal history of the DM in its relation to the observed relic density. Alternatively, other production mechanism includes Freeze-in production of DM [187] where at first the DM is out-of-equilibrium and then slowly comes into equilibrium and gets produced as the Universe expands; for this, one requires sufficiently small couplings (note that such small couplings are natural in kinetic mixing of DP scenarios). However, depending upon the mass of the DP, the final DM abundance maybe completely independent of $m_{A'}$ [165]. Cosmological history and terrestrial constraints becomes very important for DM masses between MeV and GeV. Refs. [188, 189]. On the other hand, for DM becomes lighter than an MeV, bounds from DM self-interaction, stellar emission, N_{eff} and terrestrial constraints comes into play. DM-electron couplings and their constraints and scalar-mediated nucleon couplings were discussed in Ref. [190].

In conclusion to this section, we wish to highlight the motivation for DP also lies in understanding the portal to the DM which has eluded us in all experimental searches hitherto. Next we move on to discuss a still stronger reason to look for this DP: to resolve an anomaly observed in a nuclear physics experiment.

6.4 Beryllium-8 Anomaly

The ATOMKI collaboration has observed in the excited ^{8}Be nuclear decays an anomaly which we will describe below [177, 178, 179]. This is particularly relevant for the present work in this thesis since the new experimental technique that we will illustrate to search for the dark photon is particularly well suited to test, at least in some regions of the parameter space, the particle physics explanation based on a new gauge boson with mass $m_{A'}$ of 17 MeV kinetically mixed with the photon [180].

The experimental set-up consists of a pair spectrometer that has observed the decays of ^{8}Be* with high statistics. A proton beam with centre-of-momentum energy of 1.03 MeV (resonance energy) collide with Li nuclei to form the resonant state ^{8}Be*, and a small fraction of these decay via the $^8Be^* \rightarrow ^8 Be$ e$^+$ e$^-$ process. There are plastic scintillators and multi-wire proportional chambers in the plane perpendicular to the proton beam. These give us the measurement of the electron and positron energies, as well as the opening angle of the e^+e^- pairs that travel through the detector plane; basically one gets the distributions of opening angle θ and invariant mass m$_{ee}$ of the electron-positron pairs. SM predicts that the opening angle θ and m$_{ee}$ distributions should fall monotonically.

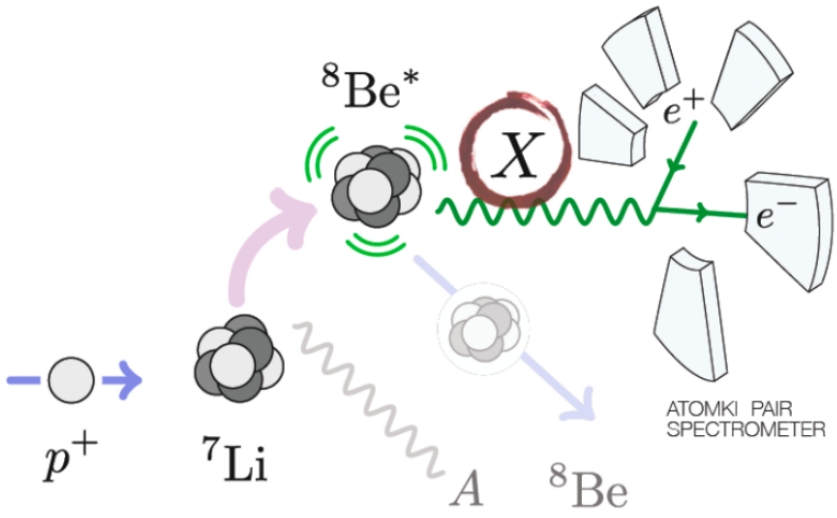

Figure 6.2: Schematic description of the ^{8}Be experiment.

But the experiment observed (see Fig. 6.3) that θ distribution consists of a high-statistics bump peaking at $\theta = 140^o$ and the behaviour becomes SM-like prediction at around $\theta = 170^o$ [177], which seems unaccountable by any known physics (schematic representation of the experiment is provided in Fig.6.2). The anomaly of observing excess pairs of electron-positrons has a high statistical significance of 6.8σ which excludes the possibility that this arises as a statistical fluctuation. The shape of the excess is remarkably consistent with that expected if a new particle with mass

$m_{A'} = 17.0 \pm 0.2(\text{stat}) \pm 0.5(\text{sys})\,\text{MeV}$ [179] is being produced in these decays. The strength of the A' coupling to e^+e^- pairs, parameterized as $\epsilon = \sqrt{\alpha'/\alpha}$ with α ($= \frac{1}{137}$) being the QED coupling and α' the $U(1)'$ fine structure constant, the later being constrained by several experimental considerations which we will describe in details in the next section. In the Atomki setup, $A' \to e^+e^-$ decays must occur in the few cm distance between the target and the detectors. This implies a lower limit $\epsilon/\sqrt{\text{Br}(A' \to e^+e^-)} \gtrsim 1.3 \times 10^{-5}$. In the following we will assume for simplicity $\text{Br}(A' \to e^+e^-) = 1$; if the A' decays with a non-negligible rate into invisible dark particles χ, with $m_\chi < m_{A'}/2$, the quoted limits need to be accordingly re-scaled. However, in case the invisible decay channel becomes largely dominant, other limits different from the ones discussed in this paper apply. We refer to Ref. [191] for details.

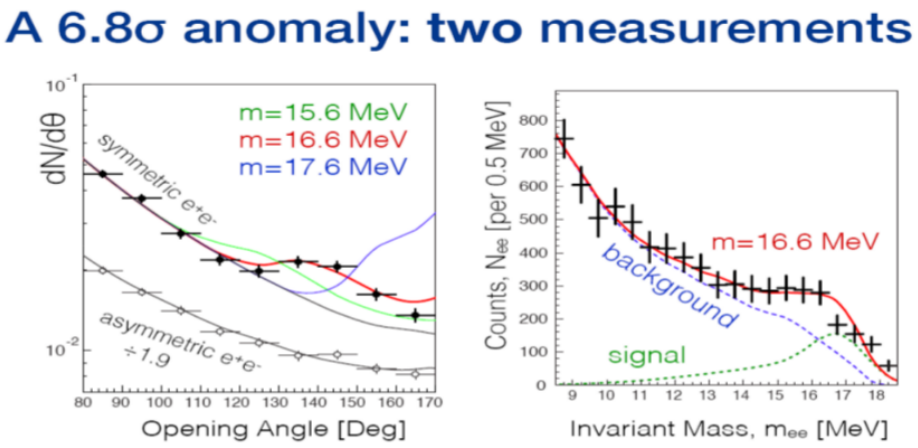

Figure 6.3: Plot adopted from Ref. [177].

Thus we see a light gauge boson is favored by the experimental anomaly and the need to contemplate searches for this particle by other methods and experiments. We will develop a new method for producing this DP in a laboratory experiment (PADME) and the key idea on advocating this new technique lies in the observation that in Be experiment the A' (if it exists) decays to electron-positron final products. Our proposal originates from this fact because this DP particle is seen to be decaying to electron-positron pairs, it can also be *produced* from the same channel as well,

that is, from the annihilation electron-positron pairs. Before we discuss about this in details, let us briefly take a look at the methods of detection, the existing bounds and the different experiments that have already searched for this particle.

6.5 Search for DP in Experiments

Searches for new particles are part of the intensity frontier since intense beams of electrons, positrons or protons are required to produce DP in sufficient quantities to compensate for their weak coupling to ordinary matter. Current and planned DP searches are characterized by their strategies for production and detection. The main DP searches in experiments are the following:

- In e^+e^- colliders via Bremsstrahlung-like process $\mathrm{e}^{\pm}\ \mathrm{Z} \rightarrow e^{\pm}\ \mathrm{Z} + \mathrm{A}'$, for electrons (or positrons) [192].

- Fixed target experiments via resonant process: $e^+e^- \rightarrow \mathrm{A}'$ and non-resonant process: $e^+e^- \rightarrow \gamma A'$ [193].

- Meson decays (whereever produced), $\pi^0/\eta/\eta' \rightarrow \gamma A'$ and rare meson decays such as $\mathrm{K} \rightarrow \pi A'$, $\phi \rightarrow \eta A'$ and $D* \rightarrow D^0 A'$ [194].

On the other hand, the main methods for DP detection can be broadly summarized in bump hunt in visible final-state invariant mass, bump hunt in missing-mass and vertex detection. In the scenario of an invisible mediator decay, as discussed in the last section, there are two main approaches to observing a hidden sector signature: either a DP is produced at a beam-dump and promptly decays into invisible states, and the invisible states scatter off material in a detector (placed downstream from the beam-dump), or the presence of the invisible states is inferred from missing momentum and/or missing mass either at a high-energy collider or fixed-target experiment.

Let us next take a look at the existing constraints on the DP parameter space from the myriad of experiments discussed above.

6.6 Existing Bounds on Dark Photon

A beam dump is an experimental set-up designed to absorb the energy of particles within an energetic beam. Electron beam dump typically consists of a beam of electrons projected on a fixed target. Lower limits on ϵ much stronger than what implied by the Atomki experimental setup are obtained from electron beam dump experiments. Old data from KEK [195] and ORSAY [196] have been reanalyzed in Ref. [197] yielding, in the interesting mass range $m_{A'} \sim 17\,\mathrm{MeV}$, $\epsilon \gtrsim 7 \times 10^{-5}$. A stronger limit, $\epsilon \gtrsim 2 \times 10^{-4}$ was obtained in [198] from a reanalysis the E141 experiment at SLAC [199]. However, for a $m_{A'} \sim 17\,\mathrm{MeV}$ the excluded region is very close to the kinematical limit of the sensitivity (see Fig. 7.7) and it has been recently pointed out, by direct comparison with exact calculations [200], that the WW (Weizsäker-Williams) approximation [201, 202, 203] adopted to derive the limits become inaccurate in this kinematic region, tending to overestimate the reach in mass [200, 204, 194] (see Fig. 6.4). For primary energies in the the range $10 - 20\,\mathrm{GeV}$, as was the case for the E141 beam [199], and for $m_{A'} \sim 20\,\mathrm{MeV}$, the WW approximation yields an A' production cross section about 50% larger than the exact calculation (see Fig. 2 in Ref. [194]) and it also overestimates the A' emission spectrum at large energies (see Fig.4 in the same reference), in which case the number of expected positrons falling within the 1.1 mrad angular acceptance of the experiment would be overestimated both because of the larger boost, and also because of the larger lifetime dilation that would cause the A' to decay closer to the detector. Besides this, let us note that an A' slightly heavier than the benchmark value of 17 MeV would in any case evade the E141 limit. It is then questionable if, for $m_{A'} \gtrsim 17\,\mathrm{MeV}$, the E141 constraints on the A' couplings can be considered as firmly established. Conservatively, we will assume that the corresponding region is still viable.

Upper bounds on ϵ in the relevant A' mass range also exist, see Fig. 7.7 and also Ref. [204]. The KLOE-2 experiment has searched for $e^+e^- \to \gamma A'$ followed by $A' \to e^+e^-$ setting the limit $\epsilon < 2 \times 10^{-3}$ [206], while constrains from the anomalous magnetic moment of the electron [207] yield $\epsilon < 1.4 \times 10^{-3}$ [208, 209].

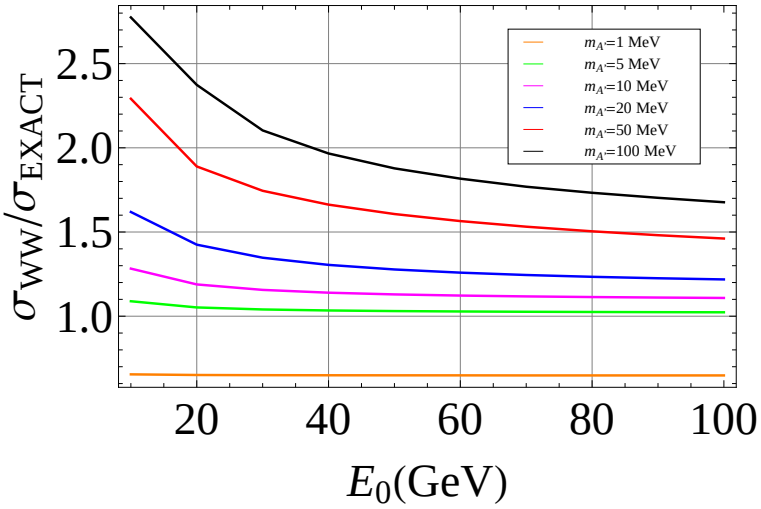

Figure 6.4: WW approximation and exact production for A′ in e- Z → e- Z + A′ as a function of the electron energy E_0 for various A′ masses. (figure taken from Ref. [194]).

A comparable limit stems from BaBar searches for $A' \to e^+e^-$ decays, but it only applies for $m_{A'} > 20\,\text{MeV}$ [210] and other fixed target experiment [211]. In summary, we will take the interval

$$7 \times 10^{-5} \leq \epsilon \leq 1.4 \times 10^{-3}\,, \tag{6.5}$$

as the window allowed for a 17 MeV A' decaying dominantly into e^+e^-. This corresponds to a DP width $2.0 \times 10^{-4} \leq \Gamma_{A'}/\text{eV} \leq 8.1 \times 10^{-2}$.

After this discussion we move on the description of the novel method for searching for the DP in the PADME experiment and presenting the results obtained from our study.

Chapter 7

Dark Sector Physics: Dark Photon Search at PADME

7.1 Introduction

This chapter is primarily based on the work in Ref.[212]. We will develop and describe a new method for resonant production of dark photon at the PADME experiment in the Frascati National Laboratory. Moreover we will show how this method is particularly suited for the search for the DP in the parameter range suited to explain the 8 Be anomaly of the ATOMKI experiment. This connection is very natural since the DP if it exits decays to electron-positron pairs in the nuclear experiment and PADME (beam from DAΦNE) is capable of searching the DP using the same channel in production.

7.2 PADME experiment at LNF

Collider searches for dark photons have been carried out in electron beam dump experiments (see [197] for a review) assuming A'-strahlung as the leading production mechanism in electron-nucleon scattering. In terms of perturbative expansion of Feynman diagrams, it can be seen that this process is of order α^3, see Fig. 7.2(a). Therefore the production is expected to be small. Another is the usual QED process of positron annihilation off an atomic target electron with two final state photons, where one photon is replaced by one A' see Fig. 7.2(b), corresponding to a process

of $O(\alpha^2)$. This we expect to be one order-of-magnitude less than that of the A'-strahlung process. However to perform this search strategy, one needs positron beams impinging on a fixed target consisting of free electrons in context to beam dump experiments. Only few facilities with positron beams exist in the world, thus A' searches with positron beams is somewhat unique. Frascati Beam test Facility will be able to provide beams suitable for fixed target experiments, and correspondingly only a few experimental proposals have been put forth [213, 214, 193]. We will describe this process and specific resonant production process that can be carried out in the Frascati PADME experiment [193].

	pot/yr	E_{min} (MeV)	E_{max} (MeV)
e^+	10^{18}	250	550
e^-	10^{18}	250	800

Table 7.1: *Beam parameters for the Frascati BTF.*

7.3 Experimental Setup

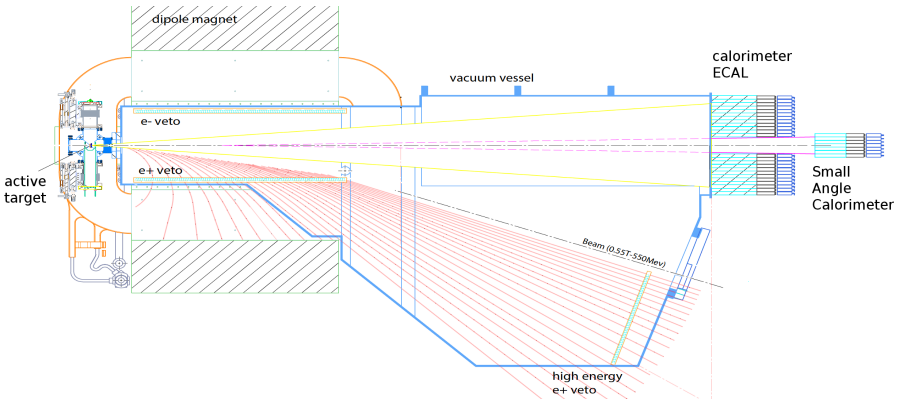

Figure 7.1: *Schematic of the PADME Experiment. Figure taken from Ref. [215].*

The PADME experiment [216, 193] at the DAΦNE LINAC Beam Test Facility (BTF) [217] of the INFN Laboratori Nazionali di Frascati (LNF) has been designed to search for DP by using a positron beam [218] impinging on a thin target of low

atomic number. The A' can be detected in the invisible channel by searching for a narrow bump in the spectrum of the missing mass measured in single photon final states, originated via $e^+e^- \to \gamma A'$. The experiment will use a 550 MeV positron beam on a 100μm thick active target made of polycrystalline diamond ($Z = 6$). To keep under control the counting rates the beam intensity will be kept at $\sim 10^{13}$ positrons on target per year (pot/yr), that is well below the maximum available intensity (cfr.Tab 7.1). The low Z and very thin target are intended to minimize the probability of photon interaction inside the target since, in order to reconstruct accurately the missing mass, the measurement requires a precise determination of the four-momentum of the γ produced in the annihilation. The recoil photons will be detected by a quasi cylindrical calorimeter made of inorganic crystals located 3.3 m downstream the target, while the non-interacted positrons, which constitute the vast majority of the incoming particles, are deflected outside the acceptance of the calorimeter by a 1 m long dipole magnet. Three different sets of plastic scintillator bars will serve to detect electrons and positrons. Profiting by the presence of a strong magnetic field, these detectors, intended to provide an efficient veto for the positron bremsstrahlung background, can also be used to measure the charged particles momentum. The PADME detector is thus able to detect photons and charged particles and it will be sensitive to invisible ($A' \to \chi\bar{\chi}$) as well as to visible ($A' \to e^+e^-$) DP decays.

7.4 A' production via resonant e^+e^- annihilation

A very important observation is that for A' masses $\gtrsim 1\,\mathrm{MeV}$, the process of resonant e^+e^- annihilation into on-shell A' becomes possible. The Feynman diagram for this process is in Fig.7.2(c), and the process being of $O(\alpha)$, is parametrically enhanced with respect to the previous two production channels. Moreoever being sufficiently close to this resonant process one may look to reduce other backgrunds due to its enhanced cross-section. For a positron beam fixed target experiment like PADME in a dedicated mode this is particularly impeccable to strategize and implement since the beam energy can be suitably tuned with a particular peaked centre-of-momentum

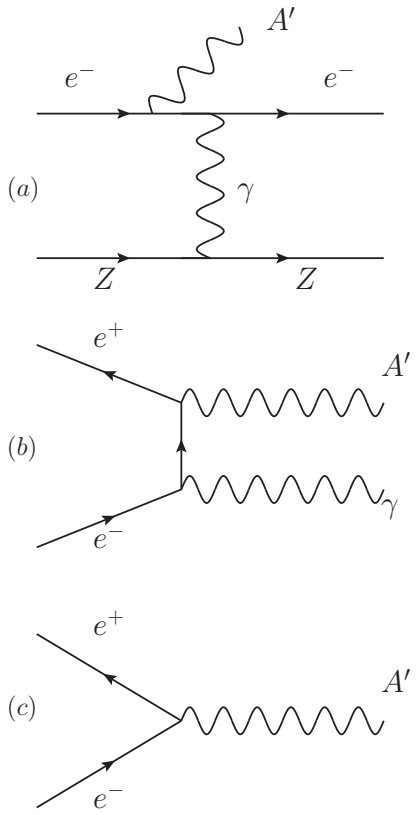

Figure 7.2: *A production modes in fixed target e-/e+ beam experiments. (a) A'-strahlung in e–nucleon scattering; (b) A' -strahlung in e- e+ annihilation; (c) resonant A' production in e+ e- annihilation.*

energy for the positrons hitting the target. This process also contributes in electron beam dump experiments via A' production from annihilation of secondary positrons and needs to be taken into account for proper analysis [219]. In particular, it was found that due to the contribution of resonant A' production, the E137 data exclude a parameter space region larger than it was previously though [197, 198]. We have included this extended excluded region; it corresponds to the area in light grey color towards the bottom of the plot in Fig. 7.7.

7.4.1 Resonant Production of A$'$

Taking into account the importance of resonant annihilation to create DP we consider the sensitivity of the PADME experiment to the production process $e^+e^- \to A' \to$

e^+e^-. We need to modify trifle the experimental configuration to implement this resonant production mechanism to its fullest advantage. The thin diamond target should be replaced by a tungsten target of several cms of length. This is mainly due to:

1. The thick target will absorb most of the incoming positron beam and the related EM showers, and in any case degrade sufficiently the energy of the residual emerging particles. This means that the charged particles background can be easily deflected and disposed of sufficiently due to thickess of the target. The A' produced in e^+e^- annihilation, if long lived enough, will emerge out of the dump and escape without interacting, decaying inside the downstream vacuum vessel, producing an e^+e^- pairs of well defined energy. Therefore we straight-off gain five orders of magnitude with respect to the thin target running mode, (see Table 7.1) for the full beam intensity of 10^{18} pot/yr [1].

2. The second advantage is that a thick enough target provides a more-or-less continuous energy loss for the incoming positrons propagating through the dump; this basically means that they can efficiently 'scan' radiatively in energy for locating very narrow resonances in the regions throughout the parameter space (DP mass).

To correctly consider this second point it is necessary to study the energy distribution of positrons inside the BTF beam which is tuneable to a nominal energy E_b within the range $250 \leq E_b/\mathrm{MeV} \leq 550$, and can hence be described by a Gaussian function $\mathcal{G}(E) = \mathcal{G}(E; E_b, \sigma_b)$ where $\sigma_b/E_b \sim 1\%$ is the energy spread. The probability that a positron with initial energy E will have an energy E_e after traversing $t = \rho \cdot z/X_0$ radiation lengths (with ρ the density of the material in g/cm^{-3} and $X_0 = 6.76\,\mathrm{g/cm^{-2}}$ the unit radiation length in tungsten), is given by [220, 221]

$$I(E, E_e, t) = \frac{\theta(E - E_e)}{E\,\Gamma(bt)} \left[\log \frac{E}{E_e}\right]^{bt-1}, \tag{7.1}$$

[1] The maximum number of $e^\pm$ deliverable in one year given in Table 7.1 is LNF site authorization limited by the efficiency of the existing radiation shielding. However, technically the BTF could deliver up to 10^{20} electrons or positrons on target per year.

where $b = 4/3$ and Γ is the Euler gamma function. Eqn. 7.1 neglects secondary positrons from EM showers, as well as the loss of primary positrons from $e^+e^- \to \gamma\gamma$ annihilation, but is still sufficiently accurate for our purposes. The e^+ energy distribution after t radiation length is given by:

$$\mathcal{T}(E_e, t) = \int_0^\infty (E)\; I(E, E_e, t)\; dE\,. \tag{7.2}$$

Integrating $\mathcal{T}(E_e, t)$ in t one would obtain the track-length distribution for primary positrons. However, for an accurate determination of the detectable number of A', the coordinate $z = tX_0/\rho$ of the production point is important, especially for the larger ϵ, and hence shorter decay lengths. Thus, the integration in t should be performed only when accounting for the probability of A' decaying outside the dump. We fix the origin of the longitudinal coordinate at the beginning of the dump, z_D is the end point of the dump, and $z_{\rm det}$ is the distance between the origin and the detector. The A' decay length

$$\ell_\epsilon = c\,\gamma\tau_{A'}, \tag{7.3}$$

with $\gamma = \frac{m_{A'}}{2m_e}$ the time dilation factor, depends quadratically on ϵ through the lifetime $\tau_{A'} = 1/\Gamma_{A'}$ (but it does not depend on $m_{A'}$, see below). For the range of ϵ given in Eqn. 6.5, $16 \gtrsim \ell_\epsilon/\text{mm} \gtrsim 0.04$.

7.4.2 Cross-section

Let us first look at the cross-section for the resonant production and detection, of A', $\sigma_{\rm res}$ via the $e^+e^- \to A' \to e^+e^-$ process. For the essential s-channel process the scattering amplitude is enhanced when the beam energy is close to the A' mass. It is important to note that this process neither interferes with the analogous QED process with an off-shell γ, nor with t-channel amplitudes that can then be neglected. Using the narrow width approximation $\sigma_{\rm res}$ is given by:

$$\sigma_{\rm res}(E_e) = \sigma_{\rm peak}\frac{\Gamma_{A'}^2/4}{(\sqrt{s} - m_{A'})^2 + \Gamma_{A'}^2/4}\,, \tag{7.4}$$

with $s \simeq 2m_e E_e$ and $\Gamma_{A'} \simeq \epsilon^2 \alpha m_{A'}/3$. The peak of this cross-section is achieved when $\sigma_{\text{peak}} \simeq 12\pi/m_{A'}^2$. Since ϵ and $m_{A'}$ are the only independent parameters in the model, we expect heavier DP to be sensitive to lower ϵ values since there exists parabolic relation between the two parameters for a fixed value of the cross-section. The picture we presented is a simplified one and one needs to consider cross-section including initial state radiation effects. Let us sketch the calculation for this process next.

$e^+e^- \to A' \to e^+e^-$ cross section

According to Ref. [222] , the cross section for the process $e^+e^- \to A' \to e^+e^-$ corresponding to diagram in Fig. 7.3 (a), including 1-loop electromagnetic corrections and taking into account soft photon bremsstrahlung (also considering the finite width of the A′ boson) can be written as:

$$\frac{d\sigma}{d\Omega} = \epsilon^4 \frac{\alpha^2}{4s} |\chi(S)|^2 \times C_\theta \times C_{IR}(1 + c_\Phi + c_S), \tag{7.5}$$

where

$$\chi(S) = \frac{s}{s - m_{A'}^2 + i m_{A'} \Gamma_{A'}} \tag{7.6}$$

is known as the reduced propagator and $\Gamma_{A'}$ is the A' decay width expressed as:

$$\Gamma_{A'} = \epsilon^2 \frac{\alpha m_{A'}}{3} \sqrt{1 - \frac{4m_e^2}{m_{A'}^2}} \left(1 + \frac{2m_e^2}{m_{A'}^2}\right) \tag{7.7}$$

The expressions for C_θ and $C_{IR}(1+c_\Phi+c_S)$ correspond to bremsstrahlung and virtual electromagnetic corrections, respectively. C_θ is:

$$C_\theta = \left[1 + \frac{8m_e^2}{s} + (1 - \frac{4m_e^2}{s}) \cos^2\theta\right] \tag{7.8}$$

and $C_{IR}(1 + c_\Phi + c_S)$ is given by:

$$\left|\frac{\Delta E}{E}\frac{1}{1-\frac{\Delta E}{E}\chi(s)}\right|^{(\frac{2\alpha}{\pi}\beta_e)} \times \left[1 + \frac{2\alpha}{\pi}\beta_e\frac{s-m_{A'}^2}{m_{A'}\Gamma_{A'}}(\Phi - \Phi_{A'}) + \frac{\alpha}{\pi}(\frac{3}{2}\beta_e + \frac{1}{3}\phi^2 + \frac{1}{2})\right] \quad (7.9)$$

where

$$\tan\Phi = \frac{m_{A'}^2 - s(1-\frac{\Delta E}{E})}{m_{A'}\Gamma_{A'}}$$

$$\tan\Phi_{A'} = \frac{m_{A'}^2 - s}{m_{A'}\Gamma_{A'}}$$

$$\beta_e = log(\frac{s}{m_e^2}) - 1$$

with E the energy of the incoming particle and ΔE the energy up to which soft photons emission is included ($\frac{\Delta E}{E} \sim 1\%$).

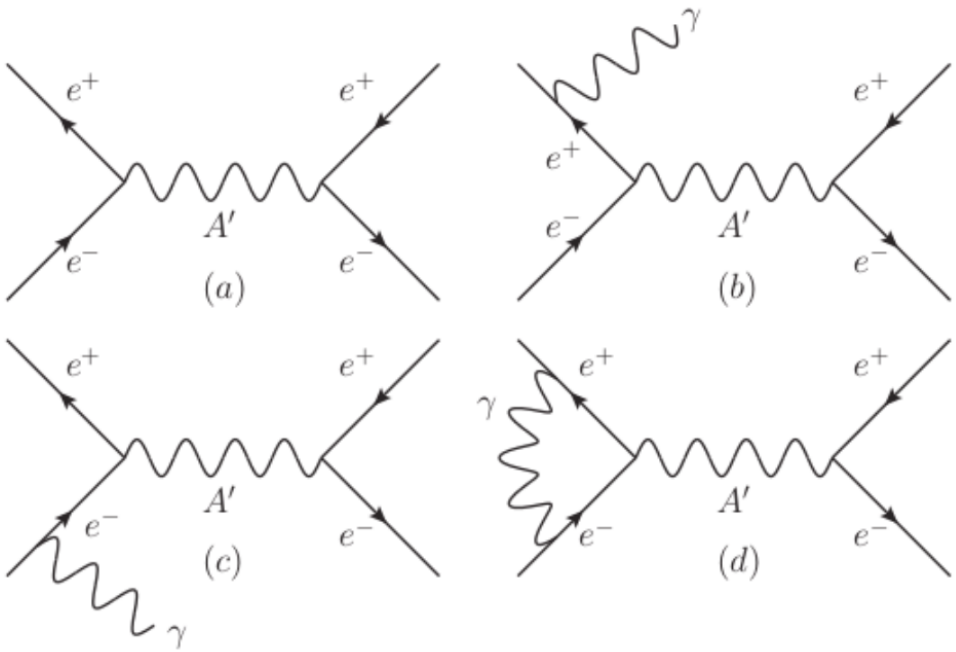

Figure 7.3: *Feynman diagrams of the process e+ e- → A' → e+ e- : (a) correspond to the tree level process, while (b)-(c) and (d) represent bremsstrahlung and virtual electromagnetic corrections, respectively.*

This expression is actually $\frac{\Delta E}{E_e}$ to be precise with E_e representing the positron energy in the specific collision, but the difference is irrelevant here. In the bremsstrahlung

case (diagrams Figs. 7.3 (b) and (c)) the soft photon can also be radiated from the electron external leg. Taking the e^+ energy to be E_e after t units of radiation length and considering the electrons inside the target at rest, i.e., the centre-of-momentum energy as $s = 2m_e(E_e + m_e)$, one gets the relevant cross section in the laboratory frame.

7.4.3 Estimation of Number of Events

Typically, the number of detectable DP events is given by:

$$N_{A'} = \frac{N_{e^+} N_0 X_0 Z}{A} e^{-\frac{z_D}{\ell_\epsilon}} \int_0^T dt\, e^{\frac{X_0}{\rho \ell_\epsilon} t} \int_0^\infty dE_e\, \mathcal{T}(E_e, t)\, \sigma_{\rm res}(E_e)\,, \tag{7.10}$$

with N_{e^+} the number of incident positrons, N_0 the Avogadro number, $A = 184$ the atomic mass of tungsten, $Z = 74$ is the atomic number and $\sigma_{\rm res}(E_e)$ the differential resonant cross section. Eqn.7.10 takes into account the fact that the probability to detect an A' produced at z is given by the expression:

$$d\mathcal{P}/dz = (1/\ell_\epsilon) e^{-z/\ell_\epsilon} \tag{7.11}$$

between $z_D - z$ and $z_{\rm det} \to \infty$, where the limit is justified since $z_D \sim O(1\,\text{m})$. It is noteworthy that even if the initial beam energy is not much above the resonance, after just a fraction of a radiation length ($\rho X_0 = 3.5\,\text{mm}$ for tungsten) the energy of most positrons will have already degraded below the threshold for resonant production, so that setting $T = 1$ for the upper limit of the integration is also a good approximation. This is clearly depicted in Fig. 7.4. As the positrons from the beam cross each unit radiation length the tail of the distribution gets elongated that is, probability of finding an energetic enough positron becomes negligible. Also, one can note that as it crosses each unit radiation length a positron which was initially not at resonant energy to produce on-shell DP might degrade energy and come to resonance creating DP. Thus this process effectively "scans" the parameter space of DP masses. The first exponential factor in Eqn.7.10 accounts for the fact that the larger is the length of

the dump, the smallest is the number of A' that can be detected. For $z_D \sim 10\,\text{cm}$ we can expect that virtually all the background from the EM showers will be absorbed in the dump. However, only a few A' will decay outside. By decreasing the dump length z_D one looks to increase the statistics but then the SM background begins to kick in and it is difficult to control beyond 1 cm or so. In the lack of a dedicated simulation of the detector/background for the resonant annihilation process, we will present results for variable dump length values considering optimistic and pessimistic cases to be $z_D = 2\,\text{cm}$ and $z_D = 10\,\text{cm}$ respectively. And also consider a value in between of $z_D = 5\,\text{cm}$.

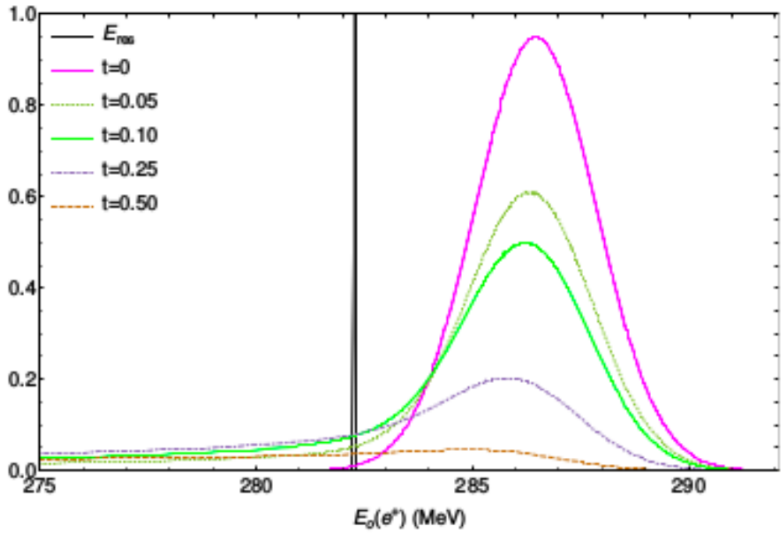

Figure 7.4: *Evolution of the positron energy distribution at different radiation lengths t. The vertical axis represents the positron energy distribution $\mathcal{T}(E_e, t)$. All the curves are normalized to one. The vertical narrow black strip represents the A' resonance of a 17 MeV DP.*

In the numerical computation we take into account m_e effects both in the cross section and in the width, and we also account for the emission of soft photons from the initial state (see e.g. [222]) up to energies $\Delta E/E_b \approx 1\%$, which can radiatively enhance the resonance width, and thus the production rate, E_b being the beam energy.

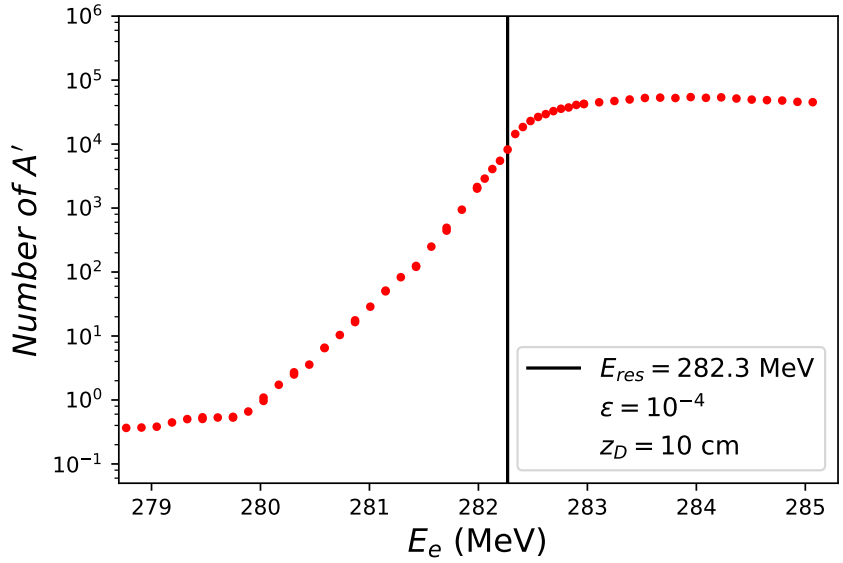

Figure 7.5: *The number of DPs decaying outside the dump as a function of the beam energy for* $\epsilon = 10^{-4}$*. The vertical line corresponds to the energy for resonant production of a 17 MeV DP. A dump length* $z_D = 10$ *cm and a background free measurement have been assumed.*

7.5 Comments on the Salient Features

Some of the distinct features of this resonant production mechanism when compared to other DP production mechanisms are as follows:

(i) The peak cross section of the process is only determined by the mass of the DP. In terms of the kinetic mixing, the total resonant cross section has only quadratic dependence in ϵ ($\sim \epsilon^2\alpha$). Therefore we see an interplay between the smallness of the coupling and the enhancement due to the resonance process which leads to observable number of electron-positron pairs from A' decays. Small ϵ suppression is overcompensated by the strong enhancement from the larger decay length $\sim \exp(-\epsilon^2)$ thereby increasing the number of A' that decay outside the dump. In thick target experiments this is particularly useful and we are able to explore the parameter space for smaller and smaller ϵ values.

(ii) For constant ϵ values, the A' decay length $\ell_\epsilon = \gamma\, c\, \tau_{A'}$ is insensitive to the A' mass. This $m_{A'}$ cancels between the boost factor $\gamma \sim m_{A'}/(2m_e)$ and the lifetime

$\tau_{A'} \propto 1/m_{A'}$. For all A' masses the decay length then becomes fixed $\ell_\epsilon \sim 3/(2m_e\alpha\epsilon^2)$. Therefore, the entire $m_{A'}$ range within the reach of the beam energy can be probed with the same sensitivity. This is clearly evident from Fig. 7.7. This also implies that by varying the dump length we can scan the ϵ values.

(iii) When the beam energy is varied by only a few MeV, the background (if it is constant) can be directly measured from the data (see Fig. 7.5). When the beam energy lies well below the resonance, the background for e^+e^- pairs (a case for $z_D = 10\,\text{cm}$ in the picture is assumed to be background-free) can be directly measured. However, once the beam energy is increased, and is approaching resonant production, the number of e^+e^- pairs *produced* increases to a maximum value, after which it remains approximately constant even if the energy increases due to positron energy losses in the material, which drive their energy towards E_{res}. Clearly, even in the presence of a significant number N_{BG} of e^+e^- background pair events, as long as $N_{A'} > \sqrt{N_{BG}}$ a good signal of A' decays can be detected. Also note that Fig. 7.5t if obtained from the experiment is clearly a smoking-gun signature for the resonant DP production process unless if the A' resonance lies somewhat below the minimum beam energy, since one would always measure e^+e^- resonantly produced by primary e^+ degraded in energy, together with backgrounds. However, in this case by raising the beam energy and stepping further away from the resonance, the number of di-lepton pairs resonantly produced would drop because of the degradation of the primary beam quality due to EM showering. The behavior of a 'background' which decreases with increasing beam energy would still be a signal of beyond the SM physics.

7.6 Effects of target electrons velocities

Considering electrons at rest inside materials are approximations only; in reality, especially for large atomic numbers, like tungsten ${}_{74}\text{W}$, electrons can have large velocities, especially the ones in the inner core shells. This is supported when one takes a look at electrons virial velocities $\langle v_{nl}\rangle \approx \alpha Z_{\text{eff}}^{(nl)}$ in terms of the effective nuclear charge $Z_{\text{eff}}^{(nl)}$ felt by electrons in the (nl) shell (a complete list of effective nuclear charges

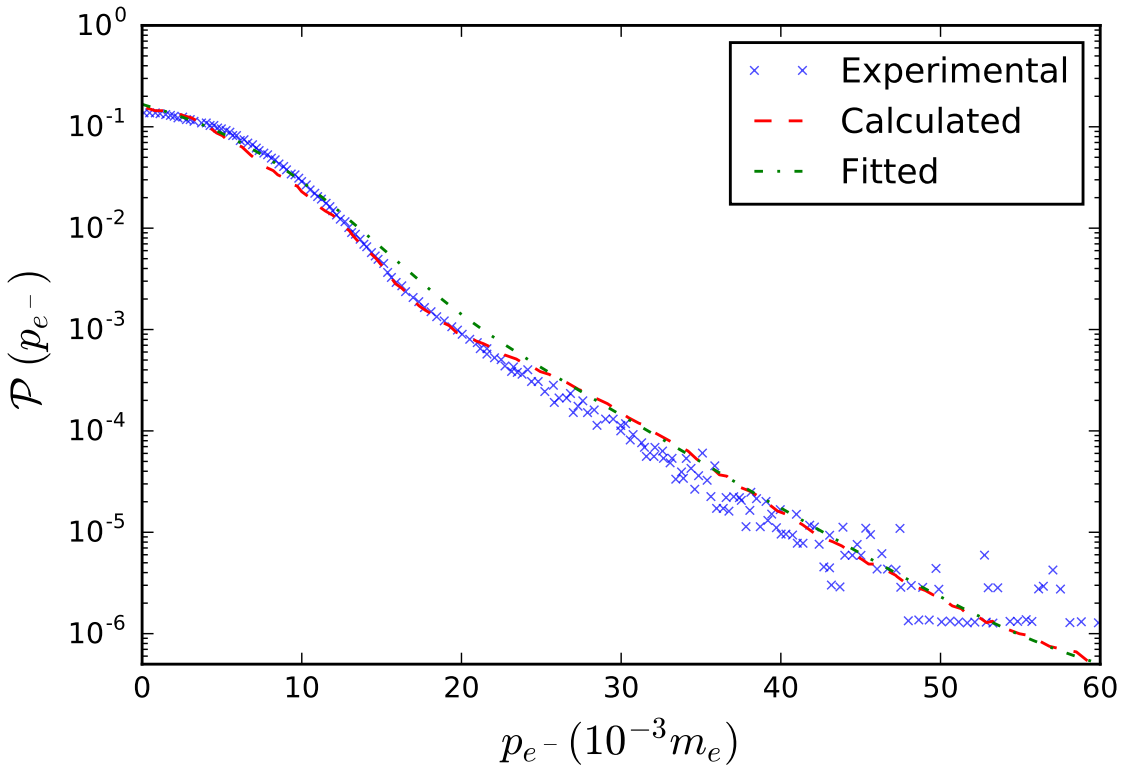

Figure 7.6: *The positron annihilation probability as a function of the target electron momentum for tungsten (figure adapted from Ref. [223]). The blue crosses represent experimental points, while the red dashed line is the result of the calculation method adopted in [223]. The green dot-dashed line corresponds to the fit given by the function in Eqn 7.12.*

can be found in Ref. [224]). However, for targets of small atomic numbers, like ${}_6$C or ${}_{13}$Al, virial velocities are small too, and the effects of target electrons motion is likely to be negligible. Particularly, for ${}_{74}$W one finds that the average velocities span a rather large range $0.003 \lesssim \langle v_{nl} \rangle \lesssim 0.5$ when going from valence or conduction electrons (with Fermi energy $\epsilon_F \sim 4.5\,\text{eV}$) to inner core electrons. What this means is our estimations regarding the center of mass (c.m.) energy from the beam energy, energy spread, energy loss due to in-matter propagation, and assuming electrons at rest can be largely different from the actual values. To give an example, already for a longitudinal velocity component $v_z \sim 0.03$ the effect of shifting the c.m. energy away from the resonant value is three time larger than the effect of the intrinsic $\sim 1\%$

energy spread in the beam energy. To rectify this, we will consider the positron annihilation probability as a function of the electron momentum, since annihilation with de-localized and weakly bound valence electrons, which contribute to the low-momentum part of the momentum distribution, is more likely than annihilation with the localized and tightly bound core electrons contributing to the high-momentum part.

For positron annihilation at rest, the annihilation probability distribution as a function of the electron momentum is directly measured from the Doppler broadening by the amount $\Delta E = p_L/2$ of the 511 keV photon line, with p_L the e^- momentum component along the direction of γ emission (the relative direction of the two γ's also deviates from 180^o by the small angle $\theta = p_L/m_e$). In Fig. 7.6 (adapted from [223]) a large set of experimental points for ${}_{74}$W is represented with blue crosses. The red dashed line represents a theoretical calculation performed in the same paper. Up to $p_{e^-} \sim 15 \cdot 10^{-3}\, m_e$ the main contribution to the annihilation comes from electrons in the 5d shell, beyond that point 4f electrons dominate, while the contribution of the high momentum core electrons becomes relevant only for $p_{e^-} \gtrsim 40 \cdot 10^{-3}\, m_e$ where, however, the annihilation probability is suppressed below 10^{-5}. Accordingly, we find that a good fit to the experimental and calculated distributions [223] can be obtained with the sum of just three terms:

$$\mathcal{P}(v_e) = \frac{1}{N}\Big(1.015^{-v_e^2} + 1.112^{-2v_e} + \theta(v_e - 40)\, 3 \cdot 10^{-6+\frac{1}{v_e}}\Big), \tag{7.12}$$

where $v_e = p_{e^-}/m_e$, $N \sim 12$ is a normalization factor, and the first term in parenthesis accounts for 5d electrons, the second for 4f electrons, and the last one, which is non zero only for $v_e \geq 40$, accounts for core electrons. To take into account target electron motion we thus replace the Mandelstam variable s in $\sigma_{\rm res}$ by

$$s(v_e, \chi) = 2m_e \left[E_e \left(1 - \mathcal{P}(v_e) v_e \frac{1}{2} s_\chi c_\chi\right) + m_e\right], \tag{7.13}$$

where $c_\chi = \cos\chi$ accounts for the projection of $\vec{v}_e$ along the z-direction of the incoming

positron, $s_\chi/2$ with $s_\chi = \sin\chi$ is the probability distribution for the angle χ. We integrate the cross section in c_χ and $v_e \in [0, 0.06]$. Tab. 7.2 collects some results that illustrate how the number of DP *produced* within the first radiation length of tungsten depends on various effects. The second column gives the results for three different values of ϵ for a beam energy tuned at the resonant energy $E_{\rm res} = 282.3\,{\rm MeV}$, when the motion of the target electrons is neglected. The third column gives the results obtained when the electron velocity is taken into account according to the distribution in Eqn. 7.12. We see that the shift of the c.m. energy due to the electron momentum has the effect of reducing the number of DP produced by about a factor of five. The last column gives the results for a beam energy tuned above the resonance $E_b = E_{\rm res} + 2\sigma_b$. The number of DP is increased by about a factor of three because of the positron energy losses, which brings on resonance also positrons in the high energy tail of the initial energy distribution.

Of course, using the annihilation probability distribution for positrons at rest in the problem at hand, is a crude way of proceeding. We can expect that target electron motion effects can be significantly large for in-flight annihilation of short wavelength positrons with energies of $O(100\,{\rm MeV})$, since the annihilation probability with electrons in the inner shells will be enhanced. Therefore, our estimate of the production rates might be optimistic by a factor of a few. On the other hand, while positron energy loss, which proceed mainly via bremsstrahlung, constitute a quantized process, the dependence of the c.m. energy on the angle χ characterizing the electron momentum is continuous, and this justifies modeling positron energy losses as a continuous process.

7.7 Discussions

We briefly summarize our investigations and the salient features of our whole study. First we compare the two PADME search strategies: the brehmsrahlung one and the resonant method. Then we discuss to some extent the effects of background in this experimental phenomenology and related instrumentation and finally list out few

$\epsilon \Big/ N_{A'}^{\rm prod}$	$E_{\rm res}$ $(v_e = 0)$	$E_{\rm res}$	$E_{\rm res} + 2\sigma_b$
1.0×10^{-3}	7.69×10^{11}	1.51×10^{11}	4.72×10^{11}
5.0×10^{-4}	1.81×10^{11}	3.79×10^{10}	1.17×10^{11}
1.0×10^{-4}	7.25×10^{9}	1.49×10^{9}	4.73×10^{9}

Table 7.2: *Number of* 17 *MeV DP produced in the first radiation length of a tungsten target for* 10^{18} *positrons on target, for three different values of* ϵ*. The second and third columns are for a beam energy tuned to the resonant value* $E_{\rm res} = 282.3\,MeV$*, assuming respectively electron at rest and with the velocity distribution in Eqn.7.12. The last column, also including* v_e *effects, is for a beam energy* $E_b = E_{\rm res} + 2\sigma_b$*.*

important take-aways from our work.

7.7.1 Comparison of PADME search modes

In Fig. 7.7 we show the status of the current limits for DP searches assuming visible A' decays into e^+e^- pairs with unit branching fraction and suppressed couplings to the proton. As is discussed in Ref. [225] the last assumption is required in order to evade the tight constraints from $\pi^0 \to \gamma A'$ obtained by the NA48/2 experiment [226], and to render thus viable an explanation of the ^{8}Be anomaly via an intermediate A' vector boson. For this reason we have not included in Fig. 7.7 the limits from the NA48/2 experiment [226] nor those from the ν-Cal I experiment at the U70 accelerator at IHEP Serpukhov [227, 228] which also do not apply for protophobic A'. In the figure, the vertical black line gives the location of the DP resonance at $m_{A'} = 17\,\text{MeV}$. Leaving aside the limits from the SLAC E141 experiment for which, as explained in the introduction, the reach in A' mass might be overestimated, a viable window remains between the Orsay/KEK lines ($\epsilon \gtrsim 7 \cdot 10^{-5}$) and the $(g-2)_e$ line ($\epsilon \lesssim 1.4 \cdot 10^{-3}$). The black hatched region depicts the fore-casted sensitivity of PADME in thin target mode, that will search for DP via the $e^+e^- \to A'\gamma$ process. The limits assume $10^{13}\,\text{pot/yr}$. The light cyan trapezoidal regions represent instead the constraints that PADME could set by running in thick target mode with $10^{18}\,\text{pot/yr}$, and are respectively for tungsten targets of 10 cm, 5 cm and 2 cm of length, and neglecting backgrounds. The BTF energy range for positron beams $250 \lesssim E_b/\text{MeV} \lesssim 550$

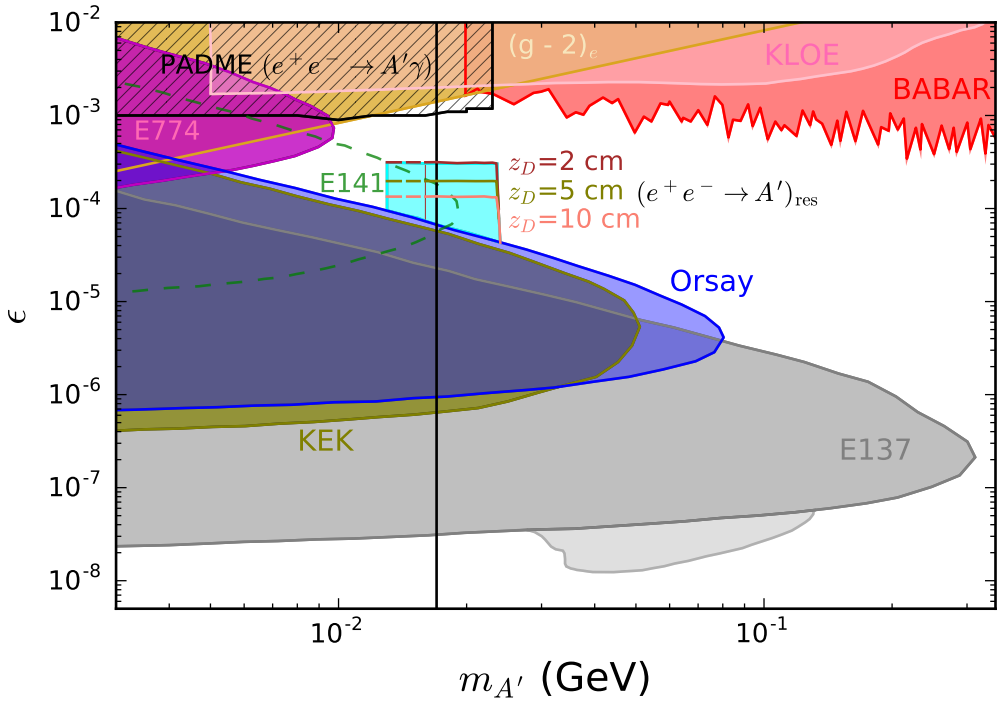

Figure 7.7: *Limits on the DP kinetic mixing ϵ as a function of the mass $m_{A'}$ from different experiments. For $m_{A'} \approx 17\,MeV$ (vertical black line) we consider still viable the region bounded from below by the Orsay and KEK blue and green-yellowish lines [197] and from above by the $(g-2)_e$ orange line [208, 209]. For reasons explained in the text we do not consider as firmly excluded the region around $m_{A'} \approx 17\,MeV$ delimited by the black-dashed curve of the E141 SLAC experiment [198, 197]. The region that could be excluded by PADME running in thin target mode is hatched in black, while the three trapezoidal-shaped areas give the PADME reach in thick target mode, respectively for a 10, 5 and 2 cm tungsten dump, assuming zero background. These regions extend to A' masses lower than the mass corresponding to the minimum beam energy ($m_{A'} \sim 16\,MeV$ for $E_b^{\rm min} = 250\,MeV$ depicted with the thin brown vertical line) because of positron energy losses in propagating through the material. The lower region in light gray extending the E137 exclusion limits is from the reanalysis in Ref. [219].*

corresponds to c.m. energies in the interval $16 \lesssim E_{\rm c.m.}/{\rm MeV} \lesssim 23.7$. Neglecting a possible small c.m. energy increase from target electron velocities, the upper value sets the upper limit on the A' masses that can be produced. The lower c.m. energy limit is indicated by the thin vertical brown line. However, because of positron energy losses, the region at low $m_{A'}$ that can be explored extends to values smaller than 16 MeV, as indicated in the figure. Of course, in propagating well inside the

dump, the beam gets degraded in energy, directions of particle momenta, number of positrons, by several effects that we are neglecting. Therefore, we can expect that the experimental sensitivity could be extended down to $m_{A'}$ values lower than 16 MeV by no more than a few MeV. This might still be sufficient to reach into the region where the E141 exclusion limits can be trusted.

The two PADME search strategies are complementary in the sense that they will be surely able to set new bounds in the regions of large $O(10^{-3})$ and small $O(10^{-4})$ coupling ϵ values of the DP with SM. We envisage the new regions in Fig. 7.7 to be explored within one year of run time of the time from the date of beginning of PADME. Very specifically the parameter space window that lay un-excluded for the explanation for ^{8}Be anomaly involving a DP can be explored impeccably and be reduced, if not ruled out fully. In the process one may also observe the experimental signature for DP and discover this dark particle and open up the window for a whole new possible dark sector of particles to follow.

7.7.2 Background Processes

Before concluding a few words on backgrounds are in order. The PADME spectrometers can detect e^+e^- pairs with good resolution for coincidence in time and momentum. The A' angular spread due to the transverse momentum of atomic electrons is much less than the intrinsic angular spread of the beam (~ 1 mrad) and it does not affect the reconstruction of the coincidence. For targets of sufficient thickness, background from secondary e^- detected in coincidence with primary or secondary e^+ can be avoided by measuring their depleted momentum via electromagnetic deflection. For targets of smaller length a certain number of e^+e^- pairs retaining a large fraction of the beam energy can exit the dump, and in this case the data driven method of searching for a 'knee' in the number of e^+e^- pairs versus beam energy (see Fig. 7.5) can provide a precious tool for revealing the onset of resonant e^+e^- production on top of the background. Punch-through photons, produced via bremsstrahlung in the very first layers of the dump, carrying a large fraction of the original beam energy,

and converting in e^+e^- in the last millimeter or so, constitute the most dangerous background. This background could be significantly suppressed by equipping the experiment with a plastic scintillator veto few mm thick, or a silicon detector of a few hundreds of μm, placed right at the end of the dump, to ensure that the e^+e^- pairs originate from decays in the vacuum vessel outside the dump. Additionally, if the experiment could be equipped with a suitable tracker, able to provide an accurate e^+e^- invariant mass reconstruction, many sources of backgrounds could be further reduced. In particular, given that the invariant mass of the e^+e^- originating from photon conversion $m^2_{e^+e^-} = 0$ is very far from $m^2_{e^+e^-} \sim (17\,\mathrm{MeV})^2$ expected from resonant annihilation, the punch-through photon background could be efficiently eliminated.

7.7.3 Conclusions

- DP of 17 MeV mass explains the anomaly observed in ^{8}Be nuclear transitions [177, 178, 179]. In this chapter we developed a novel way to search for narrow Breit-Wigner type resonances, and to look for DP coupled to e^+e^- pairs, via this kind of resonant production in e^+e^- annihilation channel.

- The Frascati BTF possesses positron beams and provide with energy range in between $250 - 550\,\mathrm{MeV}$. This means the threshold production for DP through resonant annihilation is $\sqrt{250}$ or about 16 MeV and can go upto $\sqrt{550}$ or about 23 MeV. Due to this we can search for the DP in context to the ^{8}Be nuclear anomaly. We presented our sensitivity bounds in Fig. 7.7.

- In particular from Fig.7.7 we can see there is a gap between the large ϵ region that can be bounded by searching for A' produced via $e^+e^- \to \gamma A'$, and the small ϵ region that can be efficiently explored via resonant $e^+e^- \to A'$ production. This is because the brehmsstrahlung processes are of order $O(\alpha^2\epsilon^2)$, therefore looses sensitivity very quickly with respect to the decrease of ϵ values. However, the resonant A' production is largely inefficient when ϵ becomes too large, so that most of the $A' \to e^+e^-$ decays occur inside the dump and cannot be detected.

- Resonant production is not so much advantageous for PADME with a thin target since the large beam energy $E_b \sim 550\,\text{MeV}$ implies that positrons will always have energies far from any narrow resonance with mass $\lesssim 23.7\,\text{MeV}$, given that positron energy losses in the $100\,\mu$m diamond target are negligible.

- For a reduced beam energy of $\sim 282\,\text{MeV}$, and replacing the thin target by a thicker one (few $100\,\mu$m) one can look to enhance A' resonant production, and keeping the beam intensity well below 10^{18} pot/yr to keep counting rates inside the detector under control, at least part of the remaining region for the 17 MeV DP could be explored. Thus after running of the PADME experiment there may remain no parameter space left for the DP thereby confirming or excluding this solution to the ^{8}Be anomaly in this region of parameter space.

7.7.4 Some Remarks

So far we considered only the visible decay of the DP into electrons whose branching ratio was taken to be 1. Using the method of resonant production of DPs, a similar proposal was made for lepton beam - dump experiments, in general, and particularly for LDMX proposal [229, 230] where decay of the DP was considered with the decay products being dark matter candidates. They obtained weaker bounds on the parameter space since it is essentially similar to the case of invisible decay of DP. The results push down the limits presented here by an order of magnitude if such invisible decays of DP occur.

Chapter 8

Summary and Conclusion

Neutrino oscillations prove beyond doubt the need to go beyond the Standard Model of particle physics. Many experiments are ongoing and are planned to study neutrinos arising from several sources, both artificial and natural, ranging over from μeV to EeV energy ranges.

The Deep Underground Neutrino Experiment (DUNE) will be a long baseline neutrino oscillation experiment located in the USA. It will consist of a near site situated at Fermilab in Batavia, Illinois, and a far site, situated 1300 km north-west at the Soudan Laboratories in South Dakota. In the near site, the near detector (which has not been designed yet) and the beam facility will be placed. The LBNF (Long Baseline Neutrino Facility) beam will be a ν_μ (or $\bar{\nu}_\mu$) beam with a small contamination of ν_e. It will be able to run in neutrino or in anti-neutrino modes by changing the polarization of the magnet in the focusing horn. At the far site, four 10kt Liquid Argon Time Projection Chamber (LAr-TPC) detectors will be built deep underground. This kind of detector is particularly suited to performing neutrino experiments, since it has a very good imaging capability and a good energy resolution. Its long read-out time, which is the main LAr-TPC's disadvantage, does not affect much neutrino searches, since neutrino interactions are not so frequent.

As per plan, after 7 years running (3.5 in neutrino mode and 3.5 in anti-neutrino mode) of DUNE we will be able to collect a huge statistics which will shed light on:

- Determining the oscillation parameters θ_{13}, θ_{23} and Δm^2_{31} with great precision values.

- Determining the sign of the atmospheric mass splitting Δm^2_{31}, leading to resolution of the neutrino mass ordering problem.

- Measuring the leptonic CP violating phase with good accuracy. Particularly, DUNE will be able to reach a 5 σ sensitivity to the phase if $|\sin\delta_{CP}| \sim 1$.

- Determining the octant in which θ_{23} lies at 3 σ if this angle is smaller than 43° or bigger than 47°.

However, the standard configuration of DUNE includes only the ν_e-appearance and ν_μ-disappearance channels. In this thesis, we considered a new oscillation channel, namely the ν_τ appearance channel, on top of the standard DUNE channels. This was motivated on one hand by the recent observation of ν_τ events in OPERA experiment and the fact that DUNE in any case will be able to collect a significant statistics for ν_τ sample which has not been able to achieve in any other experiments till date. Nevertheless, detecting ν_τ events are difficult, and only two accelerator experiments (DONUT and OPERA) were able to detect such events, due to very high energy threshold (3.4 GeV) of ν_τ, and the prompt decays of τ leptons. It is in fact too fast to be detected in terms of its final state lepton or hadrons with missing energy carried by neutrinos. In this thesis the tau electronic decay channel has been considered as detection channel for DUNE following along the lines of the ICARUS proposal, which had the first LAr-TPC to be used in a neutrino experiment, the CERN Neutrinos to Gran Sasso (CNGS) long baseline experiment.

Using the standard neutrino flux (which is optimized for studying the CP-violation and mass hierarchy searches in DUNE), we found that despite the number of ν_τ events in DUNE being larger than the number of ν_τ events ever seen, it will be much smaller than the number of ν_e and ν_μ events that the experiment will collect, mainly due to the energy threshold for charged current interactions. It is also to some extent due to the fact that for energetic neutrinos the $\nu_\mu \to \nu_\tau$ transition probability is not maximized in DUNE configuration which needs a longer baseline (larger L/E) to reach the peak of the oscillation [111]. For increasing the statistics for ν_τ events, we studied the physics potential for another flux known as ν_τ-optimized flux which

is being proposed by the DUNE collaboration. We presented the constraints on the oscillation parameters using both fluxes. Optimized flux helps to ameliorate the performances in the ν_τ appearance channel. But the sensitivity reaches from the other two channels are always better in the standard flux case. We understood that this is mainly due to the increased number of background events to the ν_μ disappearance and ν_e appearance signal in the optimized case. In order to circumvent this issue and take advantage of both fluxes to maximize the ν_τ-channel capabilities on the final sensitivity, it can be proposed that the running time of the experiment be shared between the two fluxes.

The addition of the ν_τ appearance channel, even with the optimized flux, does not improve the sensitivities of the measurements of the standard neutrino oscillation parameters. This happens due to smaller number of events (compared to other channels) on one hand. On the other hand, the $\nu_\mu \to \nu_\tau$ transition probability dictates that it will be driven by the the leading order only on Δm^2_{31} and θ_{23}, which are same as in $\nu_\mu \to \nu_\mu$ probability. Having had similar dependencies, ν_μ disappearance channel wins over the ν_τ appearance channel in terms of sensitivity since the latter is the dominant contributor to DUNE statistics.

We found the ν_τ appearance channel can be very useful in new physics scenarios. In particular, in this thesis, we studied the BSM physics encoded via NSI. It is a very useful way to capture the effect of new physics in the neutrino oscillation phenomenon in terms of NSI parameters. We found that particularly the bound on $|\epsilon_{\mu\tau}|$ can be significantly improved from the current constraints that exist today on this parameter. To supplement this investigation, we studied the impact the systematics, τ-detection efficiency and various "experimental reaches" (S/B values) may have on the measurements. The overall improvement of sensitivity for this parameter is about 15% than in the case without considering the ν_τ channel.

In the second half of the thesis, we were concerned with the study of dark photons. New light, weakly coupled particles are motivated by some of the most important questions in particle physics such as DM, the strong CP problem and several discrepancies between the SM and experimental results. Besides, the new light particles

may constitute the DM, or be the mediators responsible for DM interactions. As a low-energy remnants of UV-scale models, BSM U(1)$'$ predict such DP with its coupling and mass as the independent parameters to be constrained by experiments or observations. Different experiments with different strategies focus to search for this particle in different regions of its parameter space.

In particular, in order to explain the Beryllium anomaly of the ATOMKI experiment a gauge boson of 17 MeV of mass decaying into electron-positron pairs is considered in this thesis. We developed a new way to search this new gauge boson in positron beam-dump experiments. This is suited for an important region in the DP parameter space, namely of the range of ϵ between $10^{-4} - 10^{-3}$. This novel technique is proposed to be implemented in the PADME experiment. Essentially DP coupled to positron-electron pairs maybe produced via resonant production in positron-electron annihilation scenario. Frascati BTF is able to provide positron beams with energy between 250 - 550 MeV. This range covers precisely the centre-of-momentum energy needed to produce via resonant positron-electron annihilation the $m_{A'} \sim 17$ MeV DP invoked to explain the anomaly observed in ^{8}Be nuclear transitions. We investigated the sensitivity reach in PADME and presented our results in context to all existing bounds on the DP. Furthermore we compared the sensitivity reach of PADME resonant mode with that in PADME A'-strahlung mode and showed these two strategies are complementary in the sense they can be used to search in different regions of the parameter space. We also remarked that resonant $e^+e^- \to A'$ production can be relevant also for electron beam dump experiments as well since it involves secondary positrons that could trigger the annihilation process are abundantly produced in electromagnetic showers. This lead to re-analysing and improving the bounds on existing constraints from such experiments. The overall sensitivty for PADME in resonant production mode is to scan the DP parameter space region of mass about 16 to 23 MeV mass and coupling strength of ϵ between $10^{-4} - 10^{-3}$ range.

The phenomena of both neutrino oscillation and the dark photon are weakly interacting sector physics beyond the Standard Model. With many experiments planned and running for both the cases, in this decade we are going to study precisely the

physics involved in this type of scenarios. Under these circumstances we studied in this thesis the phenomenology related to the DUNE experiment and the PADME experiment in particular and predicted sensitivity reaches for the experiments. We hope this study in totality or partially will be able to guide the experimental effort on this sector on one hand and we will able to verify our predictions from the data given by the experiment on the other hand.

Chapter 9

Appendix: Neutrino Oscillation

9.1 Matter potential experienced by anti-neutrinos

The charge conjugate field ν_{eL}^C consists of anti-neutrino current in the following manner:

$$\begin{aligned} j_\nu^C &= \bar{\nu}_{eL}^C \gamma^0 \nu_{eL}^C & (9.1) \\ &= -\nu_{eL}^T C^{-1} \gamma^0 C \bar{\nu}_{eL}^T, & (9.2) \end{aligned}$$

where C is the charge conjugation operator. Due to the identity,

$$C^{-1}\gamma^0 C = (-\gamma^0)^T, \tag{9.3}$$

we find

$$\begin{aligned} j_\nu^C &= \nu_{eL}^T (\gamma^0)^T \bar{\nu}_{eL}^T & (9.4) \\ &= -\bar{\nu}_{eL}\gamma^0 \nu_{eL}. & (9.5) \end{aligned}$$

In terms of the effective Hamiltonian,

$$\bar{H}_{\text{eff}} = -\sqrt{2} G_F N_e \bar{\nu}_{eL} \gamma^0 \nu_{eL}, \tag{9.6}$$

which corresponds to

$$\bar{v}_{CC} = -\sqrt{2} G_F N_e. \tag{9.7}$$

9.2 Correlations in Standard DUNE analysis

Here we present the results when only ν_e appearance and ν_μ disappearance channels are considered in DUNE. We present correlations plots between the standard oscillation parameters that are involved, namely θ_{13}, θ_{23}, δ_{CP} and Δm^2_{31}.

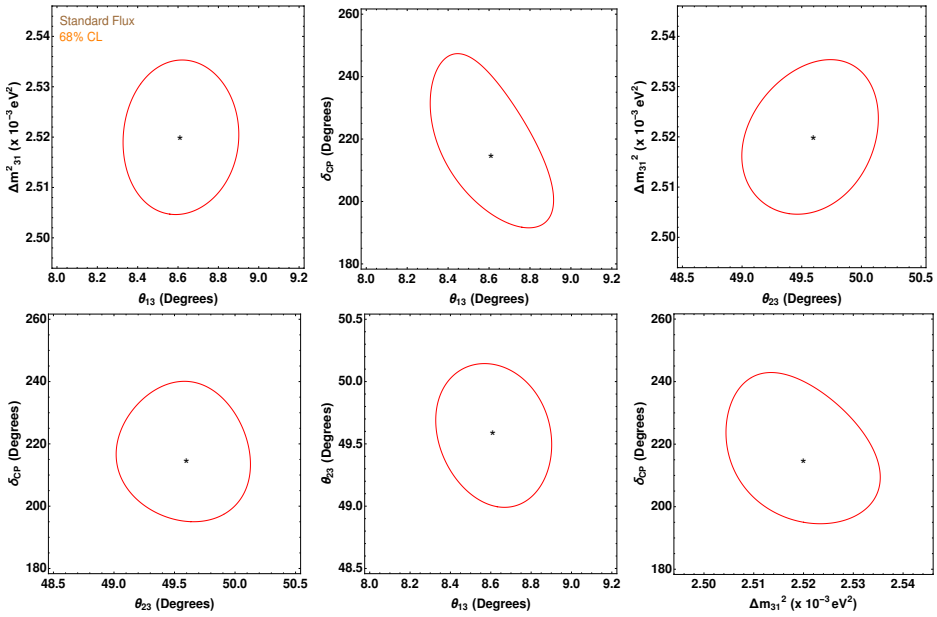

Figure 9.1: *Correlations among oscillation parameters using ν_μ disappearance and ν_e appearance channels with standard flux. The curve shows the allowed parameters space region at 68% confidence level. The star represent the best fit point. Normal Hierarchy is assumed. For brevity, only values of θ_{23} bigger than 45° have been shown in the plots. Standard flux is used.*

Central values and uncertainties from Tab. 4.1 have been used for for the oscillation parameters while performing the χ^2 analysis. The plots represent $\chi^2 = 2.3$ contours in the correlation parameter space which correspond to 68% confidence level.

The synergy between the two channels used in these simulation is very strong in the case of the standard flux. Indeed, the plots in Fig. 9.1 show that each parameter is constrained in the same way in all the planes where it is involved. This

means that there are no particular degeneracies and all the parameters can be measured independently in a very good way. The plots lead to give the following regions in the parameter space from which the individual values of the parameters maybe constrained with the standard flux:

$$\begin{aligned} \theta_{13} &\in [8.34^\circ, 8.91^\circ] \\ \theta_{23} &\in [49.02^\circ, 50.15^\circ] \\ \delta_{CP} &\in [190^\circ, 245^\circ] \\ \Delta m^2_{31} &\in [2.505, 2.533] \times 10^{-3}\ eV^2. \end{aligned} \tag{9.8}$$

Chapter 10

Appendix: Dark Photons

10.1 Origin of the Kinetic Mixing

In this appendix we present an example of the origin of kinetic mixing. Let a model of particle physics has an initial SU(2) $\times$ U(1) symmetry in its action with two fermions. The SU(2) symmetry is broken with an adjoint representation of Higgs field. The remnant U(1) mediators of the broken SU(2) mixes kinetically with the original U(1) gauge group by the combination of the two fermion loop diagrams. This derivation encompasses all the features necessary tounderstand the result in terms of an effective Lagrangian for the kinetic mixing phenomenon. The Lagrangian of the SU(2) $\times$ U(1) theory has [231, 232]:

$$\mathcal{L} = -\frac{1}{4}G^{a,\mu\nu}G^{a}_{\mu\nu} - \frac{1}{2}D_{\mu}\phi D^{\mu}\phi^{a} - V((\phi^{a})^{2}) - \frac{1}{4}F^{\mu\nu}F_{\mu\nu} - \epsilon\phi^{a}G^{a,\mu\nu}F_{\mu\nu} \qquad (10.1)$$

where the symbols have their usual meaning. It is the final term that will lead to kinetic mixing after the spontaneous breaking of SU(2) $\rightarrow$ U(1). The ϵ-term is the kinetic mixing parameter.

10.2 Stuckelberg Mechanism

If we want to give mass to a vector particle in a gauge invariant manner, electrodynamics Maxwell Lagrangian maybe added with a Stueckelberg part [233, 234]:

$$\mathcal{L} = -\frac{1}{4}\left(\partial_\mu A_\nu - \partial_\nu A_\mu\right)^2 + \frac{1}{2}m_A^2\left(A_\mu + \frac{1}{m_A}\partial_\mu\sigma\right)^2; \tag{10.2}$$

It is easily seen with the following transformations

$$\begin{aligned} A_\mu &\rightarrow A_\mu + \partial_\mu\Omega \\ \sigma &\rightarrow \sigma - m_s\Omega. \end{aligned} \tag{10.3}$$

that the theory is gauge-invariant. Now if one adds a gauge fixing term,

$$\mathcal{L}_{gf} = -\frac{1}{2\xi}(\partial\cdot A - \xi m_A\sigma)^2 \tag{10.4}$$

then A_μ and σ becomes decoupled. The propagator or the 2-point correlator for the field A_μ becomes

$$\langle A_\mu A_\nu\rangle = \frac{-i}{k^2 - m_A^2}\left(g_{\mu\nu} - \frac{(1-\xi)k_\mu k_\nu}{k^2 - \xi m_A^2}\right). \tag{10.5}$$

One can retrieve transverse-only degrees of freedom in a "unitary" gauge when $\xi = 0$.

Bibliography

[1] P. W. Higgs, Phys. Rev. Lett. **13**, 508 (1964). doi:10.1103/PhysRevLett.13.508

[2] P. W. Higgs, Phys. Lett. **12**, 132 (1964). doi:10.1016/0031-9163(64)91136-9

[3] F. Englert and R. Brout, Phys. Rev. Lett. **13**, 321 (1964). doi:10.1103/PhysRevLett.13.321

[4] G. S. Guralnik, C. R. Hagen and T. W. B. Kibble, Phys. Rev. Lett. **13**, 585 (1964). doi:10.1103/PhysRevLett.13.585

[5] G. Aad *et al.* [ATLAS Collaboration], Phys. Lett. B **716**, 1 (2012) doi:10.1016/j.physletb.2012.08.020 [arXiv:1207.7214 [hep-ex]].

[6] S. Chatrchyan *et al.* [CMS Collaboration], Phys. Lett. B **716**, 30 (2012) doi:10.1016/j.physletb.2012.08.021 [arXiv:1207.7235 [hep-ex]].

[7] P. M. Watkins, Contemp. Phys. **27**, 291 (1986). doi:10.1080/00107518608211015

[8] G. S. Abrams *et al.* [MARK-II Collaboration], Phys. Rev. Lett. **63**, 1558 (1989). doi:10.1103/PhysRevLett.63.1558

[9] G. Goldhaber, In *Boston 1990, Proceedings, Particles, strings and cosmology* 3-19 and Lawrence Berkeley Lab. - LBL-29712 (90/03,rec.Feb.91) 16 p

[10] B. W. Lynn and C. Verzegnassi, Nuovo Cim. A **94**, 15 (1986). doi:10.1007/BF02894802

[11] C. L. Cowan, F. Reines, F. B. Harrison, H. W. Kruse and A. D. McGuire, Science **124**, 103 (1956). doi:10.1126/science.124.3212.103

[12] G. Danby, J. M. Gaillard, K. A. Goulianos, L. M. Lederman, N. B. Mistry, M. Schwartz and J. Steinberger, Phys. Rev. Lett. **9**, 36 (1962). doi:10.1103/PhysRevLett.9.36

[13] K. Kodama *et al.* [DONUT Collaboration], Phys. Lett. B **504**, 218 (2001) doi:10.1016/S0370-2693(01)00307-0 [hep-ex/0012035].

[14] S. Weinberg, Phys. Rev. Lett. **19**, 1264 (1967). doi:10.1103/PhysRevLett.19.1264

[15] M. Gell-Mann and A. Pais, Phys. Rev. **97**, 1387 (1955). doi:10.1103/PhysRev.97.1387

[16] B. Pontecorvo, Sov. Phys. JETP **6**, 429 (1957) [Zh. Eksp. Teor. Fiz. **33**, 549 (1957)].

[17] Z. Maki, M. Nakagawa and S. Sakata, Prog. Theor. Phys. **28**, 870 (1962). doi:10.1143/PTP.28.870

[18] R. Davis, Jr., D. S. Harmer and K. C. Hoffman, Phys. Rev. Lett. **20**, 1205 (1968). doi:10.1103/PhysRevLett.20.1205

[19] J. N. Abdurashitov *et al.* [SAGE Collaboration], Phys. Rev. C **60**, 055801 (1999) doi:10.1103/PhysRevC.60.055801 [astro-ph/9907113].

[20] J. N. Abdurashitov *et al.* [SAGE Collaboration], J. Exp. Theor. Phys. **95**, 181 (2002) [Zh. Eksp. Teor. Fiz. **122**, 211 (2002)] doi:10.1134/1.1506424 [astro-ph/0204245].

[21] L. Wolfenstein, Phys. Rev. D **17**, 2369 (1978). doi:10.1103/PhysRevD.17.2369

[22] Y. Fukuda *et al.* [Super-Kamiokande Collaboration], Phys. Rev. Lett. **81**, 1158 (1998) Erratum: [Phys. Rev. Lett. **81**, 4279 (1998)] doi:10.1103/PhysRevLett.81.1158, 10.1103/PhysRevLett.81.4279 [hep-ex/9805021].

[23] S. Fukuda *et al.* [Super-Kamiokande Collaboration], Phys. Rev. Lett. **86**, 5651 (2001) doi:10.1103/PhysRevLett.86.5651 [hep-ex/0103032].

[24] Q. R. Ahmad *et al.* [SNO Collaboration], Phys. Rev. Lett. **87**, 071301 (2001) doi:10.1103/PhysRevLett.87.071301 [nucl-ex/0106015].

[25] Q. R. Ahmad *et al.* [SNO Collaboration], Phys. Rev. Lett. **89**, 011301 (2002) doi:10.1103/PhysRevLett.89.011301 [nucl-ex/0204008].

[26] Y. Ashie *et al.* [Super-Kamiokande Collaboration], Phys. Rev. Lett. **93**, 101801 (2004) doi:10.1103/PhysRevLett.93.101801 [hep-ex/0404034].

[27] K. Eguchi *et al.* [KamLAND Collaboration], Phys. Rev. Lett. **90**, 021802 (2003) doi:10.1103/PhysRevLett.90.021802 [hep-ex/0212021].

[28] D. Adey *et al.* [Daya Bay Collaboration], Phys. Rev. Lett. **121**, no. 24, 241805 (2018) doi:10.1103/PhysRevLett.121.241805 [arXiv:1809.02261 [hep-ex]].

[29] E. Aliu *et al.* [K2K Collaboration], Phys. Rev. Lett. **94**, 081802 (2005) doi:10.1103/PhysRevLett.94.081802 [hep-ex/0411038].

[30] P. Adamson *et al.* [NOvA Collaboration], Phys. Rev. Lett. **118**, no. 23, 231801 (2017) doi:10.1103/PhysRevLett.118.231801 [arXiv:1703.03328 [hep-ex]].

[31] S. V. Cao [T2K Collaboration], arXiv:1805.05917 [hep-ex].

[32] D. G. Michael *et al.* [MINOS Collaboration], Phys. Rev. Lett. **97**, 191801 (2006) doi:10.1103/PhysRevLett.97.191801 [hep-ex/0607088].

[33] N. Agafonova *et al.* [OPERA Collaboration], Phys. Rev. D **89**, no. 5, 051102 (2014) doi:10.1103/PhysRevD.89.051102 [arXiv:1401.2079 [hep-ex]].

[34] N. Agafonova *et al.* [OPERA Collaboration], Phys. Rev. Lett. **120**, no. 21, 211801 (2018) Erratum: [Phys. Rev. Lett. **121**, no. 13, 139901 (2018)] doi:10.1103/PhysRevLett.121.139901, 10.1103/PhysRevLett.120.211801 [arXiv:1804.04912 [hep-ex]].

[35] M. Tanabashi *et al.* [Particle Data Group], Phys. Rev. D **98**, no. 3, 030001 (2018). doi:10.1103/PhysRevD.98.030001

[36] J.H.Oort "The force exerted by the stellar system in the direction perpendicular to the galactic plane and some related problems, Bulletin of the Astronomical Institutes of the Netherlands 6 (1932) 249

[37] M. Roos, arXiv:1001.0316 [astro-ph.CO].

[38] V. Rubin, "Dark Matter in Spiral Galaxies" Scientific American 248 (June, 1983) 96106

[39] G. Battistoni *et al.*, Phys. Lett. **133B**, 454 (1983). doi:10.1016/0370-2693(83)90827-4

[40] G. Jungman, M. Kamionkowski and K. Griest, Phys. Rept. **267**, 195 (1996) doi:10.1016/0370-1573(95)00058-5 [hep-ph/9506380].

[41] G. Bertone, D. Hooper and J. Silk, Phys. Rept. **405**, 279 (2005) doi:10.1016/j.physrep.2004.08.031 [hep-ph/0404175].

[42] G. Arcadi, M. Dutra, P. Ghosh, M. Lindner, Y. Mambrini, M. Pierre, S. Profumo and F. S. Queiroz, Eur. Phys. J. C **78**, no. 3, 203 (2018) doi:10.1140/epjc/s10052-018-5662-y [arXiv:1703.07364 [hep-ph]].

[43] B. Prontecorvo, Sov.Phys.JETP 6, 429 (1957)

[44] V. N. Aseev *et al.* [Troitsk Collaboration], Phys. Rev. D **84**, 112003 (2011) doi:10.1103/PhysRevD.84.112003 [arXiv:1108.5034 [hep-ex]].

[45] C. Kraus *et al.*, Eur. Phys. J. C **40**, 447 (2005) doi:10.1140/epjc/s2005-02139-7 [hep-ex/0412056].

[46] K. Assamagan *et al.*, Phys. Rev. D **53**, 6065 (1996). doi:10.1103/PhysRevD.53.6065

[47] F. Cerutti, hep-ex/9903062.

[48] F. Priester, M. Sturm and B. Bornschein, Vacuum **116**, 42 (2015). doi:10.1016/j.vacuum.2015.02.030

[49] Y. R. Yen, arXiv:1906.10168 [nucl-ex].

[50] N. Aghanim *et al.* [Planck Collaboration], arXiv:1807.06209 [astro-ph.CO].

[51] M. Tanabashi *et al.* [Particle Data Group], Phys. Rev. D **98**, no. 3, 030001 (2018). doi:10.1103/PhysRevD.98.030001

[52] E. K. Akhmedov, R. Johansson, M. Lindner, T. Ohlsson and T. Schwetz, JHEP **0404**, 078 (2004) doi:10.1088/1126-6708/2004/04/078 [hep-ph/0402175].

[53] R. Acciarri *et al.* [DUNE Collaboration], arXiv:1601.05471 [physics.ins-det].

[54] A. Aguilar-Arevalo *et al.* [LSND Collaboration], Phys. Rev. D **64**, 112007 (2001) doi:10.1103/PhysRevD.64.112007 [hep-ex/0104049].

[55] H. L. Ray [MiniBooNE Collaboration], hep-ex/0701040.

[56] M. H. Ahn *et al.* [K2K Collaboration], Phys. Rev. D **74**, 072003 (2006) doi:10.1103/PhysRevD.74.072003 [hep-ex/0606032].

[57] P. Adamson *et al.* [MINOS Collaboration], Phys. Rev. Lett. **107**, 181802 (2011) doi:10.1103/PhysRevLett.107.181802 [arXiv:1108.0015 [hep-ex]].

[58] K. Abe *et al.* [T2K Collaboration], Phys. Rev. D **91**, no. 7, 072010 (2015) doi:10.1103/PhysRevD.91.072010 [arXiv:1502.01550 [hep-ex]].

[59] D. S. Ayres *et al.* [NOvA Collaboration], doi:10.2172/935497

[60] M. Fukugita and T. Yanagida, Berlin, Germany: Springer (2003) 593 p

[61] P. B. Pal, Int. J. Mod. Phys. A **7**, 5387 (1992). doi:10.1142/S0217751X92002465

[62] E. Roulet, Phys. Rev. D **44** (1991) 935 [Phys. Rev. D **44** (1991) R935]. doi:10.1103/PhysRevD.44.R935

[63] H. A. Bethe, Phys. Rev. Lett. **56**, 1305 (1986). doi:10.1103/PhysRevLett.56.1305

[64] M. M. Guzzo, A. Masiero and S. T. Petcov, Phys. Lett. B **260** (1991) 154. doi:10.1016/0370-2693(91)90984-X

[65] K. Ichimura [KamLAND Collaboration], arXiv:0810.3448 [hep-ex].

[66] F. P. An *et al.* [Daya Bay Collaboration], Phys. Rev. D **95**, no. 7, 072006 (2017) doi:10.1103/PhysRevD.95.072006 [arXiv:1610.04802 [hep-ex]].

[67] J. K. Ahn *et al.* [RENO Collaboration], arXiv:1003.1391 [hep-ex].

[68] J. I. Crespo-Anadn [Double Chooz Collaboration], Nucl. Part. Phys. Proc. **265-266**, 99 (2015) doi:10.1016/j.nuclphysbps.2015.06.025 [arXiv:1412.3698 [hep-ex]].

[69] I. Esteban, M. C. Gonzalez-Garcia, A. Hernandez-Cabezudo, M. Maltoni and T. Schwetz, JHEP **1901**, 106 (2019) doi:10.1007/JHEP01(2019)106 [arXiv:1811.05487 [hep-ph]].

[70] S. Goswami, Pramana **62**, 241 (2004) doi:10.1007/BF02705086 [hep-ph/0307224].

[71] R. Gandhi, P. Ghoshal, S. Goswami, P. Mehta and S. U. Sankar, Phys. Rev. D **73**, 053001 (2006) doi:10.1103/PhysRevD.73.053001 [hep-ph/0411252].

[72] H. Minakata, H. Sugiyama, O. Yasuda, K. Inoue and F. Suekane, Phys. Rev. D **68**, 033017 (2003) Erratum: [Phys. Rev. D **70**, 059901 (2004)] doi:10.1103/PhysRevD.70.059901, 10.1103/PhysRevD.68.033017 [hep-ph/0211111].

[73] A. Samanta, Phys. Rev. D **80**, 073008 (2009) doi:10.1103/PhysRevD.80.073008 [arXiv:0907.3978 [hep-ph]].

[74] M. Ghosh, P. Ghoshal, S. Goswami and S. K. Raut, Nucl. Phys. B **884**, 274 (2014) doi:10.1016/j.nuclphysb.2014.04.013 [arXiv:1401.7243 [hep-ph]].

[75] J. Burguet-Castell, M. B. Gavela, J. J. Gomez-Cadenas, P. Hernandez and O. Mena, Nucl. Phys. B **646**, 301 (2002) doi:10.1016/S0550-3213(02)00872-6 [hep-ph/0207080].

[76] H. Minakata and H. Nunokawa, JHEP **0110**, 001 (2001) doi:10.1088/1126-6708/2001/10/001 [hep-ph/0108085].

[77] G. L. Fogli and E. Lisi, Phys. Rev. D **54**, 3667 (1996) doi:10.1103/PhysRevD.54.3667 [hep-ph/9604415].

[78] V. Barger, D. Marfatia and K. Whisnant, Phys. Rev. D **65**, 073023 (2002) doi:10.1103/PhysRevD.65.073023 [hep-ph/0112119].

[79] A. Donini, D. and P. Migliozzi, Nucl. Phys. B **646**, 321 (2002) doi:10.1016/S0550-3213(02)00894-5 [hep-ph/0206034].

[80] V. Barger, D. Marfatia and K. Whisnant, Phys. Rev. D **66**, 053007 (2002) doi:10.1103/PhysRevD.66.053007 [hep-ph/0206038].

[81] O. Mena, S. Palomares-Ruiz and S. Pascoli, Phys. Rev. D **73**, 073007 (2006) doi:10.1103/PhysRevD.73.073007 [hep-ph/0510182].

[82] M. Narayan and S. U. Sankar, Phys. Rev. D **61**, 013003 (2000) doi:10.1103/PhysRevD.61.013003 [hep-ph/9904302].

[83] M. Ishitsuka, T. Kajita, H. Minakata and H. Nunokawa, Phys. Rev. D **72**, 033003 (2005) doi:10.1103/PhysRevD.72.033003 [hep-ph/0504026].

[84] T. Kajita, H. Minakata, S. Nakayama and H. Nunokawa, Phys. Rev. D **75**, 013006 (2007) doi:10.1103/PhysRevD.75.013006 [hep-ph/0609286].

[85] K. Hagiwara, N. Okamura and K. i. Senda, Phys. Lett. B **637**, 266 (2006) Erratum: [Phys. Lett. B **641**, 491 (2006)] doi:10.1016/j.physletb.2006.09.003, 10.1016/j.physletb.2006.04.041 [hep-ph/0504061].

[86] V. Barger, D. Marfatia and K. Whisnant, Phys. Lett. B **560**, 75 (2003) doi:10.1016/S0370-2693(03)00334-4 [hep-ph/0210428].

[87] P. Huber, M. Lindner and W. Winter, Nucl. Phys. B **654**, 3 (2003) doi:10.1016/S0550-3213(03)00063-4 [hep-ph/0211300].

[88] P. Huber, M. Lindner, T. Schwetz and W. Winter, Nucl. Phys. B **665**, 487 (2003) doi:10.1016/S0550-3213(03)00493-0 [hep-ph/0303232].

[89] O. Mena and S. J. Parke, Phys. Rev. D **70**, 093011 (2004) doi:10.1103/PhysRevD.70.093011 [hep-ph/0408070].

[90] O. Mena, Mod. Phys. Lett. A **20**, 1 (2005) doi:10.1142/S0217732305016269 [hep-ph/0503097].

[91] S. K. Agarwalla, S. Prakash and S. U. Sankar, JHEP **1307**, 131 (2013) doi:10.1007/JHEP07(2013)131 [arXiv:1301.2574 [hep-ph]].

[92] R. Acciarri *et al.* [DUNE Collaboration], arXiv:1512.06148 [physics.ins-det].

[93] V. De Romeri, E. Fernandez-Martinez and M. Sorel, JHEP **1609**, 030 (2016) doi:10.1007/JHEP09(2016)030 [arXiv:1607.00293 [hep-ph]].

[94] A. Friedland and S. W. Li, Phys. Rev. D **99**, no. 3, 036009 (2019) doi:10.1103/PhysRevD.99.036009 [arXiv:1811.06159 [hep-ph]].

[95] https://indico.cern.ch/event/721473/

[96] P. Ballett, T. Boschi and S. Pascoli, arXiv:1905.00284 [hep-ph].

[97] L. Emberger and F. Simon, J. Phys. Conf. Ser. **1162**, no. 1, 012033 (2019) doi:10.1088/1742-6596/1162/1/012033 [arXiv:1810.03677 [physics.ins-det]].

[98] J. Martin-Albo [DUNE Collaboration], J. Phys. Conf. Ser. **888**, no. 1, 012154 (2017) doi:10.1088/1742-6596/888/1/012154 [arXiv:1610.07803 [physics.ins-det]].

[99] A. Scarpelli [DUNE Collaboration], PoS NOW **2018**, 036 (2019) doi:10.22323/1.337.0036 [arXiv:1902.04780 [physics.ins-det]].

[100] M. Antonello *et al.* [MicroBooNE and LAr1-ND and ICARUS-WA104 Collaborations], arXiv:1503.01520 [physics.ins-det].

[101] P. A. Machado, O. Palamara and D. W. Schmitz, Ann. Rev. Nucl. Part. Sci. **69** [arXiv:1903.04608 [hep-ex]].

[102] F. Capozzi, S. W. Li, G. Zhu and J. F. Beacom, arXiv:1808.08232 [hep-ph].

[103] B. Abi *et al.* [DUNE Collaboration], arXiv:1706.07081 [physics.ins-det].

[104] C. Rott, S. In, J. Kumar and D. Yaylali, arXiv:1710.03822 [hep-ph].

[105] P. Adamson *et al.*, Nucl. Instrum. Meth. A **806** (2016) 279 doi:10.1016/j.nima.2015.08.063 [arXiv:1507.06690 [physics.acc-ph]].

[106] T. Alion *et al.* [DUNE Collaboration], arXiv:1606.09550 [physics.ins-det].

[107] "http://home.fnal.gov/ ljf26/DUNEFluxes/"

[108] M. Bishai and M. Dolce, "Optimization of the LBNF/DUNE beamline for tau neutrinos", in Document Database (DocDB) for DUNE and LBNF.

[109] P. Aprili *et al.* [ICARUS Collaboration], CERN-SPSC-2002-027, CERN-SPSC-P-323.

[110] V. D. Barger, A. M. Gago, D. Marfatia, W. J. C. Teves, B. P. Wood and R. Zukanovich Funchal, Phys. Rev. D **65**, 053016 (2002) doi:10.1103/PhysRevD.65.053016 [hep-ph/0110393].

[111] A. De Gouvêa, K. J. Kelly, G. V. Stenico and P. Pasquini, arXiv:1904.07265 [hep-ph].

[112] A. Rashed and A. Datta, Int. J. Mod. Phys. A **32**, no. 11, 1750060 (2017) doi:10.1142/S0217751X17500609 [arXiv:1603.09031 [hep-ph]].

[113] A. Ghoshal, A. Giarnetti and D. Meloni, arXiv:1906.06212 [hep-ph].

[114] N. Agafonova *et al.* [OPERA Collaboration], Phys. Rev. D **89**, no. 5, 051102 (2014) doi:10.1103/PhysRevD.89.051102 [arXiv:1401.2079 [hep-ex]].

[115] G. Galati *et al.*, Nuovo Cim. C **40**, no. 5, 160 (2017). doi:10.1393/ncc/i2017-17160-0

[116] N. Agafonova *et al.* [OPERA Collaboration], Phys. Rev. Lett. **120**, no. 21, 211801 (2018) doi:10.1103/PhysRevLett.120.211801 [arXiv:1804.04912 [hep-ex]].

[117] D. Meloni, Phys. Lett. B **792** (2019) 199 doi:10.1016/j.physletb.2019.03.042 [arXiv:1903.08933 [hep-ph]].

[118] P. Huber, M. Lindner and W. Winter, Comput. Phys. Commun. **167**, 195 (2005) doi:10.1016/j.cpc.2005.01.003 [hep-ph/0407333].

[119] P. Huber, J. Kopp, M. Lindner, M. Rolinec and W. Winter, Comput. Phys. Commun. **177** (2007) 432 doi:10.1016/j.cpc.2007.05.004 [hep-ph/0701187].

[120] P. Huber, M. Lindner and W. Winter, Nucl. Phys. B **645** (2002) 3 doi:10.1016/S0550-3213(02)00825-8 [hep-ph/0204352].

[121] G. L. Fogli, E. Lisi, A. Marrone, D. Montanino and A. Palazzo, Phys. Rev. D **66** (2002) 053010 doi:10.1103/PhysRevD.66.053010 [hep-ph/0206162].

[122] A. M. Ankowski and C. Mariani, J. Phys. G **44** (2017) no.5, 054001 doi:10.1088/1361-6471/aa61b2 [arXiv:1609.00258 [hep-ph]].

[123] S. K. Raut, Mod. Phys. Lett. A **28**, 1350093 (2013) doi:10.1142/S0217732313500934 [arXiv:1209.5658 [hep-ph]].

[124] K. Kodama *et al.* [DONUT Collaboration], Phys. Lett. B **504**, 218 (2001) doi:10.1016/S0370-2693(01)00307-0 [hep-ex/0012035].

[125] K. Kodama *et al.* [DONuT Collaboration], Phys. Rev. D **78**, 052002 (2008) doi:10.1103/PhysRevD.78.052002 [arXiv:0711.0728 [hep-ex]].

[126] T. Ohlsson, Rept. Prog. Phys. **76**, 044201 (2013) doi:10.1088/0034-4885/76/4/044201 [arXiv:1209.2710 [hep-ph]].

[127] O. G. Miranda and H. Nunokawa, New J. Phys. **17**, no. 9, 095002 (2015) doi:10.1088/1367-2630/17/9/095002 [arXiv:1505.06254 [hep-ph]].

[128] V. Brdar, J. Kopp, J. Liu, P. Prass and X. P. Wang, Phys. Rev. D **97**, no. 4, 043001 (2018) doi:10.1103/PhysRevD.97.043001 [arXiv:1705.09455 [hep-ph]].

[129] A. Greljo, G. Isidori and D. Marzocca, JHEP **1507**, 142 (2015) doi:10.1007/JHEP07(2015)142 [arXiv:1506.01705 [hep-ph]].

[130] L. Wolfenstein, Phys. Rev. D **17**, 2369 (1978). doi:10.1103/PhysRevD.17.2369

[131] S. Davidson, C. Pena-Garay, N. Rius and A. Santamaria, JHEP **0303**, 011 (2003) doi:10.1088/1126-6708/2003/03/011 [hep-ph/0302093].

[132] L. J. Flores, E. A. Garcs and O. G. Miranda, Phys. Rev. D **98**, no. 3, 035030 (2018) doi:10.1103/PhysRevD.98.035030 [arXiv:1806.07951 [hep-ph]].

[133] P. Adamson *et al.* [MINOS Collaboration], Phys. Rev. D **88**, no. 7, 072011 (2013) doi:10.1103/PhysRevD.88.072011 [arXiv:1303.5314 [hep-ex]].

[134] G. Mitsuka *et al.* [Super-Kamiokande Collaboration], Phys. Rev. D **84**, 113008 (2011) doi:10.1103/PhysRevD.84.113008 [arXiv:1109.1889 [hep-ex]].

[135] S. Choubey, A. Ghosh, T. Ohlsson and D. Tiwari, JHEP **1512**, 126 (2015) doi:10.1007/JHEP12(2015)126 [arXiv:1507.02211 [hep-ph]].

[136] T. Kikuchi, H. Minakata and S. Uchinami, JHEP **0903**, 114 (2009) doi:10.1088/1126-6708/2009/03/114 [arXiv:0809.3312 [hep-ph]].

[137] D. Meloni, T. Ohlsson and H. Zhang, JHEP **0904**, 033 (2009) doi:10.1088/1126-6708/2009/04/033 [arXiv:0901.1784 [hep-ph]].

[138] S. K. Agarwalla, Y. Kao, D. Saha and T. Takeuchi, JHEP **1511**, 035 (2015) doi:10.1007/JHEP11(2015)035 [arXiv:1506.08464 [hep-ph]].

[139] Y. Farzan and M. Tortola, Front. in Phys. **6**, 10 (2018) doi:10.3389/fphy.2018.00010 [arXiv:1710.09360 [hep-ph]].

[140] M. Masud, A. Chatterjee and P. Mehta, J. Phys. G **43** (2016) no.9, 095005 doi:10.1088/0954-3899/43/9/095005/meta, 10.1088/0954-3899/43/9/095005 [arXiv:1510.08261 [hep-ph]].

[141] A. de Gouvêa and K. J. Kelly, Nucl. Phys. B **908** (2016) 318 doi:10.1016/j.nuclphysb.2016.03.013 [arXiv:1511.05562 [hep-ph]].

[142] P. Coloma, JHEP **1603**, 016 (2016) doi:10.1007/JHEP03(2016)016 [arXiv:1511.06357 [hep-ph]].

[143] A. de Gouva and K. J. Kelly, arXiv:1605.09376 [hep-ph].

[144] M. Blennow, P. Coloma, E. Fernandez-Martinez, J. Hernandez-Garcia and J. Lopez-Pavon, JHEP **1704**, 153 (2017) doi:10.1007/JHEP04(2017)153 [arXiv:1609.08637 [hep-ph]].

[145] A. Friedland, C. Lunardini and M. Maltoni, Phys. Rev. D **70**, 111301 (2004) doi:10.1103/PhysRevD.70.111301 [hep-ph/0408264].

[146] M. C. Gonzalez-Garcia, M. Maltoni and J. Salvado, JHEP **1105**, 075 (2011) doi:10.1007/JHEP05(2011)075 [arXiv:1103.4365 [hep-ph]].

[147] M. Masud and P. Mehta, Phys. Rev. D **94**, no. 5, 053007 (2016) doi:10.1103/PhysRevD.94.053007 [arXiv:1606.05662 [hep-ph]].

[148] M. Masud and P. Mehta, Phys. Rev. D **94** (2016) 013014 doi:10.1103/PhysRevD.94.013014 [arXiv:1603.01380 [hep-ph]].

[149] M. Masud and P. Mehta, Pramana **89**, no. 4, 62 (2017). doi:10.1007/s12043-017-1457-1

[150] M. Masud, S. Roy and P. Mehta, Phys. Rev. D **99**, no. 11, 115032 (2019) doi:10.1103/PhysRevD.99.115032 [arXiv:1812.10290 [hep-ph]].

[151] S. Fukasawa, M. Ghosh and O. Yasuda, Phys. Rev. D **95** (2017) no.5, 055005 doi:10.1103/PhysRevD.95.055005 [arXiv:1611.06141 [hep-ph]].

[152] J. Liao, D. Marfatia and K. Whisnant, JHEP **1701** (2017) 071 doi:10.1007/JHEP01(2017)071 [arXiv:1612.01443 [hep-ph]].

[153] S. Verma and S. Bhardwaj, arXiv:1808.04263 [hep-ph].

[154] K. Huitu, T. J. Kärkkäinen, J. Maalampi and S. Vihonen, Phys. Rev. D **93** (2016) no.5, 053016 doi:10.1103/PhysRevD.93.053016 [arXiv:1601.07730 [hep-ph]].

[155] M. Blennow, S. Choubey, T. Ohlsson, D. Pramanik and S. K. Raut, JHEP **1608** (2016) 090 doi:10.1007/JHEP08(2016)090 [arXiv:1606.08851 [hep-ph]].

[156] J. Liao, D. Marfatia and K. Whisnant, Phys. Rev. D **93**, no. 9, 093016 (2016) doi:10.1103/PhysRevD.93.093016 [arXiv:1601.00927 [hep-ph]].

[157] M. Ghosh and O. Yasuda, Phys. Rev. D **96**, no. 1, 013001 (2017) doi:10.1103/PhysRevD.96.013001 [arXiv:1702.06482 [hep-ph]].

[158] C. Biggio, M. Blennow and E. Fernandez-Martinez, JHEP **0908**, 090 (2009) doi:10.1088/1126-6708/2009/08/090 [arXiv:0907.0097 [hep-ph]].

[159] M. C. Gonzalez-Garcia and M. Maltoni, JHEP **1309**, 152 (2013) doi:10.1007/JHEP09(2013)152 [arXiv:1307.3092 [hep-ph]].

[160] I. Esteban, M. C. Gonzalez-Garcia and M. Maltoni, arXiv:1905.05203 [hep-ph].

[161] D. Meloni, JHEP **1808**, 028 (2018) doi:10.1007/JHEP08(2018)028 [arXiv:1805.01747 [hep-ph]].

[162] J. Kopp, M. Lindner, T. Ota and J. Sato, Phys. Rev. D **77** (2008) 013007 doi:10.1103/PhysRevD.77.013007 [arXiv:0708.0152 [hep-ph]].

[163] M. Blennow, D. Meloni, T. Ohlsson, F. Terranova and M. Westerberg, Eur. Phys. J. C **56** (2008) 529 doi:10.1140/epjc/s10052-008-0683-6 [arXiv:0804.2744 [hep-ph]].

[164] R. Keloth, A. Aurisano, A. Sousa, G. S. Davies, L. Suter and R. K. Plunkett, arXiv:1710.00295 [hep-ex].

[165] J. Alexander *et al.*, arXiv:1608.08632 [hep-ph].

[166] M. Battaglieri *et al.*, arXiv:1707.04591 [hep-ph].

[167] T. Blum, A. Denig, I. Logashenko, E. de Rafael, B. L. Roberts, T. Teubner and G. Venanzoni, arXiv:1311.2198 [hep-ph].

[168] G. Arcadi, M. Dutra, P. Ghosh, M. Lindner, Y. Mambrini, M. Pierre, S. Profumo and F. S. Queiroz, Eur. Phys. J. C **78**, no. 3, 203 (2018) doi:10.1140/epjc/s10052-018-5662-y [arXiv:1703.07364 [hep-ph]].

[169] B. Holdom, Phys. Lett. **166B**, 196 (1986). doi:10.1016/0370-2693(86)91377-8

[170] J. Jaeckel, Frascati Phys. Ser. **56**, 172 (2012) [arXiv:1303.1821 [hep-ph]].

[171] R. Essig, J. Kaplan, P. Schuster and N. Toro, [arXiv:1004.0691 [hep-ph]].

[172] F. del Aguila, G. D. Coughlan and M. Quiros, Nucl. Phys. B **307**, 633 (1988) Erratum: [Nucl. Phys. B **312**, 751 (1989)]. doi:10.1016/0550-3213(88)90266-0

[173] N. Arkani-Hamed and N. Weiner, JHEP **0812**, 104 (2008) doi:10.1088/1126-6708/2008/12/104 [arXiv:0810.0714 [hep-ph]].

[174] M. Goodsell, J. Jaeckel, J. Redondo and A. Ringwald, JHEP **0911**, 027 (2009) doi:10.1088/1126-6708/2009/11/027 [arXiv:0909.0515 [hep-ph]].

[175] M. Ahlers, J. Jaeckel, J. Redondo and A. Ringwald, Phys. Rev. D **78**, 075005 (2008) doi:10.1103/PhysRevD.78.075005 [arXiv:0807.4143 [hep-ph]].

[176] J. L. Hewett *et al.*, doi:10.2172/1042577 arXiv:1205.2671 [hep-ex].

[177] A. J. Krasznahorkay *et al.*, Phys. Rev. Lett. **116**, no. 4, 042501 (2016) doi:10.1103/PhysRevLett.116.042501 [arXiv:1504.01527 [nucl-ex]].

[178] A. J. Krasznahorkay *et al.*, EPJ Web Conf. **142**, 01019 (2017). doi:10.1051/epjconf/201714201019

[179] A. J. Krasznahorkay *et al.*, EPJ Web Conf. **137**, 08010 (2017). doi:10.1051/epjconf/201713708010

[180] J. L. Feng, B. Fornal, I. Galon, S. Gardner, J. Smolinsky, T. M. P. Tait and P. Tanedo, Phys. Rev. D **95**, no. 3, 035017 (2017) doi:10.1103/PhysRevD.95.035017 [arXiv:1608.03591 [hep-ph]].

[181] J. Redondo and A. Ringwald, Contemp. Phys. **52**, 211 (2011) doi:10.1080/00107514.2011.563516 [arXiv:1011.3741 [hep-ph]].

[182] V. Anastassopoulos *et al.* [CAST Collaboration], Nature Phys. **13**, 584 (2017) doi:10.1038/nphys4109 [arXiv:1705.02290 [hep-ex]].

[183] M. Pospelov, A. Ritz and M. B. Voloshin, Phys. Rev. D **78**, 115012 (2008) doi:10.1103/PhysRevD.78.115012 [arXiv:0807.3279 [hep-ph]].

[184] J. Redondo and M. Postma, JCAP **0902**, 005 (2009) doi:10.1088/1475-7516/2009/02/005 [arXiv:0811.0326 [hep-ph]].

[185] M. Pospelov, J. Pradler, J. T. Ruderman and A. Urbano, Phys. Rev. Lett. **121**, no. 3, 031103 (2018) doi:10.1103/PhysRevLett.121.031103 [arXiv:1803.07048 [hep-ph]].

[186] M. Pospelov, A. Ritz and M. B. Voloshin, Phys. Lett. B **662**, 53 (2008) doi:10.1016/j.physletb.2008.02.052 [arXiv:0711.4866 [hep-ph]].

[187] L. J. Hall, K. Jedamzik, J. March-Russell and S. M. West, JHEP **1003**, 080 (2010) doi:10.1007/JHEP03(2010)080 [arXiv:0911.1120 [hep-ph]].

[188] G. Krnjaic, Phys. Rev. D **94**, no. 7, 073009 (2016) doi:10.1103/PhysRevD.94.073009 [arXiv:1512.04119 [hep-ph]].

[189] C. Boehm, M. J. Dolan and C. McCabe, JCAP **1308**, 041 (2013) doi:10.1088/1475-7516/2013/08/041 [arXiv:1303.6270 [hep-ph]].

[190] D. Green and S. Rajendran, JHEP **1710**, 013 (2017) doi:10.1007/JHEP10(2017)013 [arXiv:1701.08750 [hep-ph]].

[191] E. Izaguirre, G. Krnjaic, P. Schuster and N. Toro, Phys. Rev. D **91**, no. 9, 094026 (2015) doi:10.1103/PhysRevD.91.094026 [arXiv:1411.1404 [hep-ph]].

[192] I. Jaegle [Belle Collaboration], Phys. Rev. Lett. **114**, no. 21, 211801 (2015) doi:10.1103/PhysRevLett.114.211801 [arXiv:1502.00084 [hep-ex]].

[193] M. Raggi, V. Kozhuharov and P. Valente, EPJ Web Conf. **96**, 01025 (2015) doi:10.1051/epjconf/20159601025 [arXiv:1501.01867 [hep-ex]].

[194] D. Banerjee *et al.* [NA64 Collaboration], Phys. Rev. D **97**, no. 7, 072002 (2018) doi:10.1103/PhysRevD.97.072002 [arXiv:1710.00971 [hep-ex]].

[195] A. Konaka *et al.*, Phys. Rev. Lett. **57**, 659 (1986). doi:10.1103/PhysRevLett.57.659

[196] M. Davier and H. Nguyen Ngoc, Phys. Lett. B **229**, 150 (1989). doi:10.1016/0370-2693(89)90174-3

[197] S. Andreas, C. Niebuhr and A. Ringwald, Phys. Rev. D **86**, 095019 (2012) doi:10.1103/PhysRevD.86.095019 [arXiv:1209.6083 [hep-ph]].

[198] J. D. Bjorken, R. Essig, P. Schuster and N. Toro, Phys. Rev. D **80**, 075018 (2009) doi:10.1103/PhysRevD.80.075018 [arXiv:0906.0580 [hep-ph]].

[199] E. M. Riordan *et al.*, Phys. Rev. Lett. **59**, 755 (1987). doi:10.1103/PhysRevLett.59.755

[200] Y. S. Liu and G. A. Miller, Phys. Rev. D **96**, no. 1, 016004 (2017) doi:10.1103/PhysRevD.96.016004 [arXiv:1705.01633 [hep-ph]].

[201] Weizscker, C.F.. Z. Physik (1934) 88: 612. https://doi.org/10.1007/BF01333110

[202] E. J. Williams, Kong. Dan. Vid. Sel. Mat. Fys. Med. **13N4**, no. 4, 1 (1935).

[203] K. J. Kim and Y. S. Tsai, Phys. Rev. D **8**, 3109 (1973). doi:10.1103/PhysRevD.8.3109

[204] S. N. Gninenko, D. V. Kirpichnikov, M. M. Kirsanov and N. V. Krasnikov, Phys. Lett. B **782**, 406 (2018) doi:10.1016/j.physletb.2018.05.010 [arXiv:1712.05706 [hep-ph]].

[205] J. Liu, N. Weiner and W. Xue, JHEP **1508**, 050 (2015) doi:10.1007/JHEP08(2015)050 [arXiv:1412.1485 [hep-ph]].

[206] A. Anastasi *et al.*, Phys. Lett. B **750**, 633 (2015) doi:10.1016/j.physletb.2015.10.003 [arXiv:1509.00740 [hep-ex]].

[207] M. Pospelov, Phys. Rev. D **80**, 095002 (2009) doi:10.1103/PhysRevD.80.095002 [arXiv:0811.1030 [hep-ph]].

[208] M. Endo, K. Hamaguchi and G. Mishima, Phys. Rev. D **86**, 095029 (2012) doi:10.1103/PhysRevD.86.095029 [arXiv:1209.2558 [hep-ph]].

[209] H. Davoudiasl, H. S. Lee and W. J. Marciano, Phys. Rev. D **89**, no. 9, 095006 (2014) doi:10.1103/PhysRevD.89.095006 [arXiv:1402.3620 [hep-ph]].

[210] J. P. Lees *et al.* [BaBar Collaboration], Phys. Rev. Lett. **113**, no. 20, 201801 (2014) doi:10.1103/PhysRevLett.113.201801 [arXiv:1406.2980 [hep-ex]].

[211] S. Choi, New Phys. Sae Mulli **66**, no. 8, 1036 (2016). doi:10.3938/NPSM.66.1036

[212] E. Nardi, C. D. R. Carvajal, A. Ghoshal, D. Meloni and M. Raggi, Phys. Rev. D **97**, no. 9, 095004 (2018) doi:10.1103/PhysRevD.97.095004 [arXiv:1802.04756 [hep-ph]].

[213] I. Rachek, D. Nikolenko and B. Wojtsekhowski, EPJ Web Conf. **142**, 01025 (2017). doi:10.1051/epjconf/201714201025

[214] J. Alexander, EPJ Web Conf. **142**, 01001 (2017). doi:10.1051/epjconf/201714201001

[215] V. Scherini [PADME Collaboration], doi:10.3204/DESY-PROC-2017-02/scherini$_v ivianaar Xiv$: 1712.01936[$hep - ex$].

[216] M. Raggi and V. Kozhuharov, Adv. High Energy Phys. **2014**, 959802 (2014) doi:10.1155/2014/959802 [arXiv:1403.3041 [physics.ins-det]].

[217] A. Ghigo, G. Mazzitelli, F. Sannibale, P. Valente and G. Vignola, Nucl. Instrum. Meth. A **515**, 524 (2003). doi:10.1016/j.nima.2003.07.017

[218] P. Valente, EPJ Web Conf. **142**, 01028 (2017). doi:10.1051/epjconf/201714201028

[219] L. Marsicano *et al.*, Phys. Rev. D **98**, no. 1, 015031 (2018) doi:10.1103/PhysRevD.98.015031 [arXiv:1802.03794 [hep-ex]].

[220] H. Bethe and W. Heitler, Proc. Roy. Soc. Lond. A **146**, 83 (1934). doi:10.1098/rspa.1934.0140

[221] Y. S. Tsai and V. Whitis, Phys. Rev. **149**, 1248 (1966). doi:10.1103/PhysRev.149.1248

[222] M. Bohm and W. Hollik, Nucl. Phys. B **204**, 45 (1982). doi:10.1016/0550-3213(82)90421-7

[223] Ghosh, V. J. and Alatalo, M. and Asoka-Kumar, P. and Nielsen, B. and Lynn, K. G. and Kruseman, A. C. and Mijnarends, P. E., Phys. Rev. B **61**, 15 (2000) doi:10.1103/PhysRevB.61.10092, url:https://link.aps.org/doi/10.1103/PhysRevB.61.10092

[224] Clementi,E. and Raimondi,D. L. and Reinhardt,W. P., "Atomic Screening Constants from SCF Functions. II. Atoms with 37 to 86" The Journal of Chemical Physics **47**, 4 (1967) doi:10.1063/1.1712084,

[225] J. L. Feng, B. Fornal, I. Galon, S. Gardner, J. Smolinsky, T. M. P. Tait and P. Tanedo, Phys. Rev. Lett. **117**, no. 7, 071803 (2016) doi:10.1103/PhysRevLett.117.071803 [arXiv:1604.07411 [hep-ph]].

[226] J. R. Batley *et al.* [NA48/2 Collaboration], Phys. Lett. B **746**, 178 (2015) doi:10.1016/j.physletb.2015.04.068 [arXiv:1504.00607 [hep-ex]].

[227] J. Blmlein and J. Brunner, Phys. Lett. B **731**, 320 (2014) doi:10.1016/j.physletb.2014.02.029 [arXiv:1311.3870 [hep-ph]].

[228] J. Blumlein and J. Brunner, Phys. Lett. B **701**, 155 (2011) doi:10.1016/j.physletb.2011.05.046 [arXiv:1104.2747 [hep-ex]].

[229] T. Raubenheimer *et al.*, arXiv:1801.07867 [physics.acc-ph].

[230] L. Marsicano *et al.*, Phys. Rev. Lett. **121**, no. 4, 041802 (2018) doi:10.1103/PhysRevLett.121.041802 [arXiv:1807.05884 [hep-ex]].

[231] F. Brummer and J. Jaeckel, Phys. Lett. B **675**, 360 (2009) doi:10.1016/j.physletb.2009.04.041 [arXiv:0902.3615 [hep-ph]].

[232] F. Brummer, J. Jaeckel and V. V. Khoze, JHEP **0906**, 037 (2009) doi:10.1088/1126-6708/2009/06/037 [arXiv:0905.0633 [hep-ph]].

[233] E. C. G. Stueckelberg, Helv. Phys. Acta **11**, 225 (1938). doi:10.5169/seals-110852

[234] D. G. C. McKeon and T. J. Marshall, Int. J. Mod. Phys. A **23**, 741 (2008) doi:10.1142/S0217751X08039499 [hep-th/0610034].